Attitude control- and stabilisation moment generation of the DelFly using Wing Tension Modulation

R.M.J. Janssen
26 October 2016

TU Delft

Attitude control- and stabilisation moment generation of the DelFly using Wing Tension Modulation

For obtaining the degree of Master of Science in Aerospace Engineering
at Delft University of Technology

R.M.J. Janssen

October 26, 2016

Faculty of Aerospace Engineering · Delft University of Technology

TUDelft

Delft University of Technology

The undersigned hereby certify that they have read and recommend to the Faculty of Aerospace Engineering for acceptance a thesis entitled **"Attitude control- and stabilisation moment generation of the DelFly using Wing Tension Modulation"** by **R.M.J. Janssen** in partial fulfillment of the requirements for the degree of **Master of Science**.

Dated: <u>October 26, 2016</u>

Readers:

Dr. Qiping Chu

Dr.ir. Matěj Karásek

ir. Bart D.W. Remes

Dr.ir. Hans Goosen

Abstract

The hovering flight of a tail-less Flapping Wing Micro Aerial Vehicle is inherently unstable and therefore needs to be actively stabilised. For this purpose, and also for controlling the attitude and heading, pitch, roll and yaw moments have to be generated. We present a flapping wing robot with a control mechanism that modulates the tension of four wings independently, by displacing the wing roots. We demonstrate with high-speed camera recordings that changing the wing tension results in a change of the angle of attack of the wings and thus alter their thrust levels. Direct moment measurements show that this is an effective method to generate pitch and roll moments, while showing a low level of cross-coupling. The effectivity of the mechanism was successfully demonstrated in-flight.

Preface

About a year ago when I had my first meeting with my supervisors Matěj Karásek and Bart Remes, I was immediately interested in the topic of DelFly design. I liked the fact that I could combine my practical and theoretical skills to contribute to one of the Faculty's famous showpieces. Soon enough, I realised that making a DelFly fly without a tail was a real challenge, and when performing a literature review I noticed that only a few research groups in the world had managed to make a flapping robot fly without a tail. It is therefore not surprising that my research had its ups and downs and I sometimes lost my confidence that my flapping robot would ever be able to fly. However, partly due to the persistent guidance and support of my daily supervisor Matěj Karásek, I kept my motivation and managed to make it fly, for which I am extremely grateful. Next, I would like to thank Bart Remes, even while we did not always agree on the inner workings of the tail-less concepts, I really enjoyed our discussions and would like to thank him for his suggestions and support. I would further like to thank Sjoerd Tijmons, for our many discussions on future concepts of the DelFly and Erik van der Horst, who helped me with the manufacturing of the prototypes.

Additionally, I would like to thank all the people that reviewed my writings throughout my master project. I am sure that this greatly increased the readability and clarity of my thesis. Lastly, I would like to think my friends, family, and girlfriend for their direct and indirect support, especially when I did not always had the time to visit them during the last phase of my thesis. My thesis and the rest of my studies have been great, and I am really looking forward to the next step.

Contents

List of Tables

List of Figures

List of Symbols

Greek Symbols

α	Angle of attack
α_{acc}	Angular acceleration
Γ	Circulation
λ	System pole, root of characteristic equation
$\bar{\Phi}$	Flapping amplitude
ϕ	Flapping angle
ϕ	Roll angle
ψ	Yaw angle
ρ	Density
τ	Dimensionless time in s
$\tau_{net\ ext}$	Net external torque
θ	Pitch angle

Roman Symbols

b	Aerodynamic coefficient depending on wing morphology
$\bar{c}$	Mean chord length
C_D	Drag coefficient
C_L	Lift Coefficient
d	Distance between COG and a.c.
F_D	Drag force
g	Gravitational acceleration

I	Moment of inertia
L	Lift
L_p	Roll damping
m	Mass
M_x	Roll moment
M_y	Pitch moment
M_z	Yaw moment
n	Flapping frequency
p	Roll rate
q	Pitch rate
R	Wing length
r	Yaw rate
$\hat{r}_2$	Non-dimensional second moment of wing area
S	Wing area
T	Torque
T_2	Time-to-double
U_∞	Free-stream velocity
V	Body speed
V_{app}	Apparent wing speed
w	Wing speed
$\hat{X}_u, \hat{M}_u$	Stability derivatives

Acronyms

a.c.	Aerodynamic Center
CFD	Computational Fluid Dynamics
COG	Center of Gravity
DOF	Degree of Freedom
FBD	Free Body Diagram
FWMAV	Flapping Wing Micro Aerial Vehicle
LEV	Leading Edge Vortex
MAV	Micro Aerial Vehicle

Chapter 1

Introduction

The goal of this thesis is to contribute to the research on the development of a tail-less DelFly. Two main concepts were developed and tested, which both rely on the deformation of a wing with a rope in order to generate the necessary moments for stabilisation and control. This thesis consists of two parts. Part I contains an academic paper that includes a description of the final tail-less DelFly concept, and the performance of this prototype is assessed with experiments. This paper mainly presents the second concept we developed, concept B. The preliminary research that is carried out before the work described in the paper, is presented in Part II. This part contains a literature review about flapping flight in general and regarding active control strategies for insects and flapping robots developed by other research groups. Next, we present in part II our two concepts and some preliminary experiments on their moment generation.

Part I

Paper

Attitude control- and stabilisation moment generation of the DelFly using Wing Tension Modulation

Robin M.J. Janssen[*], Matěj Karásek[†] and Bart D.W. Remes[‡]

Faculty of Aerospace Engineering, TU Delft, Kluyverweg 1, 2629 HS, Delft, The Netherlands

The hovering flight of a tail-less Flapping Wing Micro Aerial Vehicle is inherently unstable and therefore needs to be actively stabilised. For this purpose, and also for controlling the attitude and heading, pitch, roll and yaw moments have to be generated. We present a flapping wing robot with a control mechanism that modulates the tension of four wings independently, by displacing the wing roots. We demonstrate with high-speed camera recordings that changing the wing tension results in a change of the angle of attack of the wings and thus alter their thrust levels. Direct moment measurements show that this is an effective method to generate pitch and roll moments, while showing a low level of cross-coupling. The effectivity of the mechanism was successfully demonstrated in-flight.

I.   Introduction

Historically, the main goal of research on Micro Aerial Vehicles (MAVs) is to arrive at insect sized aircraft. The small size of these MAVs makes them well suited for reconnaissance in places that are too small or too dangerous for humans or other vehicles to enter. Therefore, researchers, industries, governments and the military have shown great interest in development of such systems. It may come as no surprise that in the development of MAVs, researchers draw their inspiration from nature. Winged insects already roam the skies since 325 million years ago [Wootton, 1981], and have been evolving ever since. Due to natural selection, dragonflies are capable of complete 180°turns within three wing beats [Alexander, 1986], and landing on flowers buffeted by high winds. Additionally, these animals have an unmatched flight envelope: capabilities range from hovering, high-speed forward flight, backward flight and quick take-off.

Due to their large flight envelope and manoeuvrability, researchers have tried to mimic these natural flyers in the form of Flapping Wing Micro Aerial Vehicles (FWMAVs). It has also led to the Delft University of Technology's project 'DelFly', see Figure 1-(a).

DelFly started as a student project to design a small ornithopter (an aircraft with flapping wings) that was able to carry a camera system with good flight characteristics. Indeed, the DelFly II is capable of hovering, and able to fly 7 m/s forward and 1 m/s backwards [de Croon et al., 2009]. The idea behind the project is to design a flying platform using a top-down approach. One starts with a functioning, relatively large ornithopter, and by studying this ornithopter, it is gradually improved and scaled down. In 2008 the 'DelFly Micro' was developed resulting from this approach. This flapper weighs 3 grams and has a wingspan of 10 cm but is still able to carry a small camera. To date, the autonomous capabilities of the 'DelFly Explorer' are still being improved, being *"the first FWMAV with onboard vision processing for autonomous flight in generic environments"* [De Wagter et al., 2014].

Throughout the whole project, the DelFly uses a biplane configuration, since the power consumption is lower than more conventional monoplane configurations for the same size [de Croon et al., 2009]. These two pairs of wings flap in anti-phase, and they are positioned on top of each other to limit size. The DelFly carries conventional tail surfaces as seen in fixed wing aircraft for stabilisation and control.

Apart from its larger size, the fact that the DelFly carries this tail, is the most discerning feature from its natural counterpart, the dragonfly. Both CFD studies [Sun and Xiong, 2005, Wu and Sun, 2009, Zhang and Sun, 2010] and studies based on quasi-steady models [Cheng and Deng, 2011, Karásek and Preumont, 2012] conclude that hovering (tail-less) in-

---

[*]Graduate Student, Faculty of Aerospace Engineering, Department of Control & Simulation, TU Delft r.m.j.janssen-1@tudelft.nl

[†]Postdoctoral researcher, Faculty of Aerospace Engineering, Department of Control & Simulation, TU Delft, m.karasek@tudelft.nl

[‡]MAVLab coordinator, Faculty of Aerospace Engineering, Department of Control & Simulation, TU Delft, b.d.w.remes@tudelft.nl

(a) DelFly II

(b) Tail-less DelFly

Figure 1. DelFly II and Tail-less DelFly

sect flight with two wings is dynamically unstable, both longitudinally and laterally. To achieve stable flight, the insect needs to generate time-varying control forces and moments to suppress the disturbed motion of their body due to an initial disturbance [Sun, 2014]. Although the flight dynamics of a four-winged tail-less flapping robot with a wing layout comparable to the DelFly has not been studied, we expect and also noticed in our experiments that a passive tail-less DelFly is dynamically unstable. The dragonfly solves this stability issue by generating the moments needed for stable flight by using its wings, they achieve this by introducing small changes to the wing angle of attack, to the mean wing position and to the flapping amplitude [Ellington, 1999]. The dragonfly is able to alter these parameters independently for each of its wings, resulting in high manoeuvrability [Hatch, 1966].

In contrast, the DelFly fully relies on its tail for passive stabilisation, and this tail features control surfaces for manoeuvring- and steady-state control. A downside thereof is that it stays sensitive to external disturbances. During a typical envisioned mission for MAVs, the inspection of buildings, the MAV will have to fly close to obstructions such as walls. Even on a calm day these obstructions can cause drafts, severely hindering the successful completion of a mission. Removing this tail and instead using active control and stabilisation makes the DelFly potentially very agile and more resilient against wind gusts.

Another reason to use active wing control and stabilisation could lie in the improvement of controllability during hover. In current prototypes, the DelFly is controllable during hover due to the tail surfaces being in the wake of the wings. This way, the airflow over the control surfaces can be steered, which generates the necessary control moments. However, only a part of this highly turbulent wake is steered, resulting in degraded control performance with respect to forward flight, where also the airflow resulting from a forward speed is steered. The use of active wing control could bridge this gap, resulting in a more even control performance over various speeds. Additionally, removing the tail can potentially reduce the MAV's size and weight, bringing it closer to the envisioned fly-sized craft.

However, actively stabilising and controlling a FW-MAV is extremely challenging and only a few research groups have succeeded. More have demonstrated the generation of control moments on a force balance. For the control moment generation of these FWMAVs, two main strategies were used. Coleman et al. [2015], Karásek et al. [2014], Ma et al. [2013] used changes in the flapping kinematics to generate moments, such as modulations in amplitude and mean wing position.

The second strategy is the generation of moments by wing deformation. The Nano Hummingbird [Keennon et al., 2012b] uses changes in wing twist and wing rotation to control the three attitude moments and stabilise the flight without a tail.

Nevertheless, the few prototypes that achieved stable tailless free-flight —the flappers of Keennon et al. [2012b], Ma et al. [2013] and Coleman et al. [2015] —all carry only two wings. To date, tailless flight is still in its infancy on lay-outs similar to the DelFly, a lay-out which has advantages in flight efficiency due to thrust enhancing effects such as the clap-and-peel mechanism [de Croon et al., 2012].

The goal of present research is to be able to control a DelFly by using its wings not only for propulsion, but also for control. This can eventually be developed in a tail-less DelFly. We propose a novel mechanism to generate the moments to control and stabilise the four-winged DelFly, by modulating the slackness of each of the wings with rope based actuation. The final tail-less DelFly, as developed in this paper, is depicted in Figure 1-(b).

In this paper, first the requirements that are set to be able to actively control- and stabilise our prototype are described, using reference data of a similar flying robot, in section II. Next, in section III, further detailed explanation of the design of the subsystems is presented —the flapping-, control- and actuation mechanisms. In section IV the methodology, results and discussion of four main experiments we conducted are described. In this section, first an experiment of static force/torque measurements on the prototype is presented, showing the magnitude of the control moments the prototype is able to generate. Next, we show with force/torque measurements the response of the generated moments to step inputs. To obtain insight on the morphological behaviour and aerodynamic mechanisms behind the control moment generation, the motion of the DelFly during these step inputs was recorded using a high-speed camera. We continue by showing the performance of the prototype during a free flight experiment. The paper ends with conclusions and recommendations for further research.

II.   Requirements

In order to assess the various prototypes which are developed for this research, it is important to set quantitative and qualitative requirements, which meet the research goal of controlling the DelFly by means of its wings. First, a summary of the requirements is presented, after which the quantitative requirements —set using reference data—are discussed. This reference data is obtained from Keennon et al.

[2012a], since the flapping robot they describe, the Nano Hummingbird, is one of the few FWMAVs that was able to self-stabilise in-flight without using aerodynamic dampers, and is comparable in size to the DelFly.

II.A.   Summary of requirements

The requirements for active control, which also hold for active stabilisation, are identified in order of importance:

1. **Low weight**. Since the mechanism needs to be eventually able to fly, the weight of the mechanism should be low. The combined weight of the structure, flapping mechanism, control system and battery should be less than 23 grams, the weight the DelFly is able to lift for a sustained amount of time.

2. **High control moment generation**. The generated moments need to be able to control the DelFly, and in case of tail-less flight also be able to mitigate disturbing forces and moments. For stable, tail-less flight near hover, the pitch and roll angles (see Figure 2 for axis definitions) should be stabilised using attitude feedback. Yaw moment control is necessary if one wants to control the heading of the aircraft. Since a model for the DelFly tail-less dynamics is not available, reference data from the Nano Hummingbird is used to set a quantitative requirement. This analysis, as explained in section II.B, results in a requirement for the pitch and roll moments in the order of 1 to 3 Nmm.

3. **Repeatable and spectrum wide**. For the vehicle to be controllable, the moments that are to be generated should be repeatable, i.e. a certain control input should always generate the same control moment. Also, the vehicle should be able to generate both positive and negative moments, and the generated moments should preferably be linearly related to the respective control inputs.

4. **Low cross-coupling**. We need to be able to generate the moments around the attitude axes independently. If a cross-coupling exists between the various attitude commands, a combined command should be able to nullify this coupling, else undesirable accelerations occur, which will likely destabilise the FWMAV.

5. **Fast actuation**. The lag time of the control mechanism should be low (i.e. the time between a command and the moment production). Compliance to this requirement is desirable for the

control of the DelFly, but necessary for tail-less stabilisation, in order to timely mitigate disturbances. An initial requirement for the lag time of moment generation when a full range (-100% to 100%) step command is given, is in the order of 0.15 s to 0.2 s for full actuation. This was set by studying reference data of the Nano Hummingbird, as is explained below.
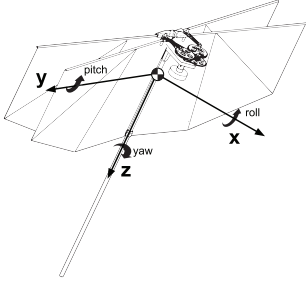
Figure 2. Body axis definitions and their rotations.

II.B.   Reference data to set the requirements

The quantitative requirements for the minimum control moments and actuation speed are set by studying reference vehicles. Keennon et al. [2012a] mention that for their prototype *"one of the more dramatic flight demonstrations was an autonomous 360° flip in the roll axis"*, and that the servos were fully deflected during this manoeuvre. This manoeuvre is shown in Figure 3.

(a) Roll angle

(b) Roll rate

(c) Roll acceleration

(d) Required roll moment
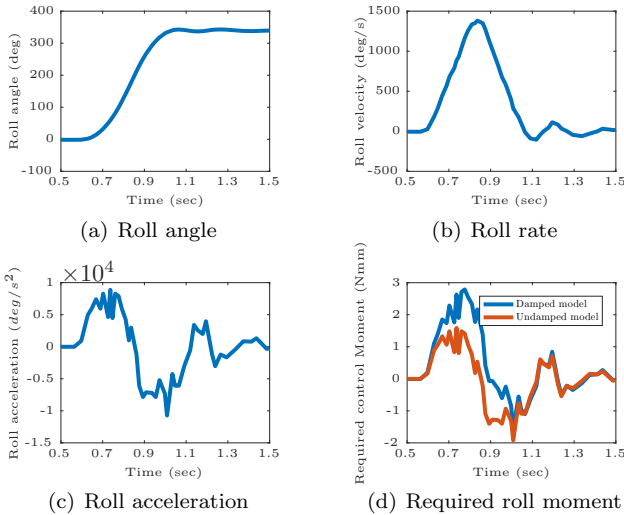
Figure 3. 360°lateral flip by the Nano Hummingbird. Data for angular velocity from Keennon et al. [2012a]

Keennon et al. [2012a] showed the roll rate for this manoeuvre in their research paper. The data was digitised and the roll angle and acceleration were

estimated by integration and derivation respectively. Using Newton's second law for rotation, the external moment on the vehicle (simplified for one degree of freedom) can be calculated from the roll acceleration and the moment of inertia around the roll axis:

$$M_{x_{\text{ext}}} = I_{xx}\ddot{\phi} \qquad (1)$$

where $M_{x_{\text{ext}}}$ is the external roll moment, I_{xx} is the moment of inertia around the roll axis and ϕ is the roll angle.

However, for this roll moment, effects acting in the opposite direction are not taken into account, such as skin friction and flapping counter-torque [Cheng and Deng, 2011].

When capturing these effects in a roll damping term, L_p, we can extend equation 1 to:

$$\ddot{\phi} = \frac{L_p}{I_{xx}}\dot{\phi} + \frac{1}{I_{xx}}M_{x_{\text{contr}}} \qquad (2)$$

where $M_{x_{\text{contr}}}$ is the roll control moment.

Cheng and Deng [2011] provide semi-analytical equations to calculate the roll damping term. However, this requires details about the flapping kinematics and performance of the Nano Hummingbird which are not available. Therefore, the non-dimensional value for the Hawkmoth (*Manduca sexta*) is taken, $L_p^+ = -0.81$ [Cheng and Deng, 2011], which is the closest insect described in the paper compared to the Nano Hummingbird in size.

This value for L_p^+ is non-dimensionalised by [Cheng and Deng, 2011]:

$$L_p = \rho U^2 R \bar{c}^2 L_p^+ / n \qquad (3)$$

where $U = 2\Phi n R \hat{r}_2$.

In these formulas, $\rho = 1.225\,kg/m^3$ is the air density, $R = 7.4 \times 10^{-2}\,m$ the wing length, $\bar{c} = 2.5 \times 10^{-2}\,m$ the mean chord length, $n = 30\,Hz$ the flapping frequency, $\Phi = 170\,^o$ the flapping amplitude and $\hat{r}_2 = 0.505$ is the non-dimensional second moment of wing area. The moment of Inertia of the Nano Hummingbird was estimated as $I_{xx} = 1.026 \times 10^{-5}\,kg \cdot m^2$, with the simplification that all the components are considered as point masses. These values have been obtained for the Nano Hummingbird either from Keennon et al. [2012a] or by estimation based on photos and available materials. $\hat{r}_2$ was taken from Cheng and Deng [2011] for the Hawkmoth.

This results in a damping coefficient of $L_p = -6.77 \cdot 10^{-5}\,Nms/rad$.

With these parameters, an estimate can be made for the required roll control moment to perform this manoeuvre with the Nano Hummingbird. The result of the undamped ($M_{x_{\text{ext}}}$) and damped ($M_{x_{\text{contr}}}$) one degree of freedom model is shown in Figure 3-(d), indicating a maximum $M_{x_{\text{contr}}}$ of 2.8 Nmm.

With this value for $M_{x_{\mathrm{contr}}}$, it is possible to make a fast 360°lateral flip with the Nano Hummingbird. Clearly, the lateral flip described above is an extreme manoeuvre and an estimation of the moment required to achieve this does not result in the magnitude of moments that are required for regular manoeuvres and stabilisation. Additionally the dimensions, number of wings (two instead of four), flapping frequency and moment of inertia for the Hummingbird are different from our prototype and we made assumptions for damping coefficient L_p, while this L_p has a substantial influence on the result. However, it does provide a benchmark to which we can later compare the generated moments for the prototype described in this paper. For now, we can estimate that the moments necessary to stabilise and control a tail-less FWMAV, comparable to the Nano Hummingbird, are in the order of 1-3 Nmm.

In order to control the DelFly with the proposed mechanism, it would also be desirable to reduce the lag time between a command and when the commanded moment is generated. A low lag time is even required in order to stabilise the DelFly to timely mitigate destabilising external forces and moments. For this requirement, the lateral flip of the Nano Hummingbird [Keennon et al., 2012a] is again used as a reference. In Figure 4 the time histories of the roll servo position command and servo feedback during the 360°lateral flip are plotted. It takes 0.09 s between the step command and when the command is actually reached, which gives an indication of the time needed to switch from extreme servo positions. We also see that the roll moment generated due to this servo positions takes approximately 0.15 to 0.20 s to settle when a step is given. Again, it is stressed that the result from these calculations should only be used as an indication for the servo speed that we need to fly tailless.

Concluding, for the DelFly, the required actuation speed is expected to be in the order of 0.1 s, which resulted for the Nano Hummingbird in a lag time between the command and the moment generation of 0.15 to 0.20 s.

III.   Prototype design

The prototype as is described in this paper, is a modified version of the DelFly II presented by de Croon et al. [2012]. The basic principles of the flapping mechanism and wing layout are the same and are explained in section III.A. The wings themselves are adapted for the use with the proposed control mechanism —wing tension modulation—and the principles of this mechanism are explained in section III.B. The wing tension control rods are actuated by a lightweight
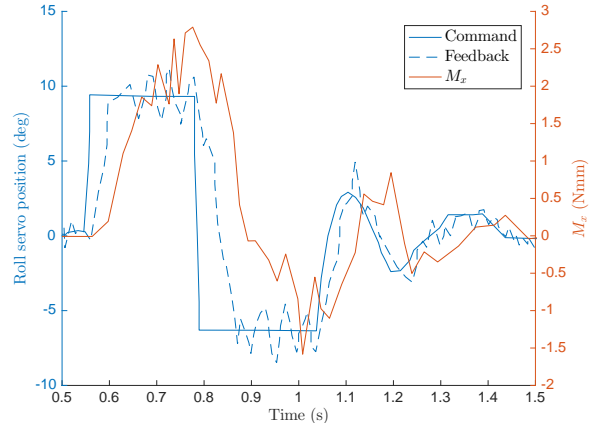
Figure 4. Roll servo position command and feedback for the 360°lateral flip of the Nano Hummingbird. Also the result of the damped model for $M_{x_{\mathrm{contr}}}$ is plotted for comparison. Data retrieved from Keennon et al. [2012a].

rope based actuation system, elaborated in section III.C. A picture of the final prototype compared to its ancestor, the DelFly II, is shown in Figure 1.

III.A.   Flapping mechanism and wings

The flapping mechanism consists of a brushless DC motor driving a crankshaft mechanism with a symmetric wing hinge, as opposed to regular DelFlies carrying a tail, which have a nonzero dihedral angle. This new hinge facilitates a four-fold symmetrical flapping motion, resulting in even performance for each wing. Additionally, no net moment is generated about any point of the flapping axis. Two cranks drive the hinge, coupling the motion of the left top wing to the right bottom wing and the right top wing to the left bottom wing. The wing design is based on a geometry optimisation from Groen et al. [2010], and the wings measure 140 mm in length from root to tip and have a mean chord length of 80 mm. They are made from 10-micron polyester membrane. The wings are hand built by using a template and a vacuum table, such that a high accuracy and repeatability is achieved. They are stiffened by carbon rods. In Figure 5 this flapping mechanism and wing layout are depicted schematically.

III.B.   Wing tension modulation

To generate control moments with the wings, the slackness of each wing is individually controlled. Keennon et al. [2012b] concluded that for the Nano Hummingbird the thrust force of a wing decreases when the slackness of a wing is increased. They exploit this phenomenon by moving the roots of the two wings to

(a) Flapping mechanism　　　　(b) Wing geometry
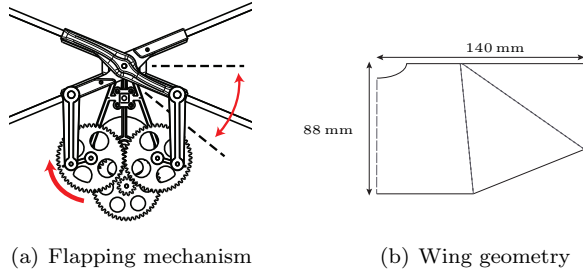
Figure 5. The symmetric flapping mechanism and wing layout

various directions. In this way, the wing foil slackness can be influenced in various phases of the flapping cycle: By moving the roots laterally and outbound, the slackness of the foil can be increased during the mid-stroke. By moving the roots in the ventral and dorsal directions, mainly the extremal flapping angles are affected. This can be used to control the roll and pitch angles, respectively.

Force balance measurements on the DelFly also indicated that the slackness of the wings affects the thrust force that is generated. For the DelFly, theoretically the roll and pitch moments can be controlled by being able to vary the slackness, and thus the thrust, for each wing individually, see Figure 6.

(a) Pitch control　　　　　　(b) Roll control
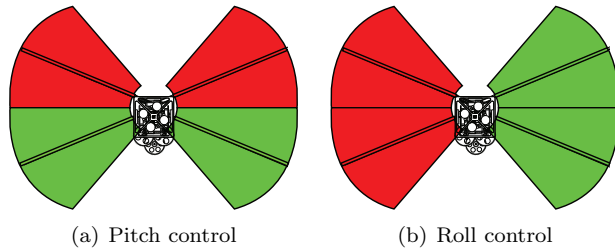
Figure 6. Top view of pitch and roll control by wing tension modulation. The wings in red are slack and therefore have a decrease in thrust compared to neutral, the wings in green are in tension and generate more thrust. This mechanism is hypothesised to generate the control moments.

To modulate this slackness, two concepts were explored, these are shown in Figure 7. For concept A the most inward wing stiffeners of the wing layout are pulled towards the fuselage with a rope in order to attempt to deform and tension the wing. However, it turned out that this method did not result in the desired effect. Instead of the slackening of the wing, the leading edge was bent and the foil between the stiffener and the root was deformed. This did not result in a modulation of the thrust; it did modulate the drag of the wing throughout a flapping cycle. This extra drag was higher during the inbound than during the outbound stroke, resulting in a net yaw moment

when one wing or a diagonal pair of wings are tensioned. We were however not able to produce pitch and roll moments.

For concept B, the usual DelFly concept with two wing pairs is abandoned; the pairs are cut in the middle. A carbon rod is glued at the root of each of the now four wings. This rod is moved towards the fuselage by pulling with a rope to stiffen the wings, and outbound by releasing the tension in the rope. The carbon control rods are clamped near the wing hinge and with respect to the fuselage point slightly outwards (see section IV.A.2 for the direction), such that when the rope is released by the actuation mechanism, the carbon rods spring outwards and the wings are made slack. A back view of a DelFly prototype with wing tension modulation according to concept B, with one of the ropes highlighted, is shown in Figure 8. This proved to be an effective method to produce pitch and roll moments and was therefore chosen for further development and testing.

(a) Concept A　　　　　(b) Concept A - back view

(c) Concept B　　　　　(d) Concept B - back view
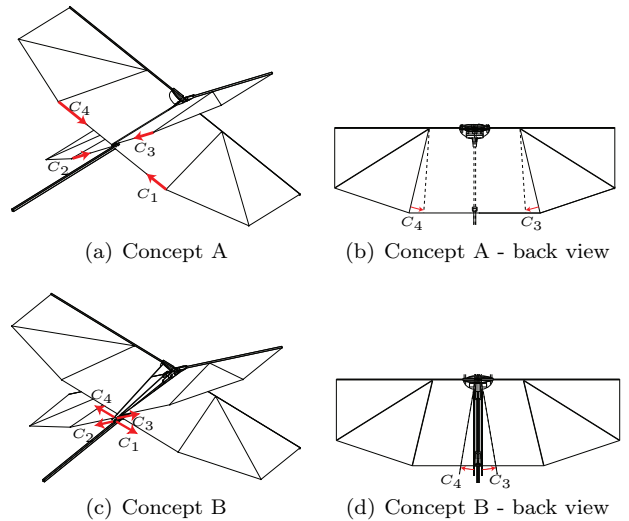
Figure 7. Concepts A and B for wing tension modulation. C_1-C_4 are the various degrees of freedom for control. The results for prototype B are presented in this paper.

III.C.　Actuation mechanism

As was already mentioned in the previous section, for both concepts A and B a lightweight rope based actuation system is proposed. A similar system was also used by Tokutake et al. [2009], who demonstrated a system with ropes connected to the wing foil to change the camber of the wing. They used one servo, and in this way they were able to generate a pitching moment. Keennon et al. [2010] patented a system that uses ropes to move a wing rod in the ventral-dorsal directions. However, their mechanism is fundamentally different from our system, since they have

two ropes per wing, one for the ventral and one for the dorsal direction, instead of our system that uses only one rope.

We use a rope-based mechanism to control the tension of the individual wings, and use a linear actuation system to vary the length of the ropes, and thus constrain the roots of the wings in their desired positions.
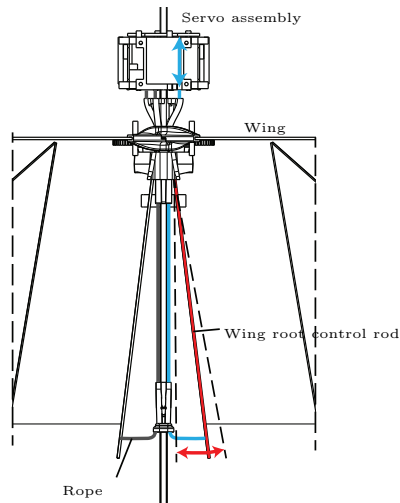
Figure 8. Back view of the prototype, with one of the four ropes highlighted in cyan. In red is the resulting motion of the control rods for concept B.

Two linear actuation concepts were designed. In the first concept, it was attempted to actuate all of the four wings, with as few servos as possible, with the goal to save weight. With the system in Figure 9-(a)-(b), the system can be controlled for pitch and roll with only two servos. Also combinations of pitch and roll can be commanded. In this system, each wing is connected with a rope to a slide on a linear slide guide rail. Moving this slide will either pull the control rods on the wings inbound, or release the rods outbound. Each slide is connected by a rope and pulley system to both the pitch and roll servo. When rotating the pitch servo clockwise, the slides on the top of the figure move outbound, tensioning these wings. At the same time, the slides of the bottom wings (not connected here for clarity) move inbound, slackening the wings. The slides are connected to the roll servo such that a rotation clockwise will tension the right pair of wings and slacken the left pair of wings, and vice versa. Also combinations of roll and pitch can be commanded in this way. A disadvantage of this system is that the effective stroke of the rope to the wings is only half the stroke of the servo, due to the moving pulley connected to the sled.

For the second concept, four readily available linear servos are used: the SuperMicro Systems Single

(a) Two-servo concept actuators

(b) Two-servo concept rope to wing

(c) Four-servo concept actuators (two servos removed)

(d) Four-servo concept rope to wing

(e) Top view four-servo concept
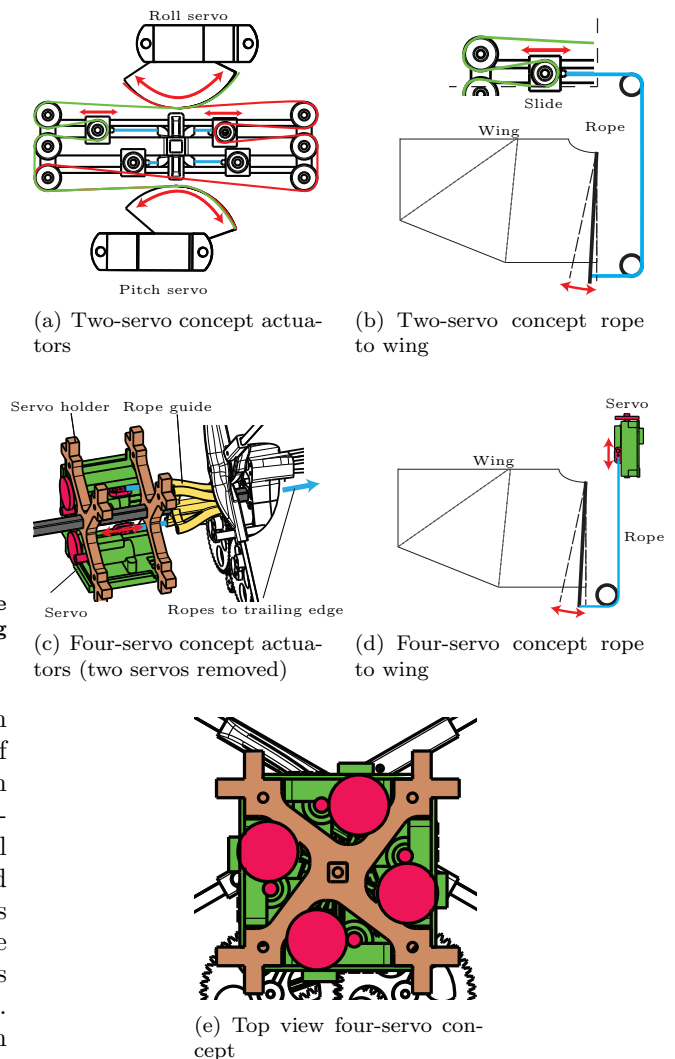
Figure 9. Actuation mechanism concepts. (a)-(b) is a concept with as few servos as possible. In this figure, two of the ropes have been omitted for clarity. In (c), the four-servo concept, two of the servos are left out in this figure for clarity. In (e) the four-servo concept is depicted with all servos visible. This four-servo concept is chosen for the flight tests in this paper.

Linear Servo. An isometric view of this system is shown in Figure 9-(c), with two servos removed for clarity. Figure 9-(d) shows how the rope is attached to the wing control rod. In (e) a top view of the system is shown with all four servos. These servos weigh 1.2 g, and can reach their full stroke of 8 mm in 0.12 s. However, during flight testing, it appeared that the motor of the servos overheated, therefore, these motors were replaced for a more powerful version, adding 0.15 g per servo.

Comparing the two concepts, it turned out that the estimate of the weight of the four-servo concept was approximately 1.5 g lighter than two-servo pulley concept, due to the extra weight of all the necessary components for the pulley system, and the large servo attachments needed in order to have enough stroke. Also, the development time is lower for the four-servo system, since it is already an off-the-shelf product. An additional advantage of the four-servo system is that each wing can be controlled individually. Therefore, the four-servo system was chosen as the actuation system for wing tension modulation. This resulted in the total system weighing 21.5 grams, including battery, in compliance with the weight requirement.

IV. Experiments

The experiments presented here include force and moment measurements on a force balance, high speed camera measurements and flight tests. In the subsequent paragraphs the experimental methods and results of these experiments will be presented. The experiments presented in this section are all performed on wing tension modulation concept B, the concept with control rods at the root of the wing.

IV.A. Static force/torque balance experiments

In the first experiments, a force/ torque balance was used to measure the forces and moments resulting from the wing tension modulation. First, the methodology of the experiment will be explained. In section IV.A.2 an experiment is conducted in order to find the optimal root displacement direction. This direction is then used for the actuated prototype, and the results of the force balance experiment for this prototype are presented in section IV.A.3.

IV.A.1. Force/torque balance set-up

In order to assess the performance of the prototypes and improve the magnitude of the moments, the prototypes were tested on a Nano17 Titanium force/ torque sensor. A Hall effect sensor in conjunction with a magnet on the main gear was used to measure

the flapping frequency during testing. A power supply with remote voltage sensing was used to keep the voltage constant at 4.0 V. The force balance set-up is shown in Figure 10.
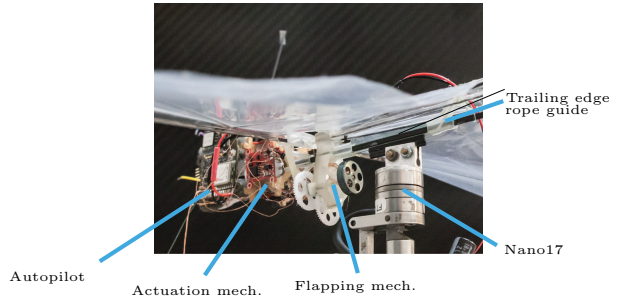
Figure 10. Force balance with actuated prototype

IV.A.2. Results for various displacement directions

To keep the number of servos required and the complexity of the prototype to a minimum, for the final prototype the control rods at the root of the wings are displaced with only one degree of freedom. The direction of the displacement of each wing is chosen by studying the effect on the attitude moments by displacing one of the control rods in various directions over a rectangular grid. For this experiment, the position of the wing root rods was varied by manually fixing them at different positions in a CNC-milled wooden plate. The other side of the rod near the flapping mechanism was mounted flexibly on the rotating wing hinge. The resulting moments and forces for various positions of the back left wing root are measured and the results are presented in Figure 11.

Figure 11 shows that the roll moment generation is affected the most by displacing the bars laterally, the pitch by displacing the bars diagonally, and, less conclusive, an effect in yaw is visible when displacing the bars longitudinally. When displacing the wing root laterally or diagonally, the resulting roll moment is negative and the pitch moment positive, respectively. This suggests that, compared to the other wings, this wing generates less thrust, since the moments would make the DelFly turn towards the slack wing. However, as Figure 11-(e) shows, the frequency of the DelFly is increasing if the wing root is moved laterally. Because of this, the thrust of the flapper as a whole actually increases when a wing is made slack.

In order to have both favourable roll and pitch moment generation characteristics, and in an attempt to still be able to generate a yaw moment, we fixed the movement direction of the control rods to half the flapping angle for next models, 22.5°. Moving the rods in this direction affects the slackness of the wing primarily in the mid-stroke. During force bal-

(a) M_x (roll)

(b) M_z (yaw)

(c) M_y (pitch)

(d) F_z (-thrust)

(e) Frequency

(f) Axis definition and measurement origin.

(g) Bottom view of DelFly, indicating the root that is displaced and its directions. The other roots are left in their original tensioned position.
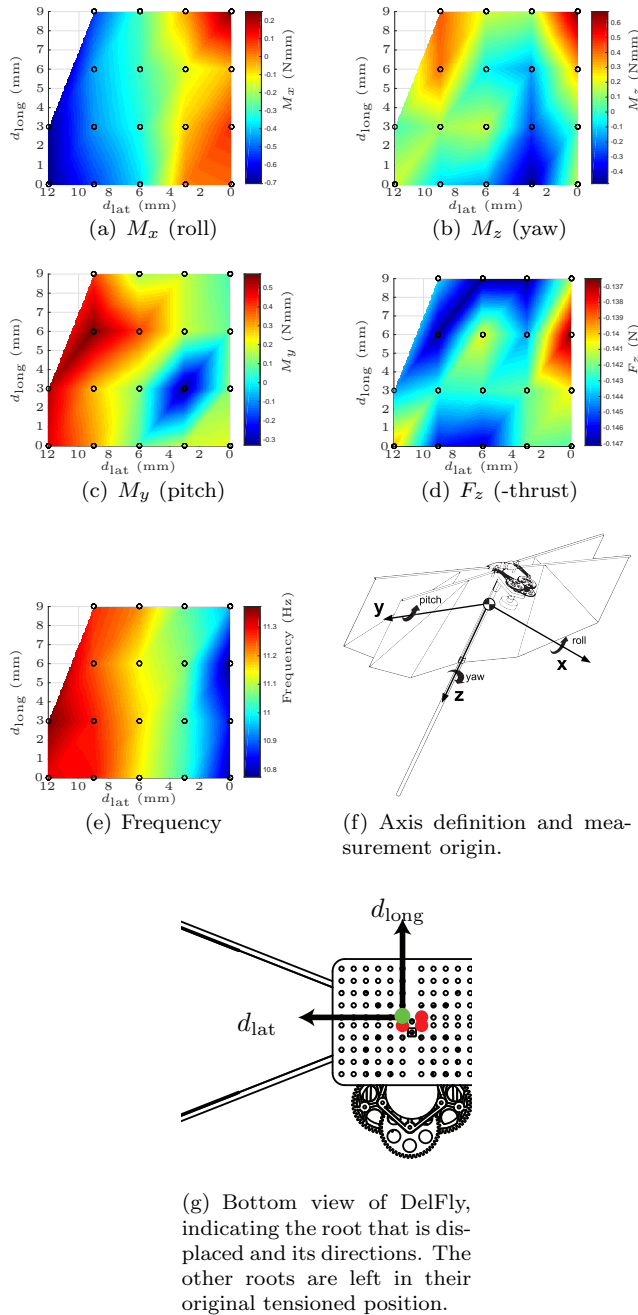
Figure 11. Forces and moments resulting from a displacement of the back left wing root (shown in (g)) in various directions. The black markers in the force and moment plots indicate the positions at which measurements were taken.

ance tests it appeared that during this mid-stroke also the maximum wing thrust is generated. This suggests that in this direction, the modulation of the magnitude of thrust will be most effective.

IV.A.3. Results for actuated prototype

In contrast to the previous experiment, in which the wing roots were manually positioned, for this experiment we used four servos with four ropes leading to the control rods. These control rods, instead of being flexibly mounted to the wing hinge as was the case in the last experiment, were firmly attached to the housing of the gear train. This was done to enable the control rods to slacken the wing due to the stiffness of the material, when the tension in the rope is released (see Section III). The control rods were mounted as close as possible to the flapping axis, such that the rods were not moving too much along with the flapping motion. The autopilot computed the servo output for each of the four wings as a linear combination of pitch and roll. Depending on the position of the servo the percentage of servo deflection is either an addition or subtraction of the pitch and roll commands. The desired servo deflections were encoded in a PWM signal to the servos.

The measurements were taken at -50, -25, 0, 25 and 50 % of the range for both pitch and roll commands, since otherwise one of the servo outputs saturates, due to the addition of pitch and roll exceeding 100% deflection. Also the extremes in both pitch and roll individually were measured. Thus, 29 measurements were taken in total. The measurements were done at a flapping frequency of around 12 Hz, in order to not degrade the wings and flapping mechanism too much. The forces and moments were measured for two seconds and averaged over a whole number of flapping cycles.

Figure 12 shows the roll and pitch moments, thrust and flapping frequency for the entire span of unsaturated pitch and roll combinations. Constant pitch and roll lines are depicted in Figure 13, which are 2D sections from the 3D surface plot.

We can see that although some cross-coupling and imperfections exist, the commands have a dominant effect on the control moment generation. We are able to generate -0.95 to 1.17 Nmm around the roll and -0.39 to 0.57 Nmm around the pitch axis. Additionally, except for the 100 % roll command, we see from Figure 13 that the relation between command and respective measured moment is monotonic and quite linear. We also observe from this figure that only minor changes occur to the slope of the roll moment when next to a roll command also a pitch command is introduced. These observations are similar for the pitch case and they indicate that the two moments

can be generated independently.

In contrast to the previous experiment —which used the milled grid to hold the wing roots in place—for this experiment the maximum thrust occurs when all wings are tensioned, and decreases as the wings are slacker. We found that for this experiment the range in measured frequencies is smaller: between 11.95 and 12.2 Hz. Additionally, the measured frequency did not seem to have any correlation to the control inputs. In contrast, with the previous various displacement experiment we found a clear correlation between the control input and the measured frequency, the latter increasing as the wing became slacker. At the same time, we saw the thrust increasing for slacker wings, thrust being a function of frequency. For the present experiment we did not measure an increase in frequency when the slackness increased; and since we do not have this variation in frequency, this also has no effect on thrust. Instead we measure what we expected: a decrease in thrust when at least one wing is slack. Additionally, since we are also now controlling a multiple of wings, this effect is enhanced.

A hypothesis for the low sensitivity of the frequency to the control input in the present experiment is that we changed the method of attachment of the control rods, and we hypothesise that this resulted in a lower hinge friction. In the experiment of section IV.A.2, when we tensioned the wing, this also introduced a force on the hinge, since the rods were directly attached to hinge. When one of the wings is slackened, this hinge friction decreases and the flapping frequency therefore increases. In the present experiment, the control rods were instead clamped by the gear train housing.

When comparing the observations above to the requirements of section II, we have to conclude that we do not meet the requirement set for the magnitude of generated pitch moment. However, we are able to generate the moments with a linear relationship to the respective commands with low cross-coupling and we can generate moments throughout the whole spectrum. The moment generation can still be increased by flapping at a higher frequency; during the flight experiment we will increase the frequency to be able to generate enough thrust. Additionally, the moments can be increased by making adjustments to the maximum tension of the wings and by increasing the stroke of the control rods by attaching the ropes to a higher point on the control rods. However, when attaching the ropes to a higher point on the control rods, also the required torque from the servos is increased, resulting into increased response times.

(a) M_x (roll)

(b) M_y (pitch)

(c) F_z (-thrust)
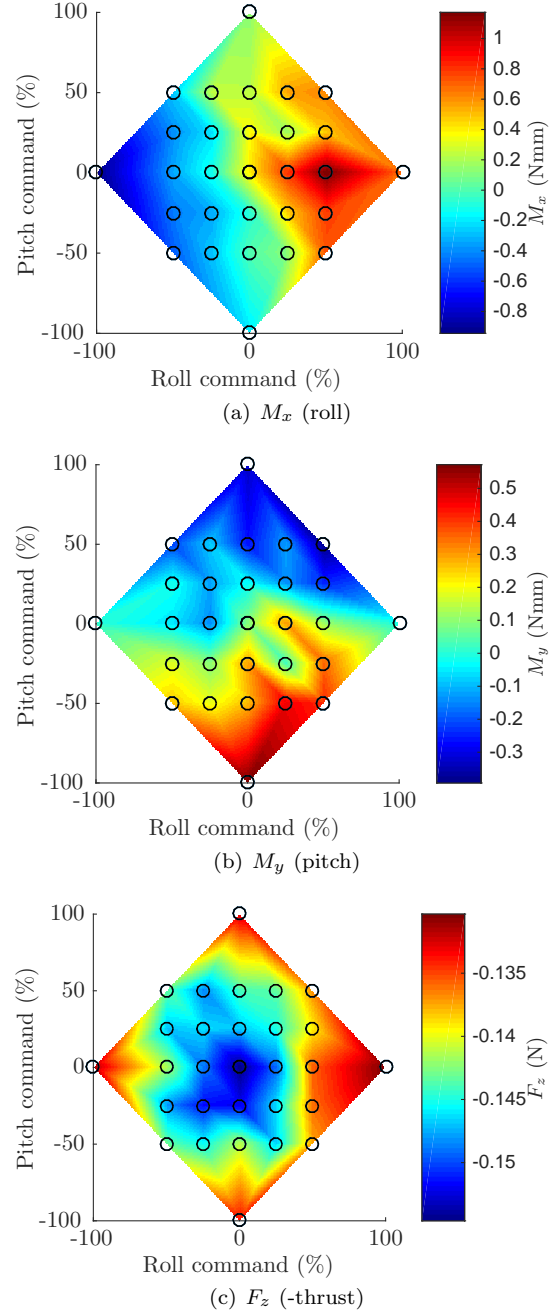
Figure 12. Forces and moments resulting from a displacement of the wing roots by the actuation system, flapping at 12 Hz. A positive roll command is defined as slackening the right pair of wings, a positive pitch command as the ventral (forward) wings slack. Black markers indicate the positions at which measurements were taken.

IV.B. Dynamic force/torque balance experiment

Figure 14 shows full range (-100% to 100%) step commands for both the roll and pitch commands. Minor adjustments have been made on the actuation system and wings, explaining the higher moment generation. Figure 14 shows that the time to control the roll moment from the full negative to the full positive reachable magnitude is 0.18 s. For the pitch moment, this lag time is slightly longer, 0.22 s. These values are close to what was found by studying the 360° lateral flip of the Nano Hummingbird, and thus comply to the moment lag requirement. For the tail-less DelFly this servo position lag is estimated using high speed camera recordings, explained in the next section.

(a) Roll moment for constant roll command

(b) Roll moment for constant pitch command

(c) Pitch moment for constant roll command

(d) Pitch moment for constant pitch command

(e) Legend for constant roll

(f) Legend for constant pitch

Figure 13. 2D sections of the 3D plot of Figure 12. The cut-outs are done at constant roll command (left), and constant pitch command (right).

(a) Roll step

(b) Pitch step

(c) Legend

Figure 14. Force balance measurements for a -100% to 100% step command in roll and pitch, respectively. The cut-off frequency of the Butterworth filter for the filtered moments is 4Hz.

IV.C. High speed camera measurements

To study the morphology of the flapping wings while varying the control input, a Photron FASTCAM SA1.1 high speed digital camera was used. A full range step command to the servos was given in roll, and the camera recorded the motion at 2000 frames per second. Figure 15 shows stills in four distinctive phases during one flapping cycle for both extremes of the roll command spectrum. It appears that the angle of the wing foil is lagging behind the leading edge more when the wing is slack than in the tension case. The angles of the leading edge and the first stiffener, as defined in Figure 17, are plotted in Figure 16. In Figure 18-(a) and (b), two excerpts of this data are shown, the first depicting a tensioned and the latter showing a slack wing. By taking the cross-correlation between the flapping angle and stiffener angle signals, Figure 18-(c) and (d), we can calculate the time delay of the stiffener angle signal with respect to the flap-

ping angle signal, which occurs when the correlation is maximal. Similarly, we can find the period of the flapping motion by taking the auto-correlation of the flapping angle signal (Figure 18-(e) and (f)). Indeed, if we calculate the lag time as a percentage of the period, we notice that the lag for the tension case is 22.97%, and for the slack case 28.39% of the period.

This extra phase lag in the slack case means that during the entire flapping cycle the angle of attack is decreased, resulting in less thrust. This (geometric) angle of attack α is the angle between the velocity vector of the leading edge (on the stroke plane) and the chord of the wing, see Figure 19. It appears that the tensioning and slackening of the wings by the control rods at the root of the wings has an effect on the passive rotational mechanism. The wings of the DelFly rotate freely around the leading edge spar, and this rotation is altered by the control input.

We have two hypotheses for this decrease in angle of attack in slack mode. The first one is that we notice in the high-speed footage that the foil itself is slack, altering the morphology of the foil during flapping, including the angle of attack. The second one is that when the tension of the wing roots is released, the roots are allowed to move more freely, also effecting the morphology of the rest of the wing, including its angle of attack.

Additionally, from the video recordings it is estimated that the time it takes the servo to switch extremal positions is 0.14 s. This value is higher than the value found in the requirements section from the analysis of the Nano Hummingbird. However, when including the results of the dynamic force/ torque measurements, and comparing this to the Nano Hummingbird, it seems that for our prototype the time between the moment in time when the servo position is reached, and the moment in time when the generated moments settle, is shorter. The explanation for this is thought to be a combination of a number of aspects: the DelFly has four wings instead of two, flaps at a lower frequency than the Nano Hummingbird, and although the fundamentals of the control methods are the same, they use a different mechanism.

IV.D. In-flight experiment

Lastly, we conducted flight experiments, to evaluate the performance of the prototype in hovering flight. To achieve stabilised flight, the center of gravity location is an important parameter and can be influenced by changing the position of the components of the prototype. An analysis for the desired center of gravity location will be given in section IV.D.1. Next, the methodology of the experiment is presented, section IV.D.2. The results of the flight test will be presented in section IV.D.3.

(a) Tensioned at min flapping angle

(b) Slack at min flapping angle

(c) Tensioned at mid rotation outbound

(d) Slack at mid rotation outbound

(e) Tensioned at max flapping angle

(f) Slack at max flapping angle

(g) Tensioned at mid rotation inbound

(h) Slack at mid rotation inbound
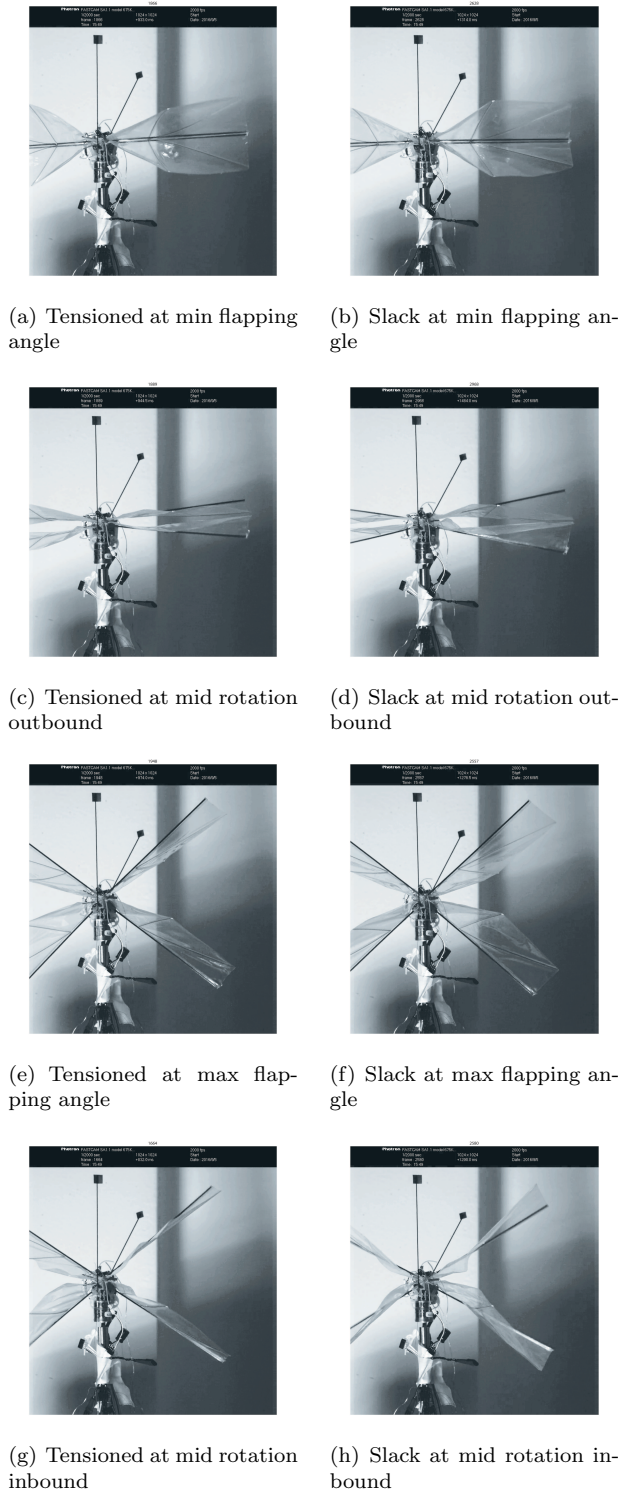
Figure 15. Stills of high-speed camera footage at various wing positions. Left the wings are tensioned by the servos, right they are in their slack position. (a)-(b) are taken at the minimum flapping angle, (c)-(d) are taken when the stiffener and the leading edge have the same angle, during outbound movement of the leading edge, (e)-(f) are at the maximum flapping angle, and (g)-(h) are when the stiffener and leading edge have the same angle, during inbound movement of the leading edge.
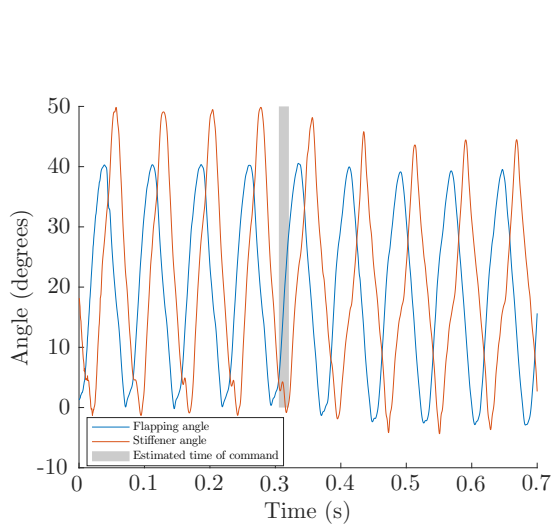
Figure 16. Angles of the leading edge (flapping angle) and stiffener, measured from the high-speed camera's footage. Shown in grey is the estimated time of a step command from a tensioned wing to a slack wing. Angle definitions are depicted in Figure 17

(a) Tension

(b) Slack

Lagtime = 0.0170 s

Lagtime = 0.0220 s

(c) Cross-correlation tension

(d) Cross-correlation slack

Period = 0.0740 s

Period = 0.0775 s

(e) Auto-correlation of ϕ tension

(f) Auto-correlation of ϕ slack
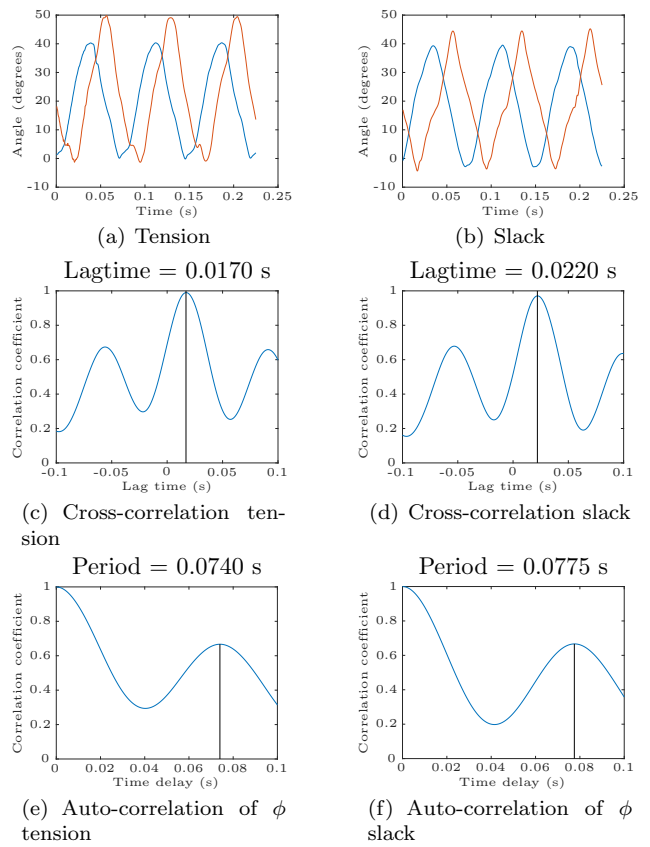
Figure 18. (a)-(b) are excerpts of Figure 16, when the wing is tensioned and slack, respectively. (c)-(d) show the cross-correlation between the flapping and stiffener angles, resulting in the lag time. (e)-(f) depict the auto-correlation of the flapping angle (ϕ), resulting in the period of the flapping motion. For angle definition, see Figure 17

(a)

Flapping angle ϕ

Stiffener angle

(b)
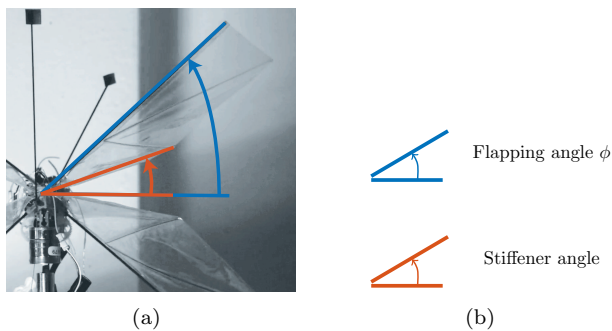
Figure 17. Definition of angles in Figures 16 and 18
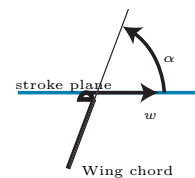
Figure 19. Geometric angle of attack α of a DelFly wing. w is the wing velocity due to the flapping motion.
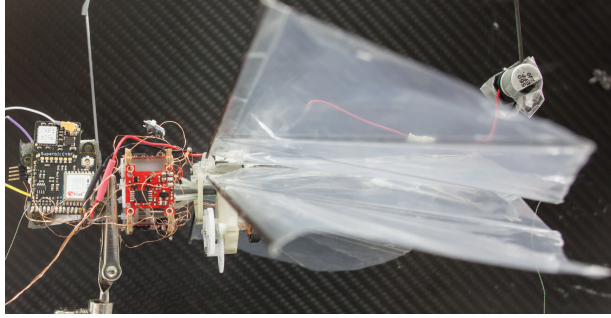
Figure 20. Side view of prototype for free flight, showing the Lisa/S, servo assembly, flapping mechanism and wings.

IV.D.1. Center of gravity location

In the introduction we mentioned that flapping flight is inherently unstable. An important parameter that has influence on the extent of this instability is the position of the center of gravity.

The first requirement to the position of the center of gravity for the tail-less DelFly is that it should coincide with the flapping axis, such that for a neutral command the weight is in line with the thrust vector. When the center of gravity does not coincide with the flapping axis, a moment is generated due to the offset of the thrust vector and the weight vector in the center of gravity, and we would then have to counteract this with a control input, which is undesirable. This sets a requirement on the x- and y-coordinate of the center of gravity.

Additionally, both the derivative of the generated moment with respect to the control input and the static pitch stability are dependent on the z-coordinate, i.e. the height of the center of gravity. When numerically shifting the measurement location of the force balance test using $\vec{M_{shift}} = \vec{M} - \vec{r} \times \vec{F}$ (which is possible since we measure all six force and moment components), we observed that the derivative of the generated moments due to the control inputs increased and became more linear when the location was more towards the top of the vehicle. Therefore, from this perspective, we want to choose a location for the center of gravity that is as high as possible.

We also argue that the z-location of the center of gravity has influence on the response of the pitch movement to a forward velocity. In Figure 21, the situation is drawn for both a high location of the center of gravity (a) and a low one (b). When pitching forward with the prototype, the control mechanism will slacken the forward wings and tension the aft wings. This extra thrust generated by the aft wings, δ_T, will generate a pitch moment M_T. However, as the body pitches forward, the thrust vector will have a nonzero forward component that will make the prototype fly

forward. A drag force F_D will be generated due to the free-stream velocity V_∞ which is now nonzero. This drag force generates either an extra contribution to the pitching moment, or generates a counteracting moment, depending on the center of gravity location. This moment is shown for both cases in Figure 21 as M_D. When an extra contribution to the pitching moment is generated as is the case for a high center of gravity location, the DelFly will pitch forward even faster; this situation is statically unstable. When the center of gravity location is in the aerodynamic center (assumed at the quarter-chord point), the situation is statically, marginally stable, and when the center of gravity is lower than the aerodynamic center this pitching motion due to forward velocity is statically stable. Naturally, when the location of the center of gravity is too low, the vehicle loses its forward flying capabilities.

(a) COG above leading edge (b) COG at trailing edge
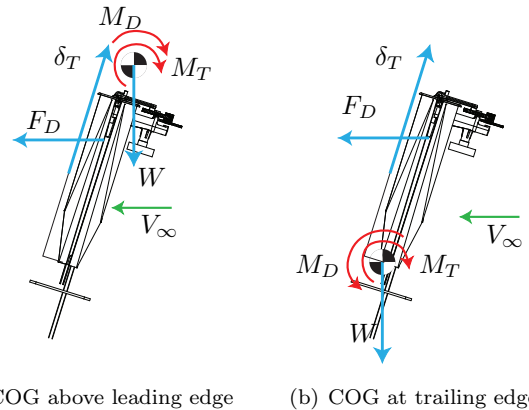
Figure 21. Pitch moments in forward flight for various center of gravity (COG) locations

We have to stress that, even while we may achieve longitudinal static stability by choosing a low center of gravity, this does not mean that the DelFly is also dynamically stable. We will illustrate this by deriving a model, based on the model by Teoh et al. [2012] and perform eigenvalue analysis to see the effect of changing the position of the center of gravity on the system's poles. The model is based on two-winged flapping flight, clearly for a flapping robot with four wings the dynamics are more complex. However, we expect the main findings to be similar.

In steady flow, the aerodynamic drag of a fixed wing due to inertial forces varies quadratically with the airspeed V, as:

$$F_D = \frac{1}{2}\rho V^2 S C_D = \beta V^2 \qquad (4)$$

where ρ is the air density, S the surface area of the wing, and C_D the drag coefficient that varies with the angle of attack. However, the drag on the wings

of two-winged insect flight varies approximately proportional to the air speed [Teoh et al., 2012]. Figure 22 shows that, in forward flight, the apparent velocity of a wing decreases for the upstroke, and increases for the downstroke. Therefore, when approximating the wing trajectory as an upward-downward sawtooth function [Teoh et al., 2012], the drag during the upstroke is $F_{D,\text{up}} = \beta(w - V)^2$ and during the downstroke the drag is $F_{D,\text{down}} = -\beta(w + V)^2$. The stroke-averaged drag force is then:

$$
\begin{aligned}
\bar{F_D} &= \frac{1}{2}\left(F_{D,\text{up}} + F_{D,\text{down}}\right) \\
&= \frac{1}{2}\beta\left(w^2 - 2wV + V^2 - \left(w^2 + 2wV + V^2\right)\right) \\
&= -2\beta wV
\end{aligned}
\tag{5}
$$
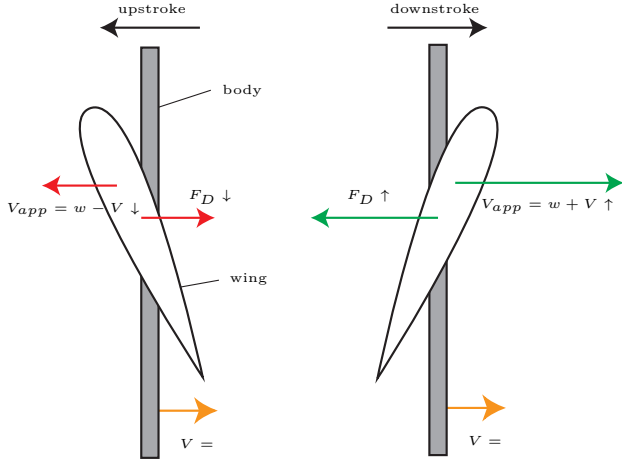
Figure 22. **Difference in wing drag in forward flight when in upstroke versus downstroke, for a two-winged flapping robot.** w **is the wing speed due to flapping, relative to the body;** V **is the velocity of the body;** F_D **is the drag of the wing and** V_{app} **is the apparent wing speed.**

This shows that for two-wing flapping robots, the drag force is proportional to V, when the flapping frequency and thus the relative wing speed due to flapping is constant. We therefore use $\bar{F_D} = -bv$, where b is an aerodynamic coefficient that depends on the wing morphology. b can be obtained by wind tunnel tests.

We then draw the forces of the two-winged robot during hover, assuming small pitch angle θ, and with an offset of the center of gravity to the aerodynamic center of d, see Figure 23. Using Newton's second law, equating the sum of the forces in x-direction to the acceleration in x-direction:

$$
\begin{aligned}
m\dot{v}_x &= \bar{F_D} + F_{T,x} \\
&= -b\left(v_x - d\omega\cos\theta\right) - F_T\sin\theta
\end{aligned}
\tag{6}
$$
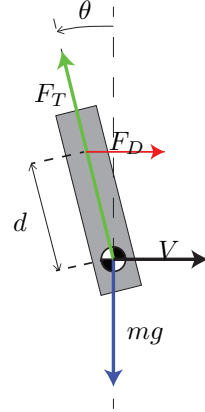
Figure 23. **Diagram for the force and torque model inspired by Teoh et al. [2012]. The parameters in the figure:** F_D **is the drag force;** θ **the pitch angle;** d **the distance between the application point of the drag force (also assumed to be the aerodynamic center, at quarter-chord) and the center of gravity, and** V **the velocity.**

where $F_{T,x}$ is the x-component of the thrust force.

Similarly, equating the torque to rotational acceleration:

$$
\begin{aligned}
J\dot{\omega} &= -d\bar{F_D}\cos\theta \\
&= db\cos\theta\left(v_x - d\omega\cos\theta\right)
\end{aligned}
\tag{7}
$$

We simplify by linearising around $\theta = 0$:

$$
\begin{aligned}
\dot{v}_x &= \frac{1}{m}\left[-bv_x + bd\omega - F_T\theta\right] \\
\dot{\theta} &= \omega \\
\dot{\omega} &= \frac{1}{J}\left[dbv_x - d^2b\omega\right]
\end{aligned}
\tag{8}
$$

When defining the state vector as $\mathbf{x} = [v_x, \theta, \omega]$ and assuming that thrust balances weight ($F_T = mg$) the state-transition matrix A in $\dot{\mathbf{x}} = A\mathbf{x}$ is:

$$
A = \begin{pmatrix} -\frac{b}{m} & -g & \frac{1}{m}bd \\ 0 & 0 & 1 \\ \frac{1}{J}bd & 0 & \frac{1}{J}d^2b \end{pmatrix}
\tag{9}
$$

The system matrix A can also be written with stability derivatives $\hat{X}_u = -\frac{b}{m}$, $\hat{X}_q = \frac{1}{m}bd$, $\hat{M}_u = \frac{1}{J}bd$ and $\hat{M}_q = \frac{1}{J}d^2b$:

$$
A = \begin{pmatrix} \hat{X}_u & -g & \hat{X}_q \\ 0 & 0 & 1 \\ \hat{M}_u & 0 & \hat{M}_q \end{pmatrix}
\tag{10}
$$

The poles of A are defined as the roots of the characteristic equation $|\lambda I - A| = 0$. We therefore obtain the equation:

$$\lambda^3 - \left(\hat{X}_u + \hat{M}_q\right)\lambda^2 + \left(\hat{X}_u\hat{M}_q - \hat{M}_u\hat{X}_q\right)\lambda + \hat{M}_u g = 0 \tag{11}$$

According to Karásek [2014], the effect of $\hat{X}_q$ on the dynamics is small and by neglecting this derivative, equation 11 can be reduced to:

$$\lambda^3 - \left(\hat{X}_u + \hat{M}_q\right)\lambda^2 + \left(\hat{X}_u\hat{M}_q\right)\lambda + \hat{M}_u g = 0 \tag{12}$$

Similar to the analysis that was performed by Karásek [2014], this equation can be rewritten as:

$$\lambda\left(\lambda - \hat{X}_u\right)\left(\lambda - \hat{M}_q\right) + \hat{M}_u g = 0 \tag{13}$$

$$1 + \hat{M}_u \frac{g}{\lambda\left(\lambda - \hat{X}_u\right)\left(\lambda - \hat{M}_q\right)} = 0 \tag{14}$$

Equation 14 has the same form as the transfer function of the closed loop of system

$$H(s) = \frac{g}{\left(\lambda\left(\lambda - \hat{X}_u\right)\left(\lambda - \hat{M}_q\right)\right)} \tag{15}$$

with feedback gain $\hat{M}_u$ [Karásek, 2014]. By comparing equation 9 to equation 10, for $b > 0$, we find that the sign of $\hat{M}_u$ is equal to the sign of d. Additionally, $\hat{X}_u < 0$ for any d and $\hat{M}_q = 0$ for $d = 0$ and $\hat{M}_q > 0$ for $d \neq 0$. If we assume that d is small ($d \ll 1[m]$), the effect of d on $\hat{M}_q$ is relatively small and we can therefore perform the root locus method to study the effect of $\hat{M}_u$ —and therefore d —on the dynamics of A.

The system $H(s)$ of equation 15 has three poles, two at the origin (of which one corresponds to $\hat{M}_q = 0$), and one at $\hat{X}_u$. Since the open-loop transfer function does not have finite zeros, we have three zeros at infinity.

For $\hat{M}_u > 0$ (thus $d > 0$), the root locus will follow asymptotes $\pm 60°$ and $180°$. For negative $\hat{M}_u$ ($d < 0$) the asymptotes are ± 120 °and $0°$. The start point of the asymptotes is $\hat{X}_u/3$, however, since $\hat{M}_q \geq 0$ for any d, the roots can never all lie in the left-half plane and we will therefore never have both static and dynamic stability.

The root locus is shown in Figure 24. We see that for a high center of gravity ($d < 0$), we have an unstable divergence mode (real positive pole) and a stable oscillatory mode (complex pole pair with negative real part), while for low center of gravity ($d > 0$) we have a stable subsidence mode (real negative pole), but now have an unstable oscillatory mode instead (complex pole pair with positive real part). When d is set to zero, two of the eigenvalues are in the origin, resulting in marginal stability. Note that the above model was derived for two-winged flight. The DelFly
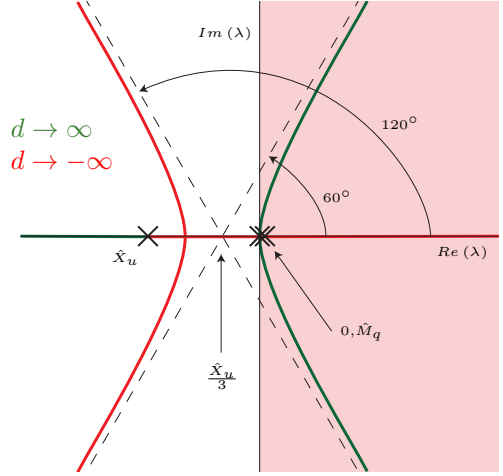
Figure 24. Root locus showing the effect of the center of gravity position with respect to the aerodyamic center. $d > 0$ **corresponds to a center of gravity position below than the aerodynamic center,** $d < 0$ **corresponds to a center of gravity position above the aerodynamic center (see Figure 23).**

dynamics are more complex, because of its four wings. We however expect the results to be similar: it is not possible to achieve both static and dynamic inherent stability. For a stable flight we need an active control system and we need to carefully choose the center of gravity.

We hypothesise that the best location for the center of gravity, for the current prototype, is at or near the aerodynamic center (at the quarter-chord point). This will give a high control authority, and we can expect a relatively low instability to marginal stability, resulting in a higher chance of successfully stabilising the DelFly. Therefore, in the design, the servo assembly and auto pilot were placed in the top of the vehicle, and by shifting the location of the battery the location of the center of gravity was tuned. The battery was ultimately placed at the bottom of the flapping robot to end up with a center of gravity near the quarter-chord point.

IV.D.2. Methodology of the flight experiment

To control the flight, a Lisa/S autopilot from 1 Bit Squared is used, equipped with a Superbit CYRF radio module, see Figure 20 [Remes et al., 2014]. The autopilot runs PaparazziUAV software. The attitude (roll and pitch) of the DelFly is controlled with a PD controller, with attitude feedback using the IMU available on the Lisa/S.

Next to the tuning of the center of gravity as we presented in the previous section, also the roll and pitch feedback gains have to be tuned. This was done using a telemetry module to connect wirelessly to the

Lisa/S, making it possible to quickly set and try different gains.

For recording the flight, the attitude angles and position of the DelFly were measured using an OptiTrack Motion Capture System, capturing the position of infrared reflective markers on the DelFly. The prototype also had a safety wire attached at the bottom. In order to keep track whether the DelFly was flying freely, markers were also placed on the operator's hand. The distance between the operator's hand and the DelFly is then indicative for the moment the DelFly is in free flight. In the next section, the results for this flight test are presented.

IV.D.3. Results in-flight experiment using Lisa/S autopilot

Figure 25 shows the attitude angles, altitude and distance to the operator's hand, for two flight tests, one using an on-board attitude feedback controller (Figure 25-(a) and (b)) and one without control (Figure 25-(c) and (d)). To obtain these results, both the center of gravity location and the feedback gains were tuned. The DelFly showed the best behaviour in terms of flight duration when the center of gravity was located near the quarter-chord point; it appears that our hypothesis for the center of gravity location is correct. The figure shows that in the first flight test the DelFly's attitude is stable for two seconds, after which it drifts in roll. During the experiment, the altitude was slowly decreasing, which indicates that the DelFly did not have enough thrust. In the second experiment, the servos were given a constant tension command. In this experiment, the DelFly was immediately pitching up when released. A similar divergence, but to varying direction, also occurred when repeating the experiment. The DelFly however seemed to have enough thrust for climbing in this case. This indicates that when the DelFly is in attitude feedback mode, the servos and motor combined are drawing too much current and level flight cannot be reached anymore. However, during its descent it was able to self-stabilise for about 2 s.

IV.D.4. Flight experiment using Lisa/MXS autopilot

During the flight experiment of the previous section, it appeared that the DelFly did not have enough thrust to maintain altitude. Therefore, a Lisa/MXS was used instead of the heavier Lisa/S. This is a prototype autopilot developed in-house by the MAVLab of Delft University of Technology. Additionally, weight was saved by removing extra connectors and by making the structure lighter. This resulted in a prototype that is 2.1 grams lighter than the Lisa/S equipped

(a) Attitude feedback mode

(b) Attitude feedback mode

(c) Neutral command
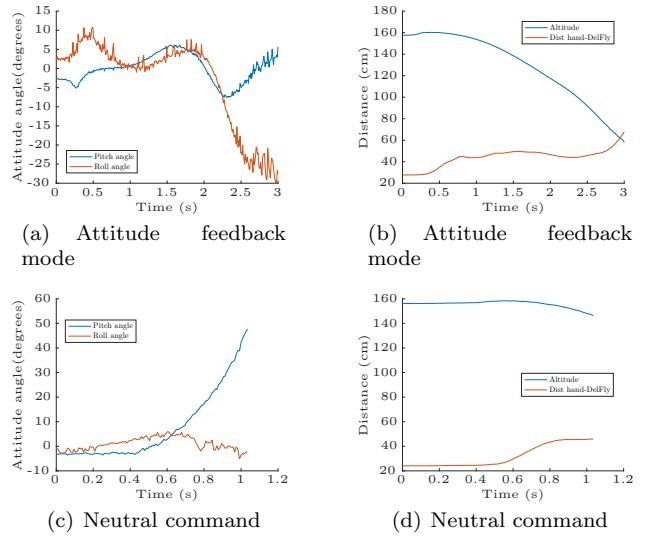
(d) Neutral command

Figure 25. OptiTrack measurements of two flight tests using the Lisa/S autopilot. For the experiment shown in (a)-(b) the control system is enabled, for (c)-(d) the servos have a constant neutral command. The parameter distance hand-DelFly is indicative for when the DelFly is released and is flying freely.

prototype, reducing the weight by 9%, resulting in a total weight of the prototype of 21.5 g. The flight tests were recorded by the OptiTrack system, and the results are shown in Figure 26. For these flights the safety wire was attached to the top of the vehicle, since it was easier to quickly perform multiple tests in a row.

From Figure 26-(a) and (b) can be deducted that in attitude feedback mode the DelFly was able to climb steadily with slight oscillation in pitch and roll angles for about five seconds. Near the end of the flight, the amplitude of these oscillations increased slightly, and five seconds into the flight the attitude angles diverged since the safety wire ran short. Unfortunately we could not increase the length of the safety wire, since otherwise the vehicle would crash into the ground if the flight diverged. We attempted to control the throttle of the DelFly to keep a constant altitude, however, the DelFly was very sensitive to changes in the thrust level. Therefore, we kept the throttle constant throughout these experiments. For additional research we recommend implementing an altitude feedback loop to control the throttle of the DelFly. Figure 26-(c) and (d) shows an example of a flight when the servos are given a neutral command, for which the attitude angles of the DelFly diverge. Similar behaviour was observed when repeating this flight.

(a) Attitude feedback mode

(b) Attitude feedback mode

(c) Neutral command
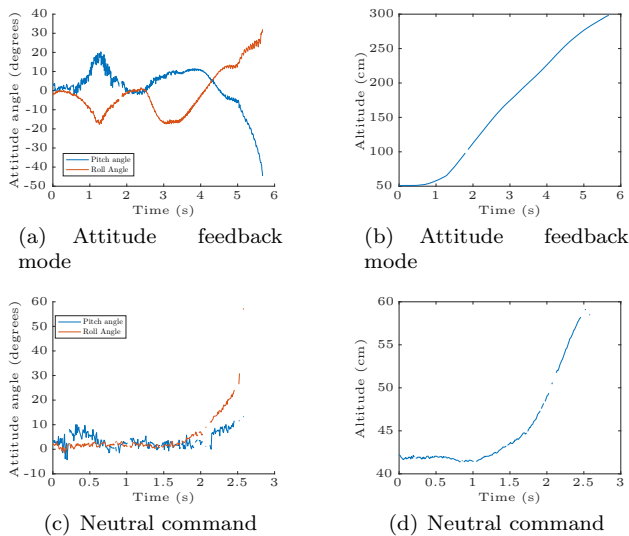
(d) Neutral command

Figure 26. OptiTrack measurements of two flight tests using the Lisa/MXS autopilot. For the experiment shown in (a)-(b) the control system is enabled, for (c)-(d) the servos have a constant neutral command.

V. Conclusion

We presented a novel control mechanism for a Flapping Wing Micro Aerial Vehicle that generates the control moments by varying the wing tension for each of its four wings. This wing tension is controlled by four linear actuators that vary the position of the control rods at the root of the wings. High-speed camera recordings show that for a slack wing the angle of attack is decreased, which results in a lower amount of thrust for that wing. We demonstrated experimentally that by individually modulating the slackness of each wing, the 21.5-gram prototype can produce roll moments of -0.95 to 1.17 Nmm and pitch moments of -0.39 to 0.57 Nmm while flapping at 12 Hz, and the transition between these minima and maxima takes approximately 0.2 s. Furthermore, low levels of cross-coupling exist for combined pitch and roll commands. With these specifications we complied to all requirements we set for tail-less flight, except the requirement for the magnitude of the pitch moment. The prototype was able to self-stabilise for five seconds in a flight experiment.

VI. Recommendations

First off, we recommend research aimed at creating a model of the flight dynamics for a tail-less DelFly. In present research, we have set the requirements for tail-less flight using a reference vehicle. When an accurate model for tail-less four-winged flight is available, one can simulate the dynamics of a DelFly,

find the characteristic dynamic modes, set more accurate requirements, and even estimate the gains for the attitude feedback loop.

Next, we recommend further work to increase magnitude of the generated control moments. In this paper, we showed that control by wing tension modulation is able to stabilise the flight in hover, however, to make the stability more robust and to allow forward flight (and afterwards return back to hover), the magnitude of the generated moments should be increased. To increase magnitude of the generated moments, we recommend to:

- Develop servos with a higher stroke (at the same speed), such that a higher moment can be generated.

- Increase the amplitude of the trajectory of each wing to 90°, such that in theory the magnitudes of the pitch and roll moments that can be generated are equal. For the present concept, the maximum pitch moment that can be generated is a factor two lower than for roll, this is due to a bigger arm for the roll moment generation. Additionally, increasing the amplitude has benefits for thrust generation, due to two clap-and-peels per stroke (see de Croon et al. [2012]).

- Optimise the wing planform and location and orientation of the carbon control rods at the root of the wings for maximum moment generation (while maintaining thrust).

Lastly, we recommend to:

- Include the possibility to generate a yaw moment, such that the heading can be controlled. This can be achieved by combining concepts A and B, see section III.B.

- Continue with the tuning of the flapping robot to remove the oscillations in attitude angles during flight.

- Include an altitude feedback loop to keep the tail-less DelFly at constant altitude during flight experiments.

- Repeat the measurements in this paper with additional prototypes, to reduce any manufacturing-related defects.

References

David E. Alexander. Wind tunnel studies of turns by flying dragonflies. *Journal of Experimental Biology*, 122(1):81–98, 1986.

Bo Cheng and Xinyan Deng. Translational and Rotational Damping of Flapping Flight and Its Dynamics and Stability at Hovering. *IEEE Transactions on Robotics*, 27(5):849–864, October 2011. ISSN 1552-3098, 1941-0468. doi: 10.1109/TRO.2011.2156170.

David Coleman, Moble Benedict, Vikram Hrishikeshavan, and Inderjit Chopra. Design, Development and Flight-Testing of a Robotic Hummingbird. In *AHS 71 st Annual Forum, Virginia Beach, Virginia, May 57, 2015*, 2015.

Guido C.H.E. de Croon, Kristien M. E. De Clercq, Rick Ruijsink, Remes, and C. De Wagter. Design, aerodynamics, and vision-based control of the DelFly. *International Journal of Micro Air Vehicles*, 1(2):71–97, 2009.

Guido C.H.E. de Croon, Mark A. Groen, Christophe De Wagter, Bart D.W. Remes, Rick Ruijsink, and Bas W. van Oudheusden. Design, aerodynamics and autonomy of the DelFly. *Bioinspiration & biomimetics*, 7(2):025003, 2012.

Christophe De Wagter, Sjoerd Tijmons, Bart D.W. Remes, and Guido C.H.E. de Croon. Autonomous flight of a 20-gram flapping wing mav with a 4-gram onboard stereo vision system. In *Robotics and Automation (ICRA), 2014 IEEE International Conference on*, pages 4982–4987. IEEE, 2014.

Charles P. Ellington. The novel aerodynamics of insect flight: applications to micro-air vehicles. *Journal of Experimental Biology*, 202(23):3439–3448, 1999.

Mark Groen, Bart Bruggeman, Bart Remes, Rick Ruijsink, Bas W. Van Oudheusden, and Hester Bijl. Improving flight performance of the flapping wing MAV DelFly II. In *Int. Micro Air Vehicle Conf. and Competition (IMAV 2010)(Braunschweig, Germany)*, 2010.

Gary Hatch. Structure and Mechanics of the Dragonfly Pterothorax. *Annals of the Entomological Society of America*, 59(4):702–714, July 1966. ISSN 0013-8746, 1938-2901. doi: 10.1093/aesa/59.4.702.

Matěj Karásek. *Robotic hummingbird: Design of a control mechanism for a hovering flapping wing micro air vehicle*. PhD thesis, Université libre de Bruxelles, 11 2014.

Matěj Karásek and André Preumont. Flapping flight stability in hover: A comparison of various aerodynamic models. *International Journal of Micro Air Vehicles*, 4(3):203–226, 2012.

Matěj Karásek, Alexandre Hua, Yanghai Nan, Mohamed Lalami, and André Preumont. Pitch and Roll Control Mechanism for a Hovering Flapping Wing MAV. *International Journal of Micro Air Vehicles*, 6(4), 2014. ISSN 1756-8293.

Matthew Keennon, Karl Klingebiel, Alexander Andriukov, Bart D. Hibbs, and John P. Zwaan. Air vehicle flight mechanism and control method, 12 2010. CA Patent App. CA 2,776,485, Fig. 19-20.

Matthew Keennon, Karl Klingebiel, and Alexander Andriukov. Tailless flapping wing propulsion and control development for the nano hummingbird micro air vehicle. In *American Helicopter Society Future Vertical Lift Aircraft Design Conference*, 2012a.

Matthew Keennon, Karl Klingebiel, Henry Won, and Alexander Andriukov. Development of the nano hummingbird: A tailless flapping wing micro air vehicle. In *50th AIAA Aerospace Sciences Meeting Including the New Horizons Forum and Aerospace Exposition, Nashville, TN. January*, pages 9–12, 2012b.

Kevin Y. Ma, Pakpong Chirarattananon, Sawyer B. Fuller, and Robert J. Wood. Controlled Flight of a Biologically Inspired, Insect-Scale Robot. *Science*, 340(6132):603–607, May 2013. ISSN 0036-8075, 1095-9203. doi: 10.1126/science.1231806.

Bart D. W. Remes, Piotr Esden-Tempski, Freek Van Tienen, Ewoud Smeur, Christophe De Wagter, and Guido C.H.E. De Croon. Lisa-s 2.8 g autopilot for gps-based flight of mavs. In *IMAV 2014: International Micro Air Vehicle Conference and Competition 2014, Delft, The Netherlands, August 12-15, 2014*. Delft University of Technology, 2014.

Mao Sun. Insect flight dynamics: Stability and control. *Reviews of Modern Physics*, 86(2):615–646, May 2014. ISSN 0034-8861, 1539-0756. doi: 10.1103/RevModPhys.86.615.

Mao Sun and Yan Xiong. Dynamic flight stability of a hovering bumblebee. *Journal of Experimental Biology*, 208(3):447–459, February 2005. ISSN 0022-0949, 1477-9145. doi: 10.1242/jeb.01407.

Zhi Ern Teoh, Sawyer B. Fuller, Pakpong Chirarattananon, Nestor O. Pérez-Arancibia, Jack D. Greenberg, and Robert J. Wood. A hovering flapping-wing microrobot with altitude control and passive upright stability. In *2012 IEEE/RSJ International Conference on Intelligent Robots and Systems*, pages 3209–3216. IEEE, 2012.

Hiroshi Tokutake, Shigeru Sunada, and Yukio Ohtsuka. Active Control of Flapping Wings Using Wing Deformation. *Transactions of the Japan Society for Aeronautical and Space Sciences*, 52(176): 98–103, 2009.

Robert J. Wootton. Palaeozoic insects. *Annual review of entomology*, 26(1):319–344, 1981.

Jianghao Wu and Mao Sun. Control for going from hovering to small speed flight of a model insect. *Acta Mechanica Sinica*, 25(3):295–302, June 2009. ISSN 0567-7718, 1614-3116. doi: 10.1007/ s10409-009-0241-y.

Yanlai Zhang and Mao Sun. Dynamic flight stability of a hovering model insect: lateral motion. *Acta Mechanica Sinica*, 26(2):175–190, May 2010. ISSN 0567-7718, 1614-3116. doi: 10.1007/ s10409-009-0303-1.

Part II

Preliminary Research

Chapter 2

Introduction to the preliminary research

A main goal of research on Micro Aerial Vehicles (MAVs) is to arrive at insect-sized aircraft. The small size of these MAVs makes them well suited for reconnaissance in places that are too small or too dangerous for humans or other vehicles to enter. Therefore researchers, industries, governments and the military have shown great interest in development of such systems. It may come as no surprise that in the development of MAVs, researchers draw their inspiration from nature. Winged insects already roam the skies since 325 million years ago (Wootton, 1981), and have been evolving ever since. Due to natural selection, dragonflies are capable of complete 180° turns within three wing beats (Alexander, 1986), and capable of landing on flowers buffeted by high winds. Additionally, these animals have an unmatched flight envelope: capabilities range from hovering, high speed forward flight, backward flight and quick take-off. On high-speed movies of dragonflies it is shown that dragonflies achieve these feats by using left-right asymmetries in wing stroke amplitude, angle of attack, mean wing position and asymmetric drag creation (Alexander, 1986).

Due to their large flight envelope and manoeuvrability, researchers have tried to mimic these natural flyers in the form of FWMAVs. It has also led to the Delft University of Technology's project 'DelFly', see Figure 2-1.

DelFly started as a student project to design a small ornithopter (an aircraft with flapping wings) that was able to carry a camera system with good flight characteristics. Indeed, the DelFly II is capable of hovering, and able to fly $7\,\mathrm{m/s}$ forward and $1\,\mathrm{m/s}$ backwards (De Croon et al., 2009). The idea behind the project is to design a flying platform using a top-down approach. One starts with a functioning, relatively large ornithopter, and by studying this ornithopter, it is gradually improved and scaled down. Recently the 'DelFly Micro' was developed resulting from this approach. This flapper weighs 3 grams and has a wingspan of $10\,\mathrm{cm}$ but is still able to carry a small camera. Currently the 'DelFly Explorer' is being developed, which is *"the first FWMAV with onboard vision processing for autonomous flight in generic environments"* (De Wagter et al., 2014).

(a) Male Emperor Dragonfly, picture by Stuart
Roebuck
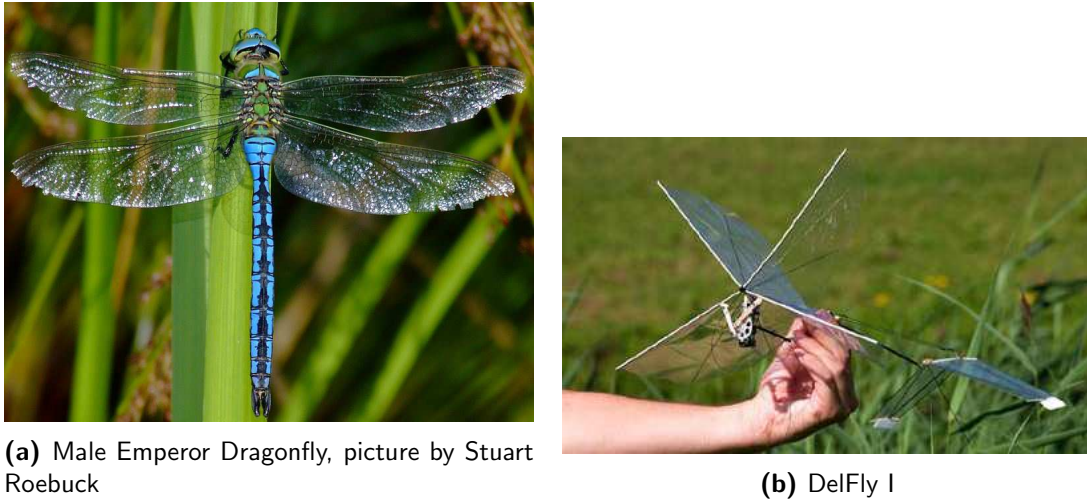
(b) DelFly I

Figure 2-1: Inspiration from nature resulted in the DelFly.

Throughout the whole project, the DelFly uses a biplane configuration, since the power
consumption is lower than more conventional monoplane configurations for the same size
(De Croon et al., 2009). These two pairs of wings flap in antiphase, which are positioned on
top of each other to limit size. The DelFly carries conventional tail surfaces as seen in fixed
wing aircraft for stabilization and control. The hovering capability results from the placement
of these tail surfaces in the wake of the flapping wings, generating an airflow over the tail-
and control surfaces even when there is no forward speed.

2-1   Motivation

Apart from its larger size, the fact that the DelFly uses tail surfaces for control and stabiliza-
tion, is the most discerning feature from its natural counterpart, the Dragonfly. Dragonflies
only use their wings to control and stabilize their flight: they actively stabilize their attitude
by small changes of the wing angle of attack, of mean wing position and of flapping amplitude
(Ellington, 1999). The dragonfly is able to alter these parameters independently for each of
its wings, resulting in high manoeuvrability (Hatch, 1966).

In contrast, the DelFly fully relies on its tail for passive stabilization. A downside thereof
is that it stays sensitive to external disturbances. During a typical envisioned mission for
MAVs, the inspection of buildings, the MAV will have to fly close to obstructions such as
walls. Even on a calm day these obstructions can cause wind gusts, severely hindering the
successful completion of a mission. Tail-less FWMAVs are inherently unstable and need to be
stabilized actively, just like their natural counterparts. In turn, this makes them potentially
very agile and more resilient against wind gusts.

Another reason to use active wing control and stabilization could lie in the improvement of
controllability during hover. In current DelFly models controllability results from the tail
surfaces being in the wake of the wings. In this way, the airflow over the control surfaces
can be steered, which generates the necessary control moments. However, in this way only a
part of this highly turbulent wake is steered, resulting in degraded control performance with

respect to forward flight, where also the airflow resulting from a forward speed is steered. The use of active wing control could bridge this gap, resulting in a more even control performance over various speeds. Additionally, removing the tail can potentially reduce the MAV's size and weight, bringing it closer to the envisioned fly-sized craft.

The successful control and stabilization of a FWMAV without using tail surfaces has been performed by few research groups (Keennon, Klingebiel, Won, & Andriukov, 2012; Ma et al., 2013; Coleman et al., 2015), however, these prototypes all carry only two wings. It has never been done on a lay-out similar to the DelFly, a lay-out which has advantages in flight efficiency due to clap-and-peel (see section 4-1-3). It is therefore desirable to be able to eventually fly a DelFly with active control and stabilization. The goal of present research is to be able to control a DelFly by using its wings not only for propulsion, but also for control. This can eventually be developed in a tail-less DelFly.

The main research question can therefore be formulated as:

What is an adequate yet simple system to control the attitude of the four-winged DelFly by using the wings not only for propulsion, but also for control, and how can this system be (eventually) employed to achieve stabilized free flight without using tail surfaces?

This research question can be sub-divided into the following sub-questions:

1. Which kinematic parameters of the flapping motion can be changed in order to generate the three attitude moments?

2. What mechanical system can be employed in order to change these kinematic parameters of the flapping motion for a DelFly prototype?

    (a) What are the requirements on the mechanical linkage system to change these kinematic parameters?

    (b) What are the requirements on the motor/servo to change these kinematic parameters?

3. What criteria are relevant for assessing the effectiveness of the various types of control by wing-deformation, and what is their order of importance?

4. What are the requirements of a test-setup to test the criteria on the DelFly prototypes?

5. What is, by comparing the concepts to the assessment criteria, the best concept for controlling a DelFly using wing-deformation?

6. What additional requirements can be identified on the control mechanism when the DelFly needs to be stabilized without using tail surfaces?

2-2   Preliminary research outline

This preliminary thesis consists of two parts. The first part is a literature survey, where inspiration is drawn from both nature and from other research groups. Chapter 3 describes

the aerodynamics of flapping flight in insects and their control strategies. Next, chapter 4 elaborates on the FWMAVs of other research groups, as well as the state-of-the-art of the DelFly project.

The second part deals with the experiment which is performed on the DelFly. In this part, first the requirements for the control mechanism will be stated, in chapter 5. After this, the test setup which is used to assess the concepts to the requirements is elaborated. This setup is then used to test the two concepts which have been developed, and their results are presented.

Lastly, the conclusions are presented in chapter 11.

<div align="right">

Chapter 3

</div>

Flapping wing aerodynamics of natural flyers

In order to come up with modifications to the DelFly, such that it can be eventually controlled and stabilized without using a tail, inspiration is drawn from nature and from other research groups. During the analysis of these animals and crafts, the focus point will be the mechanics of flight, the methods of thrust/lift generation and the mechanics of active wing control. After having analyzed these systems, this knowledge can be used to come up with an effective system for wing control of the DelFly.

To be able to understand flapping wing aerodynamics, first some basic principles need to be understood. Next, the kinematics of flapping flight will be discussed, followed by the implications on the lift creation. At the end of this chapter the (in)stability of flapping insects will be discussed, followed by how they control and actively stabilize their flight.

3-1 Classical lift-theory for thin airfoils

Before introducing the means of lift creation of flapping animals and FWMAVs, first some basic principals of aerodynamics need to be understood. Conventional aerodynamics is based on rigid wings moving at a constant velocity. Various theories exist that explain the means of lift generation, the force that is required to keep an aircraft airborne. A fundamental explanation is by using the definition of circulation around an airfoil. When the circulation is known, the lift (L) per unit span (or L') can be calculated by using the Kutta-Joukowski theorem:(Anderson Jr, 1985)

$$L' = \rho_\infty U_\infty \Gamma \tag{3-1}$$

where ρ_∞ is the density of the fluid (air), U_∞ is the free-stream velocity and Γ is the circulation, which is defined as the negative of the line integral of velocity around a closed curve C in the flow that enclosed the airfoil:
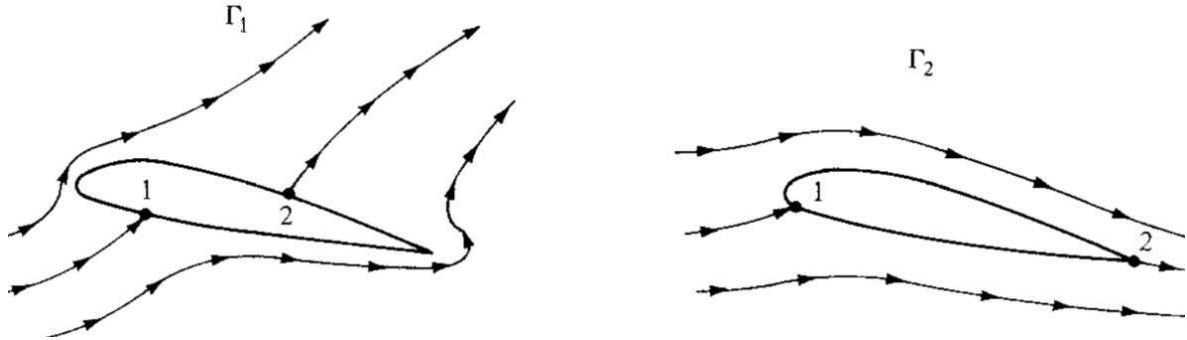
Figure 3-1: Various values of circulation Γ over an airfoil. Points 1 and 2 are stagnation points. Adapted from Anderson Jr (1985)

$$\Gamma \equiv \oint_C \boldsymbol{V} \cdot d\boldsymbol{s} \tag{3-2}$$

The potential flow around an airfoil has an infinite number of solutions for different Γ. In Figure 3-1 an airfoil is subjected to two values of circulation. Clearly, an additional condition in needed that imposes a certain value of Γ for a certain angle of attack α to get to a single solution.

Experiments by the German mathematician M. Wilhelm Kutta showed that nature imposes *"the airflow to smoothly leave the top and bottom surfaces of the airfoil at the trailing edge"* (Anderson Jr, 1985). This adaptation by nature is shown for Γ_2 in Figure 3-1 and is known as the *Kutta Condition.*

If this Kutta Condition is satisfied, it implies that an inclined plate or thin airfoil generates a downward force on the airflow, which results in a upwards reaction force. This upward reaction force is the *lift* of the airfoil.

3-2 Kinematics of flapping wings

In contrast to the airfoils considered in section 3-1, which can be considered as a stationary body subjected to a free-stream velocity U_∞, the body and wings of natural fliers beat with a complicated three-dimensional motion. This motion is composed of three components: sweeping (fore and aft movement), heaving (up and down movement) and pitching. The flapping frequency is typically between 5 and 200 Hz (Ansari et al., 2008). The stroke of an insect can be divided in four phases: two translational- (upstroke and downstroke), and two rotational phases (pronation and supination) (Dickinson et al., 1999). During the translational phases, the wings sweep through the air with a high angle of attack, and during this phase the linear motions dominate over changes in pitch. During the rotational phases, which occur at the end of a translational phase, the wings rotate (i.e. wing pitch changes rapidly) and reverse direction (i.e. stroke reversal). During this process, the leading edge always leads the trailing edge (Ansari et al., 2008). This complicated three-dimensional motion has additional implications to the flow, as will be explained in the next section.

3-3   Unsteady mechanisms that enhance lift in insects

When insect wings are placed in a wind tunnel and tested over the range of velocities encountered during flapping flight, the measured lift is substantially smaller than the lift required to keep the insect airborne (Dickinson et al., 1999). Thus, some other mechanism(s) need to be in place that boosts the lift generation of the wings beyond the forces it could generate at constant velocity or that can be explained by the conventional aerodynamic theory of section 3-1.

Indeed, a number of mechanisms have been proposed throughout the years, which typically focus on either the translational phase or the rotational phase. The dominant mechanisms that have been proposed are:

- Leading edge vortex (section 3-3-1)

- Wing rotation (Kramer effect) (section 3-3-2)

- Clap-and-fling (section 3-3-3)

- Wake capture (section 3-3-4)

3-3-1   Leading edge vortex

During the translational phases the wings of insects reach angles of attack above the stall angle. Therefore, the fluid stream separates as it crosses the leading edge, however, it reattaches before it reaches the trailing edge. In this area of separation, a Leading Edge Vortex (LEV) fills the area above the wing. From the reattachment point onwards, the flow smoothly follows the wing and leaves it at the trailing edge, resulting in the Kutta condition being maintained.

Since the wing has a high angle of attack and has additional circulation due to the LEV, the wing causes a higher downward momentum of airflow than during fixed wing flight, which results in a substantial enhancement of lift. Since normally the airfoil would have already stalled and the flow would separate completely, this effect is also called *delayed stall* (Sane, 2003). In Figure 3-2, the flapping cycle of an insect is schematically shown, with a LEV clearly visible in phase F.

3-3-2   Wing rotation, the Kramer effect

The LEVs from the previous section are predominately generated during the translational phase. The two rotational phases allow insects to have a high angle of attack during both up- and downstroke. However, the rapid change of angle of attack during rotation, has an effect on the Kutta condition, this steady state can not be achieved anymore due to rapid rotation. Instead, the stagnation point departs from the trailing edge, which leads to shear (Sane, 2003). In order to again move to the Kutta condition, additional circulation is generated, which either has a positive or an adverse effect on the net lift of the flapping wing. This phenomenon is called the *Kramer effect*, after M. Kramer who first described the effect in 1932. From the results of Dickinson et al. (1999), who tested the timing of the rotation with
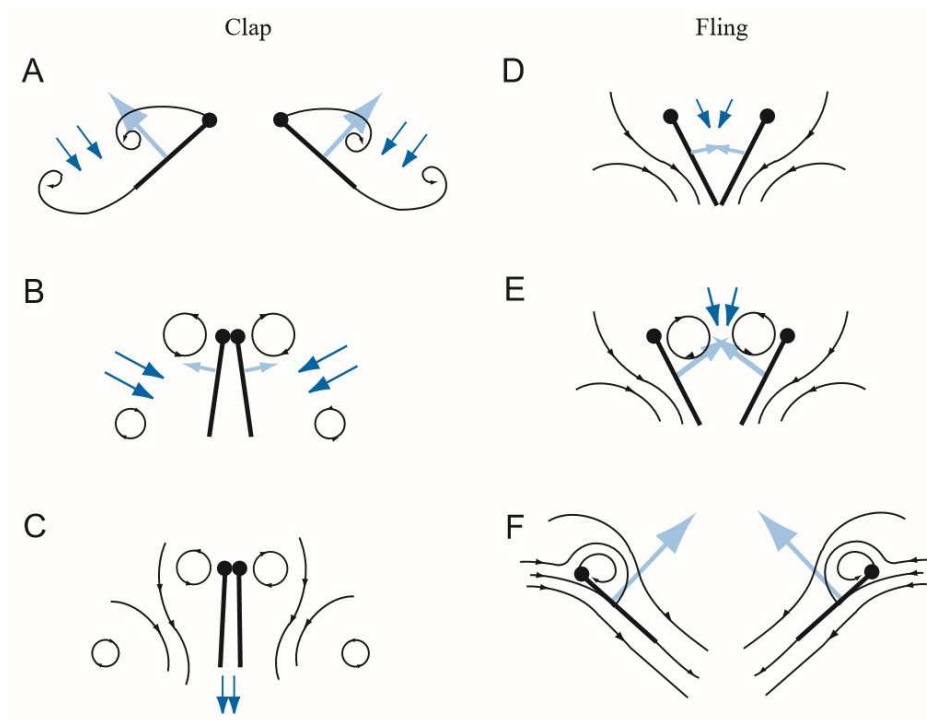
Figure 3-2: Schematic of clap (A-C) and fling (D-F). Adapted from Sane (2003)

respect to the flapping, it can be deducted that the timing of rotation has a big effect on whether an extra amount of lift is generated, or whether the Kramer effect has a adverse influence on the lift. This timing effect can also be used for control, see Section 3-4-2.

3-3-3   Clap-and-fling

The clap-and-fling mechanism was first described by Weis-Fogh (1973). The clap-and-fling is a rotational mechanism, that happens when the wings are positioned closely together during pronation (the rotation between upstroke and downstroke, i.e. at maximum flapping angle). This mechanism is used by certain insects and birds to generate a higher lift, by having a wing stroke to such an extent that the wings touch each other during rotation.

During the 'clap', the leading edges -which are leading in the flapping motion- first touch each other before the trailing edges. In this way, the gap between the wings (see Figure 3-2) is increasingly closed (Sane, 2003). Weis-Fogh (1973) argued that the opposing circulation of both wings cancel each other out during clap. This attenuates the trailing edge vorticity shed by each wing on the following stroke. Since this trailing edge vorticity normally slows down the build-up of circulation during the next stroke (via the Wagner effect[1]), the attenuation of this vorticity helps the build-up of lift in the subsequent stroke and generates the maximum

---

[1]The Wagner effect is the phenomenon that causes the circulation of a wing accelerating from rest to be lower than its steady-state value. This is due to (1) the inherent latency to reach the Kutta condition and (2) the shedding of vortices at the trailing edge, which eventually rolls up in the form of a starting vortex. This vorticity counteracts the growth of circulation bound to the wing. (Sane, 2003)

lift directly from the beginning (Arora et al., 2014). In addition, the closing gap pushes air out, creating a momentum jet (Figure 3-2-C) (Sane, 2003).

At the end of the clap, the leading edges fling apart while the trailing edge momentarily stays stationary (Figure 3-2-D). During this 'fling' phase, a low pressure region is created between the wings, and the fluid rushes into the opening gap. The result is the formation of vortices attached to the wings (i.e. LEVs) which results in extra circulation, and thus, by Equation 3-1, in more lift (Sane, 2003).

However, while the clap-and-fling could result in a modest lift enhancement, the importance must be viewed in contrast with another hypothesis: the simple hypothesis that the animal just enhances its stroke to achieve maximum stroke amplitude, which can also enhance force generation (Sane, 2003).

3-3-4 Wake capture

During the cyclic flapping motion of a flapping wing, at some point the wing will encounter the vorticity generated during a previous cycle. This is most dominant during hovering, when the wing stays in one place and the shed vortices stay in the vicinity of the wings. This interaction of the wing with its own wake is called wake capture, and this has an effect on the generated lift. Birch (2003) has researched this phenomenon, and it appeared that this effect was *"dependent on temporal changes in the distribution and magnitude of vorticity during stroke reversal"*(Birch, 2003). This distribution and vorticity is dependent on wing kinematics, most notably on the timing of the wing rotation (Dickinson et al., 1999).

3-4 Control and flight stability of natural fliers

Insects are able to hover, fly forward, fly backwards, climb, descent, and even land on flowers buffeted by wind with ease, while showing great stability. Surprisingly however, flapping flight is unstable, as described in section 3-4-1. After this section, in which the dynamic modes of insect will be described, section 3-4-2 deals about the mechanisms that are used for stabilization.

3-4-1 Flight stability of natural flyers

Dynamic stability is an inherent property of a flying system. Dynamic stability compasses the way the system behaves after it has been disturbed from an equilibrium flight state. Here, the stability during hovering is discussed, since this is also the flight mode which is used in the experiments in this paper.

To discuss the stability of a hovering insect, the eigenvalues of the linearized disturbance equations of motion need to be evaluated. Sun (2014) does this by deriving the linearized disturbance equations of motion. He uses the following state equation for an insect:

$$x = [u, v, w, p, q, r, \phi, \theta]^T \tag{3-3}$$

Table 3-1: Nondimensionalized (for flapping frequency) eigenvalues of hovering flight for the hoverfly, dronefly, bumblebee, crane fly and hawk moth (HF,DF,BB,CF and HM, respectively). Adapted from Sun (2014)

	Longitudinal modes			Lateral modes		
	$\lambda_{1,2}$ (1/s)	λ_3 (1/s)	λ_4 (1/s)	λ_1 (1/s)	$\lambda_{2,3}$ (1/s)	λ_4 (1/s)
HF	$0.074 \pm 0.144i$	-0.171	-0.020			
DF	$0.073 \pm 0.139i$	-0.165	-0.015	0.08	$-0.09 \pm 0.06i$	-0.51
BB	$0.045 \pm 0.129i$	-0.197	-0.012	0.09	$-0.12 \pm 0.07i$	-0.69
CF	$0.330 \pm 0.733i$	-0.865	-0.110			
HM	$0.269 \pm 0.608i$	-0.747	-0.092	0.26	$-0.57 \pm 0.26i$	-5.68

where u,v,w, are velocities, p,q,r, are angular velocities, ϕ is the roll angle and θ the pitch angle. He considers disturbances around an equilibrium, for which the effect can be expressed as aerodynamic derivatives, i.e. $X_u = \delta X/\delta u$, $X_v = \delta X/\delta v$. They represent the increment of the force X when there is a unit increment in u.

These derivatives can be computed by solving the Navier-Stokes equation, by using simple models, or by experiments. The derivatives compass the complete flight dynamics about a linearized point for small disturbances.

After having computed the derivatives and entering them in the equations of motion, an eigenvalue analysis of these linear equations of motion can be performed, by writing the general solution in the form of (Sun, 2014):

$$\mathbf{x}\left(t\right) = \sum_{j=1}^{4} c_j \mathbf{q}_j e^{\lambda_j t} \tag{3-4}$$

where λ_j are the eigenvalues and $\mathbf{q}_j$ are the eigenvectors (j =1,2,3,4 since for both longitudinal and lateral motion there are 4 states) and c_j are constants depending on initial conditions.

The eigenvalues as calculated by Sun (2014) from data of Sun (2005); Sun et al. (2007); Xu & Sun (2013); Zhang & Sun (2010) are depicted in Table 3-1.

In general, a system is stable if and only if $\mathfrak{Re}(\lambda_j) < 0$ for all j, since in that case $\mathbf{x} \to 0$ for $t \to \infty$ (the solution will converge). Otherwise the solution will diverge. From Table 3-1 can be deducted that all insects considered have an unstable longitudinal mode, and for the insects for which lateral modes are identified, also an unstable mode is found. Because of these unstable modes, the hovering flight of insects is **dynamically unstable**. Based on these eigenvalues, the time-to-double can be calculated, which provides an indication for the instability:

$$T_2 = \frac{ln(2)}{\lambda_j} \tag{3-5}$$

This T_2 is about 9.5 for the hoverfly and dronefly, 15.4 for the bumblebee, and 2-2.5 for the crane fly and hawk moth for the unstable longitudinal mode. These values are non-dimensionalized for the wing-beat period. When the wing-beat period is taken into account, the time to double for the hoverfly, dronefly and cranefly is 46-60 ms, and for the bumblebee

and hawkmoth 100 ms (Sun, 2014). Clearly, these animals need to be able stabilize their flight using active control. This is explained in the next section.

3-4-2   Control mechanics used by natural flyers

A flying insect inherently has six Degrees of Freedom (DOFs). It is free to translate along or rotate around any of the three orthogonal axes, which are centered in the center of gravity. A force or moment can produce an acceleration or angular acceleration, respectively, to control the position and orientation of an insect in space, by Newton's second law. However, it is usually unnecessary to control all six DOFs (Taylor, 2001). For the control of the position of an object in space, a system with three independent control inputs already suffices: independent control of the pitch angle and heading angle, and an ability to change the longitudinal acceleration. For an aircraft, usually four DOFs can be controlled, being the three rotations about the main body axes, and the control of longitudinal acceleration (i.e. controlling thrust). This is also termed three-axis control (Taylor, 2001).

DelFly as of yet does not have three-axis control. It can change its longitudinal acceleration by varying the flapping frequency, can produce a pitch moment by deflecting its elevator, and can produce either a yaw moment or a roll moment, depending on the configuration. To be able to fly the DelFly tail-less, independent three axis control is needed, to be able to prevent drift when stabilizing the attitude, as was the case in early models of the Nano Hummingbird (Keennon, Klingebiel, Won, & Andriukov, 2012). This will also improve the maneuverability of the DelFly as compared to tailed versions, since the passive stabilizing moments from the tail section will not suppress the control moments when a change of attitude is desired.

Insects are also capable of three-axis control (Sun, 2014; Taylor, 2001). Using this ability, the insect is able to perform three types of control. To account for the inherent instability of flapping flight, as was found present in section 3-4-1, an insect has to use control forces and moments for stability. This requires very fast responses, and is therefore generally performed by a reflex control system (Sun, 2014). The other types of control, being maneuvering control and steady state control are performed intentionally. Maneuvering control is for example employed to perform turns. Steady state control is used to get from one equilibrium to another, such as slowing down from forward flight to hovering.

To control their attitude, animals must overcome viscous forces as well as inertial forces (Fry et al., 2003). To achieve this, the insect needs to be able to generate the three attitude moments, which they generate by introducing changes in their wing kinematics, Sections 3-4-3-3-4-4 and body posture, Section 3-4-5.

3-4-3   Control through stroke amplitude

Historically, differences in stroke amplitude are considered as the main principle for controlling the attitude moments in flies (Götz, 1968; Taylor, 2001). This has been studied by tethering fruit flies to a torque meter and measuring the torques produced when subjecting the animal to visual stimuli based on optic flow. By studying photographs the researchers argued that it is mainly the asymmetric differences in stroke amplitude which generates the torques to perform a turn, by flapping the outer wing with a greater amplitude than the inside wing in
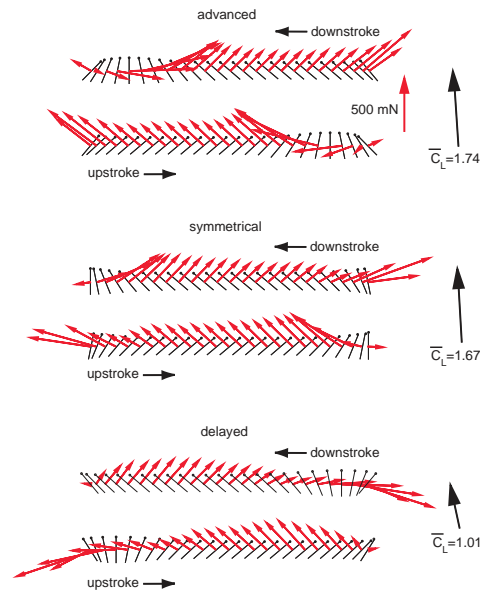
Figure 3-3: Instantaneous force vectors for three different wing motions: advanced, symmetric and delayed rotation. Adapted from Dickinson et al. (1999)

a turn (Götz, 1968). Symmetric changes to the amplitude are used for longitudinal control (Taylor, 2001). Drosophila melanogaster are, next to modulating their stroke amplitude, also able to independently vary the position of the stroke plane, which can also be used for pitch control (Zanker, 1988b).

Male dragonflies also have been studied on a tether in a wind tunnel (Alexander, 1986), and it was concluded that there are two types of turns that are used by dragonflies: rolling by changes in the wing stroke amplitude and the angle of attack of the wings, and a yaw turn, which was argued to be performed by using differential drag generation by the wings. However, it is mentioned by Alexander (1986) that this yaw turn *"could not be as closely analysed"* (Alexander, 1986).

3-4-4   Control through wing rotation timing

Recently it has been discovered that there are unsteady mechanisms in the flapping mechanism of insects that augment the lift generation that could be explained by conventional aerodynamic theory (Section 3-3), and naturally these effects are also taken into account in more recent studies in insect control. An unsteady effect which is found to be used by insects to control their attitude is wing rotation (Dickinson et al., 1993, 1999). Dickinson et al. (1999) experimentally proved that the timing of the wing rotation has a large influence on the produced lift. When wing rotation occurs before the stroke reverses, the wing rotation is called advanced. The research of Dickinson et al. has revealed that in this case the wing will generate a positive lift peak at the end of each half-stroke. When the rotation of the wing spans both the end of one half-stroke and the beginning of the next, it is called symmetric, this results in *"a positive peak before and a negative peak after the stroke reversal"* (Dickinson et al., 1999). When the rotation occurs after stroke reversal, it is termed delayed rotation, and this will result in a negative peak after stroke reversal. These three timings of

wing rotation are depicted schematically in Figure 3-3. Dickinson et al. (1993) found that Drosophila modulate this timing in rotation in order to control their flight. An increase in stroke amplitude, as was previously thought to be leading in control force generation, is correlated with an advance in timing of this wing rotation, and Drosophila can use these two effects -to a limited extent independently- to control their attitude, both longitudinally (symmetric changes) and laterally (asymmetric changes) (Dickinson et al., 1993; Sane & Dickinson, 2001). In a turn, flies advance the timing of rotation on their outer wing, and delay rotation on the inner wing. In this way, the wing on the outside will generate more lift than the inner wing, and therefore the fly will turn. Symmetrically advancing the timing of rotation on both wings allows for longitudinal control (Dickinson et al., 1999).

The DelFly has, strictly speaking, delayed wing rotation, because the leading edge is always leading the trailing edge during the flapping motion. However, the DelFly has a flexible wing, which deforms heavily during flapping, while in the research of Dickinson et al. (1999) an inflexible wing was used. Therefore, it remains to be investigated whether the delayed rotation of the DelFly has an adverse effect on the lift production.

3-4-5   Control through body posture

Next to changes in wing amplitude and rotation timing, Zanker proposes that flies use deflections of their abdomen for flight control (Zanker, 1988a,b). This mechanism can be used for both longitudinal and lateral control. For longitudinal control, the fly can deflect its center of gravity dorsally to the line of thrust, and therefore generate a pitch moment. By deflecting its body laterally, the insect can produce yaw moments (Zanker, 1988a). A lateral deflection of the body acts as a rudder, since by deflecting the abdomen to a side, the drag is locally increased. Additionally, just as was the case for the pitch moment, the center of gravity is also changed, resulting in an additional contribution to the yaw moment (Zanker, 1988a).

Chapter 4

Flapping Wing Micro Aerial Vehicles (FWMAVs)

Inspired by nature, specifically by insect aerodynamics as presented in the previous chapter, numerous research groups are making their own FWMAVs. This chapter starts with an overview of the state-of-the-art of the DelFly, the FWMAV of Delft, University of Technology. As already mentioned, this FWMAV uses tail-surfaces for passive stabilization, bearing control surfaces for attitude control. After this, a literature review is presented about FWMAVs of other research groups, with a focus on flappers with active control and stabilization. The goal of this review is to present the control methods these groups use, and to identify which of these methods are feasible to be incorporated in the four-wing DelFly design.

4-1 State-of-the-art of FWMAV DelFly

The DelFly by Delft University of Technology started as a student project in 2005, and has been developed ever since. The main design philosophy of the DelFly was to design *"an airborne camera platform with good flight characteristics"* (De Croon et al., 2009). The DelFly has a biplane configuration, with two pairs of wings placed above each other, see Figure 2-1b. These wings flap in antiphase, which has advantages for the stability, compared to other FWMAVs with only one pair of wings. It consists of tail surfaces for passive stability and control surfaces for control instead of active control and stability by using the wings, as used by some other research groups (Section 4-2).

In the next section, the components of the DelFly will be described, using the state-of-the-art DelFly Explorer as an example. The DelFly research group has conducted experiments related to the aerodynamics and mechanics of flight of the DelFly, these will be described and compared to insect flight in sections 4-1-2 and 4-1-3.
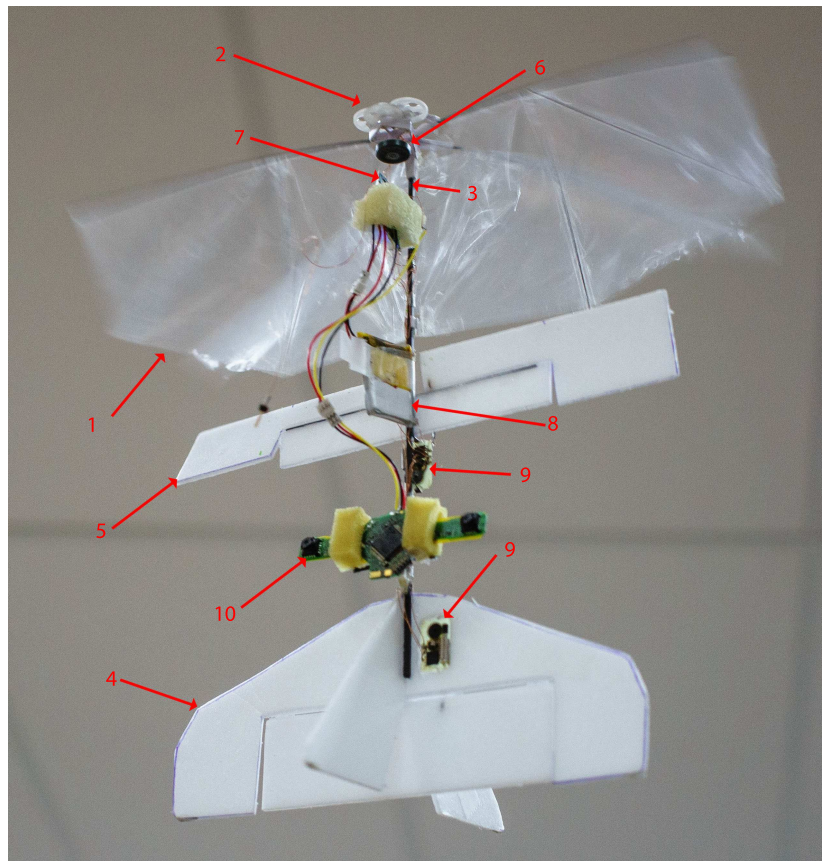
Figure 4-1: The DelFly Explorer. **(1)** Wings, **(2)** crank mechanism, **(3)** fuselage rod, **(4)** tail with elevator, **(5)** ailerons, **(6)** brushless DC motor, **(7)** Autopilot with IMU, barometer, an ATmega328P-MLF28 microcontroller and a motorcontroller, **(8)** Li-Po battery, **(9)** servos and **(10)** onboard stero vision system with STM32F405 processor for onboard vision processing. Picture by C. De Wagter.

4-1-1   The components of a DelFly

Throughout the years, many different DelFlies have been designed and built, reflecting the continuous quest for improving the DelFly both in autonomy and size, however the component layout has always been the same. The DelFly consists of five main components: the wings, the crank mechanism, a fuselage rod, the tail and the electronics. In Figure 4-1 these components are shown for the state-of-the-art DelFly, the DelFly Explorer (De Wagter et al., 2014).

The wings **(1)** are made from 10 micron Mylar foil, with stiffeners made of carbon rods. During flight, the wing shape is determined by aerodynamic, inertial and elastic forces. These forces are in turn also influenced by wing shape and stiffness of the structure, which leads to a complex interaction between fluid and structure. The result of this interaction will be explained in section 4-1-3. The wings were tested using high speed camera visualization and Particle Image Velocimetry (PIV). The locations and orientations of the wing stiffeners were investigated by de Croon et al. (2012). In this experiment, the performance was measured as a ratio of thrust over power consumption for various stiffeners layout. The improved wing layout, which is used for this thesis, has a 5% improvement in thrust-to-power ratio compared to the previous design, while keeping the the thrust approximately equal at the same flapping frequency.

The crank mechanism **(2)** has been updated several times throughout DelFly's history. In the current design, all the gear axles are parallel to each other, and all parts are housed in an injection molded part, which minimizes the friction in the mechanism. The mechanism gives a good symmetrical movement, with no rocking motion of the fuselage, in contrast to earlier mechanisms.

The crank mechanism is connected to the carbon fuselage rod **(3)**, which connects the mechanism with the tail. This rod is also used to mount the electronics and payload. The tail **(4)** is made of Polyethylene and is used for the static stability of the DelFly. It also contains an elevator used for longitudinal control.

In contrast to previous versions of the DelFly, the DelFly Explorer features a set of ailerons **(5)** just behind the wings. The older DelFly II has a rudder at the tail, causing, if deflected, the DelFly to roll (in the definitions of present paper, see Figure 8-5). The choice for ailerons is made because they are necessary for smooth turns. The ailerons cause the Explorer, in the definitions of present paper, to yaw, and since the Explorer flies almost up-right, this also influences the heading without any rotations of the camera images (De Wagter et al., 2014).

The electronics package of the Explorer is more comprehensive than previous DelFlies. The standard elements of a DelFly are the brushless DC motor **(6)**, which drives the crank mechanism, an Electronic Speed Controller (ESC) **(7)**, a Lithium Polymer battery **(8)**, and servos to drive the elevator and ailerons **(9)**. The Explorer however, also features an autopilot (combined with the ESC **(7)**), which consists of an Inertial Measurement Unit (IMU), a barometer and a microcontroller. Lastly, it has a stereo vision system **(10)**, consisting of two cameras and an STM32F405 processor (De Wagter et al., 2014).

4-1-2   DelFly kinematics

The DelFly's design results in a broad flight envelope: it is capable of $7\,\mathrm{m/s}$ in forward flight, it can hover, and it can fly backwards with $1\,\mathrm{m/s}$ (de Croon et al., 2012).

Depending on the flight velocity, the DelFly has a different orientation. During hover, the DelFly is orientated with the fuselage in a vertical position. This will orientate the flap plane horizontally. The thrust of the wings is then the main provider for the lift of the FWMAV, since this thrust is generated parallel with the fuselage. During this hover condition, the DelFly is operating with a flapping frequency of 13 Hz (de Croon et al., 2012).

When the operator wants to change to forward flight mode, he pitches the DelFly downwards. This will therefore also tilt the thrust vector. When the DelFly is almost orientated horizontally, the lift is primarily generated due to the free-stream velocity, and the thrust is used to overcome drag.

4-1-3   DelFly aerodynamics

During flight, the wing shape of the DelFly is determined by aerodynamic, inertial and elastic forces. The wings are flexible, due to the use of materials: the wings are made from Mylar foil reinforced with carbon rods as stiffeners. A D-shaped carbon rod is used for the leading edge (de Croon et al., 2012). This flexibility leads to a complex interaction between fluid and structure. Being able to explain this interaction is crucial in order to improve the designs.

The aerodynamic behaviour of the DelFly was studied by performing PIV measurements (de Croon et al., 2012). It was found that the DelFly, just like insects, appeared to have unsteady lift enhancing mechanisms: the DelFly forms Leading Edge Vortices (LEVs) and uses the clap-and-peel mechanism, which is similar to the clap-and-fling mechanism as described in section 3-3-3.

Since the DelFly's airfoil is very thin, flow separation occurs directly at the leading edge for high angles of attack. However, the wing does not stall because of reattachment further down the chord of the airfoil: a LEV is generated. The result is a suction force on the upper surface of the wing that increases both lift and drag.

By using the second lift-enhancing mechanism, the clap-and-peel, the Delfly has an 8% increase in thrust over isolated wings (de Croon et al., 2012). Flow fields derived from PIV show that the clap generates a downward momentum jet, while the peeling of the wings generates a down flow as well as a span-wise flow, see Figure 4-2. Both these effects are thought to increase thrust generation. In this picture, the vectors represent the velocity direction and magnitude, and the background color represents the absolute velocity in-plane. Also visible are leading edge vortices near the leading edge of the wings. Since the wings themselves partly inhibit the PIV measurements due to shading, areas which have low reliability have been masked.

4-1-4   DelFly flight dynamics

Similarly as the research presented for insect flight in section 3-4-1, also the flight dynamics of the DelFly have been researched. Armanini et al. (2015) has identified the forward flight dynamics of the DelFly, although the model is based on a DelFly II with tail surfaces. Because of this, it is not possible to identify the moments required to actively stabilize the DelFly, however, the research can be used to get an idea of the control and stability of the present tailed DelFly, as well as set benchmarks for he present research. Here, the model and
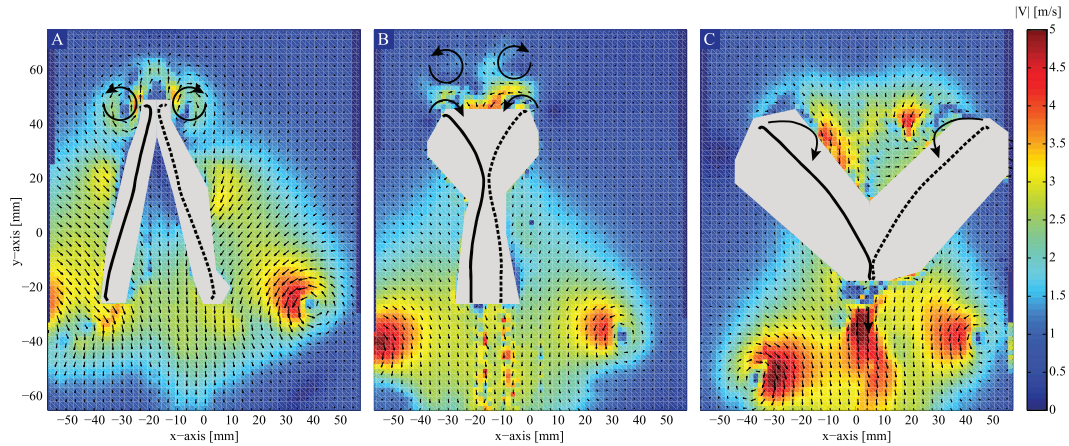
Figure 4-2: Velocity vector field of the DelFly during clap-and-peel at $13\,\mathrm{Hz}$ at a spanwise location of $0.71R$. Adapted from de Croon et al. (2012)
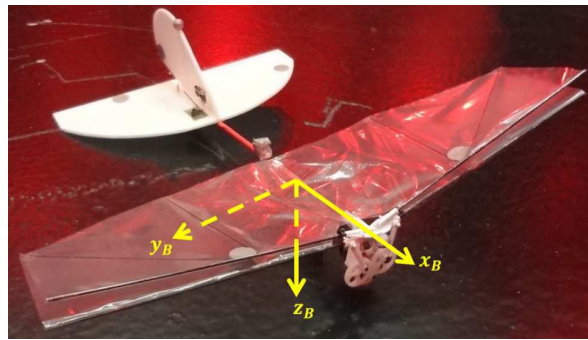
Figure 4-3: Body axis system of the dynamic model, adapted from Armanini et al. (2015)

parameter estimates will be presented, however, for a tail-less DelFly the situation will be different, and thus the parameters need to be estimated again. For the tail-less version of the DelFly, the attitude moment damping terms are expected to be much lower, since there is no damping effect from tail surfaces.

The model structure as described by Armanini et al. (2015) is split in a time-varying component and a time-averaged component, they consist of the fast time-scale processes and the cycle averaged effects, respectively. This time-scale separation assumption appeared to be valid for steady flight, however during maneuvers it was found that the model did not capture all of the time-varying dynamics. The axis system used in this research is different from the present research, it is rotated 90 degrees about the Y-axis, such that x_b is parallel to the flapping axis, see Figure 4-3.

For present research it suffices to only use the cycle-averaged component, since we want to know that the resulting long-term dynamics are when a control moment is applied to the model for the tailed version of the DelFly. Additional model identification is needed to calculate the (time-varying) control moments needed to stabilize a tail-less DelFly, this model should be based on the dynamics without a tail.

First, a linear model structure is defined for each of the six forces and moments:

$$X = X_q \Delta q + X_u \Delta u + X_w \Delta w + X_{\delta_e} \Delta_e + mg \sin \Theta_0 \tag{4-1}$$

$$Y = Y_p \Delta p + Y_r \Delta r + Y_v \Delta v + Y_{\delta_r} \Delta \delta_r \tag{4-2}$$

$$Z = Z_q \Delta q + Z_u \Delta u + Z_w \Delta w + Z_{\delta_e} \Delta \delta_e - mg \cos \Theta_0 \tag{4-3}$$

$$L = L_p \Delta p + L_r \Delta r + L_v \Delta v + L_{\delta_r} \Delta \delta_r \tag{4-4}$$

$$M = M_q \Delta q + M_u \Delta u + M_w \Delta w + M_{\delta_e} \Delta \delta_e \tag{4-5}$$

$$N = N_p \Delta p + N_r \Delta r + N_v \Delta v + N_{\delta_r} \Delta \delta_r \tag{4-6}$$

where X,Y,Z are the aerodynamic forces along x_b, y_b and z_b, L,M,N, are the aerodynamic moments around those axes, Δ is a perturbation value, Y_p, Y_r,..., are aerodynamic derivatives and δ_e, δ_r is the elevator and rudder deflection, respectively, These forces are substituted in a set of equations of motion to obtain the cycle averaged longitudinal dynamics:

$$\begin{bmatrix} \Delta \dot{q} \\ \Delta \dot{u} \\ \Delta \dot{w} \\ \Delta \dot{\Theta} \end{bmatrix} = \begin{bmatrix} \frac{M_q}{I_{yy}} & \frac{M_u}{I_{yy}} & \frac{M_w}{I_{yy}} & 0 \\ \frac{X_q}{m} - w_0 & \frac{X_u}{m} & \frac{X_w}{m} & -g \cos \Theta_0 \\ \frac{Z_q}{m} + u_0 & \frac{Z_u}{m} & \frac{Z_w}{m} & -g \sin \Theta_0 \\ 1 & 0 & 0 & 0 \end{bmatrix} \begin{bmatrix} \Delta q \\ \Delta u \\ \Delta w \\ \Delta \Theta \end{bmatrix} + \begin{bmatrix} \frac{M_{\delta_e}}{I_{yy}} & b_{\dot{q}} \\ \frac{X_{\delta_e}}{m} & b_{\dot{u}} \\ \frac{Z_{\delta_e}}{m} & b_{\dot{w}} \\ 0 & b_{\dot{\Theta}} \end{bmatrix} \begin{bmatrix} \Delta \delta_e \\ 1 \end{bmatrix} \tag{4-7}$$

and the lateral dynamics:

$$\begin{bmatrix} \Delta \dot{p} \\ \Delta \dot{r} \\ \Delta \dot{v} \\ \Delta \dot{\Phi} \end{bmatrix} = \begin{bmatrix} \frac{I_z}{I_c}L_p + \frac{I_{xz}}{I_c}N_p & \frac{I_z}{I_c}L_r + \frac{I_{xz}}{I_c}N_r & \frac{I_z}{I_c}L_v + \frac{I_{xz}}{I_c}N_v & 0 \\ \frac{I_{xz}}{I_c}L_p + \frac{I_x}{I_c}N_p & \frac{I_{xz}}{I_c}L_r + \frac{I_x}{I_c}N_r & \frac{I_{xz}}{I_c}L_v + \frac{I_x}{I_c}N_v & 0 \\ \frac{Y_p}{m} + w_0 & \frac{Y_r}{m} + u_0 & \frac{Y_v}{m} & g \cos \Theta_0 \\ 1 & \tan \Theta_0 & 0 & 0 \end{bmatrix} \begin{bmatrix} \Delta p \\ \Delta r \\ \Delta v \\ \Delta \Phi \end{bmatrix} + \begin{bmatrix} \frac{I_z}{I_c}L_{\delta_r} + \frac{I_{xz}}{I_c}N_{\delta_r} & b_{\dot{p}} \\ \frac{I_{xz}}{I_c}L_{\delta_r} + \frac{I_x}{I_c}N_{\delta_r} & b_{\dot{r}} \\ \frac{Y_{\delta_r}}{m} & b_{\dot{v}} \\ 0 & b_{\dot{\Phi}} \end{bmatrix} \begin{bmatrix} \Delta \delta_r \\ 1 \end{bmatrix} \tag{4-8}$$

where $I_c = I_x I_z - I_{xz}^2$. Just as for the case of the natural dynamics, as discussed in section 3-4-1, the states are perturbations from a steady condition.

The unknown aerodynamic derivatives are estimated using a maximum likelihood estimation, using measurements from a flight test. The resulting parameters are given in Tables 4-1 and 4-2.

Table 4-1: Parameter estimates $\hat{\Theta}$ and their estimated standard deviations $\hat{\sigma}$ for the cycle averaged longitudinal model. Adapted from Armanini et al. (2015)

Param.	$\hat{\Theta}$	$|\hat{\sigma}|$	$100\left|\hat{\sigma}/\hat{\Theta}\right|$	Param.	$\hat{\Theta}$	$|\hat{\sigma}|$	$100\left|\hat{\sigma}/\hat{\Theta}\right|$	Param.	$\hat{\Theta}$	$|\hat{\sigma}|$	$100\left|\hat{\sigma}/\hat{\Theta}\right|$
X_q	3.05E-03	2.9E-05	0.95	Z_q	-1.31E-02	2.87E-05	0.22	M_q	-1.03E-03	1.46E-06	0.14
X_u	-3.39E-02	1.48E-04	0.44	Z_u	-3.21E-02	2.18E-04	0.68	M_u	3.90E-03	8.76E-06	0.22
X_w	1.81E-02	8.58E-05	0.47	Z_w	-7.74E-02	1.29E-04	0.17	M_w	2.59E-03	4.15E-06	0.16
X_{δ_q}	2.53E-02	2.23E-04	0.88	Z_{δ_q}	-9.67E-02	1.93E-04	0.20	M_{δ_q}	-6.96E-03	1.19E-05	0.17

Table 4-2: Parameter estimates $\hat{\Theta}$ and their estimated standard deviations $\hat{\sigma}$ for the cycle averaged lateral model. Adapted from Armanini et al. (2015)

| Param.	$\hat{\Theta}$	$|\hat{\sigma}|$	$100\left|\hat{\sigma}/\hat{\Theta}\right|$	Param.	$\hat{\Theta}$	$|\hat{\sigma}|$	$100\left|\hat{\sigma}/\hat{\Theta}\right|$	Param.	$\hat{\Theta}$	$|\hat{\sigma}|$	$100\left|\hat{\sigma}/\hat{\Theta}\right|$
Y_p	3.76E-02	1.39E-02	36.90	L_p	-7.14E-06	3.80E-07	5.33	N_p	-1.98E-05	3.61E-06	18.18
Y_r	-1.49E-01	6.90E-02	46.22	L_r	3.09E-05	1.81E-06	5.86	N_r	-4.79E-04	1.43E-05	2.98
Y_v	-5.70E+00	1.36E-01	2.39	L_v	-4.47E-05	2.84E-06	6.36	N_v	-1.45E-03	2.46E-05	1.70
Y_{δ_r}	-4.00E-00	2.02E-01	5.04	L_{δ_r}	6.89E-05	3.91E-06	5.67	N_{δ_r}	-2.10E-03	2.81E-05	1.34

4-2   Flight control in FWMAVs

The generation of lift force in FWMAVs is a key research topic, since it is an essential element necessary for flight. However, to attain flight, the vehicle should also be controllable and be stable. In order for that to be the case, also the moments required to control the attitude of the aerial vehicle should be generated.

The DelFly features tail surfaces to control the roll, pitch and yaw angles; the deflection of these tail surfaces is used to control these attitude angles. Tail stabilizers in the wake of the wings keep the DelFly passively stable by increasing its aerodynamic damping (De Wagter et al., 2014). Numerous other research groups have also developed FWMAVs, some which are tail-less. Since these tail-less FWMAVs are, like their natural counterparts, unstable, they require a feedback system that senses the (changes) in the attitude and that generates moments to stabilize the FWMAV around its pitch, roll and yaw axes.

When studying natural flight, Section 3-4-2, it can be learnt that the parameters of a fly that determine the aerodynamic forces are the stroke amplitude, flapping plane orientation, timing and duration of the wing rotation and posture deviations. Also the angle of attack during flapping - which is often generated passively due to fluid-structure interaction since the material is flexible - has an influence on the forces generated (Fry et al., 2003).

Indeed, the wing mechanisms which have been employed for attitude control of tail-less FW-MAVs mostly make alterations in these kinematic wing parameters in order to alter the aerodynamic properties. The result is that these FWMAVs control their flight by changing the generation of thrust asymmetrically, or by changing the drag of the wings throughout the stroke, such that there is a net moment generated. The ways that these flappers manage to change these properties, can be divided in two main categories. The first strategy is to control the attitude by **changing the flapping kinematics**, by modulating the wing flapping amplitude, mean wing position and differences in wing velocity. This mechanism is explained in section 4-2-1. A second mechanism of attitude control moment generation is by **physically deforming the wings**, for example by changes in wing camber -pitch or -twist, this strategy is elaborated in section 4-2-2.
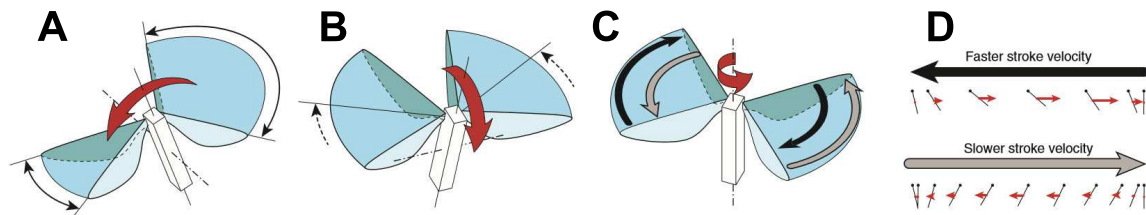
Figure 4-4: Attitude control for robotic fly by Ma et al. Image adapted from Ma et al. (2013).

4-2-1   Flapping kinematics control by FWMAVs

A first approach used for the control of FWMAVs without using tail surfaces is through a change of flapping kinematics, such as changing the wing flapping amplitude, mean wing position and wing velocity control.

Ma et al. (2013) have demonstrated this strategy with a robotic fly driven by piezoelectric flight muscles. As opposed to frequency modulation in other FWMAVs such as the DelFly, this system uses amplitude modulation to control the level of thrust, such that it remains at resonance. The robotic fly has two flight muscles, allowing each wing to be controlled independently. Because of this, control moments can be generated about all body-axes: it can control both the pitch, roll and yaw attitude. Ma et al. (2013) control system resembles that of natural flies, it uses wing stroke amplitude control (see Section 3-4-3). Roll is generated by introducing an asymmetry in wing stroke amplitude, as depicted in Figure 4-4-A. The pitch moment is generated by moving the mean wing position forward or backwards, such that thrust is generated more in the front or more at the back of the vehicle (Figure 4-4-B). Lastly, yaw (Figure 4-4-C-D) is generated by modulating the drag forces within the stroke. This is done by having an offset in stroke velocity between the up- and downstroke, using the knowledge that a higher stroke velocity results in more drag. By introducing an imbalance of velocities between the left and right wing, a net drag force is created, resulting in a yaw moment. Although Ma et al. (2013)'s fly needed to be tethered to the ground, it was able to achieve hovering flight and basic maneuvers, proving that a change in the flapping kinematics can result in stable flight. Unfortunately the mechanism from Ma et al. (2013) is not feasible for present research, because of its added complexity of piezoelectric flight muscles. The whole flapping mechanism would need to be changed, which is outside of the scope of this research.

Karásek et al. (2014) also modulates the kinematics of the flapping cycle to control their flapper, although with a different mechanism from Ma et al. (2013). Karásek et al. (2014) use a linkage mechanism connected to a single DC motor, which has a similar layout to the DelFly. Karásek et al. (2014) however use this to drive a single wing pair instead of using a biplane configuration. Via a joint displacement mechanism, both the amplitude and main wing position can be varied. The methods of roll and pitch creation are the same as was the case in Ma et al. (2013)'s research, by amplitude and mean wing position modulation, respectively. Karásek et al. (2014) mention that yaw can be created by changing the mean wing position asymmetrically, however, this was not demonstrated with results in this paper. For the DelFly this approach would mean a revision of the entire flapping mechanism. Now, the two wing pairs are coupled to each other, meaning that one of the wings on the left is kinematically connected to a wing on the right side of the fuselage. In order to change the mean flapping angle and the amplitude asymmetrically, a new flapping mechanism has to be

(a) Pitch control   **(b)** Yaw control
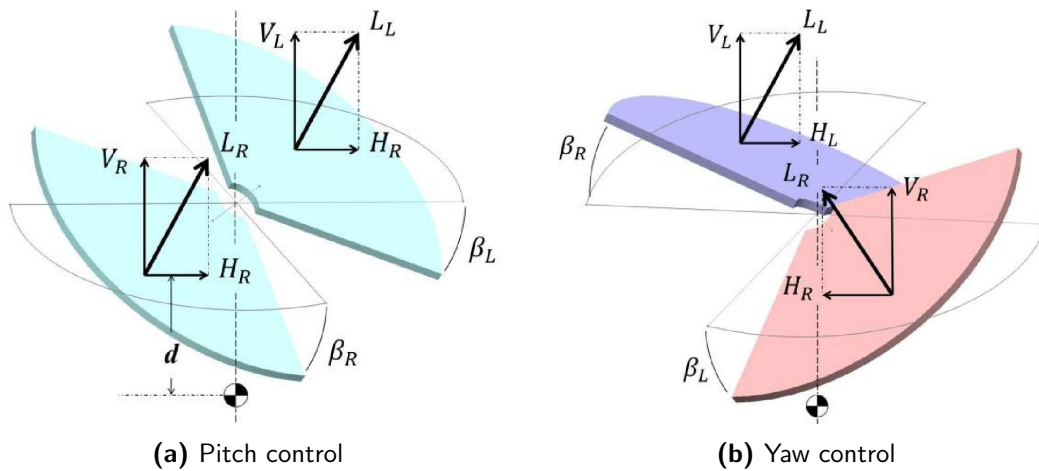
Figure 4-5: Schematic of wing plane modulation by Coleman et al. (2015).

designed without this coupling.

Coleman et al. (2015) follow a very similar approach as Karásek et al. (2014), by introducing changes in the linkages of the flapping mechanism. However, Coleman et al. (2015) use a different philosophy to control pitch and yaw. Instead of wing mean angle modulation, they rotate the entire flapping plane (Figure 4-5), resulting in a tilted lift vector. With this mechanism, Coleman et al. (2015) have demonstrated an untethered- and stable free-flight, being the first and only group demonstrating this feat in this category. However, it appears that the group managed to fly for about 5 seconds, after which it gets unstable. Coleman et al. (2015) recommend to improve the motor RPM control to increase the flight duration. Similar to Karásek et al. (2014)'s design, to implement this mechanism on the Delfly, a complete revision of the flapping mechanism is needed.

4-2-2   Control of FWMAVs using wing deformation

The second strategy is to deform the wings of the FWMAV by changes in twist or camber. A well-known research project in this area is the Nano Hummingbird (Keennon, Klingebiel, Won, & Andriukov, 2012), a small hovering ornithopter developed as part of a Defense Advanced Research Projects Agency (DARPA) program. It is a two-winged FWMAV, mimicking the appearance and flight characteristics of biological hummingbirds. During this research program, a total of fourteen prototypes were built, each getting closer to sustainable flight without using tail surfaces. The final prototype, the Nano Hummingbird, uses a string-based flapping mechanism, which consists of a rotating crank-shaft attached to two strings. These strings are each connected to two pulleys which are mounted on the wing hinge flapping axes, see Figure 4-6. The pulley system proved to have a flapping angle profile resembling a sinusoid more closely than a linkage based system, and seemed more symmetric (less left-right asymmetries).

Since this flapping mechanism links the left and right wing, similarly as the DelFly, the motion of the leading edge spars is fixed. Instead of changes in the flapping mechanism link layout to control amplitude and wing position, this mechanism uses a separate control system
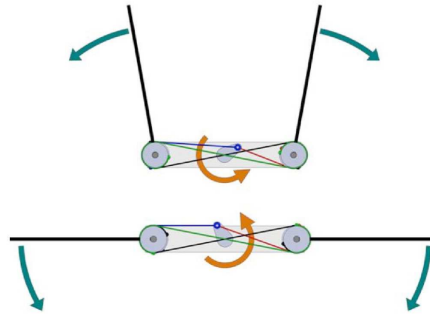
Figure 4-6: String based flapping mechanism lay-out. Adapted fromKeennon, Klingebiel, Won, & Andriukov (2012).

connected directly to the wings. During the conceptual phase, the focus was placed on two different mechanisms: wing rotation modulation (1) and twist modulation (2).

1. **Wing rotation modulation** The wings of the Nano Hummingbird are allowed to rotate, or 'pitch', passively around the leading edge, similarly to the DelFly. However, two adjustable 'stops' limit the extent in which each wing can pitch, see Figure 4-7a. This basically sets the nominal wing position during each half-stroke. This results in changes in both lift and drag. The system had acoustic noise and precision problems, and less efficiency than twist modulation, but it did allow for successful control.

2. **Twist modulation** With twist modulation, control moments are generated by varying the amount of twist in the wing foil. It was found experimentally that the lift and drag of the wing could be modulated by changing wing twist distribution. Similarly to the DelFly, the wing foil highly deforms during flapping, but this can be influenced by tightening or loosening the membrane. According to Keennon, Klingebiel, Won, & Andriukov (2012), a tight foil results in more lift, and a slack foil results in a decrease in lift. This effect can be used for control, by modulating the root spar position, as is shown in Figure 4-7b. If the root of the wing was moved laterally, this effected the slackness of the membrane primarily near the mid-stroke, which was used for roll control. If the roots of the wing were moved forward and backwards, this resulted in an effect near the end of the strokes, which was used for pitch. By combining the movements, it was shown by experiments that small changes in the twist of the wing resulted in large control moments, and resulted in a controllability of all three axes.

In the final prototype of the Nano Hummingbird, a hybrid between the two strategies was used to counter an undesired coupling with the roll axis during pitch and yaw commands. Wing rotation modulation was used for yaw control and wing twist modulation for roll and pitch control, since yaw seemed to have the highest authority with wing rotation and was easiest to implement. The final design of the control system of the Nano Hummingbird is depicted in Figure 4-8.

Synthesizing, the Nano Hummingbird is able to achieve free flight with its hybrid mechanism of wing deformation. However, since primarily the magnitude of the lift force is altered, one

(a) Wing rotation modulation

(b) Wing twist modulation
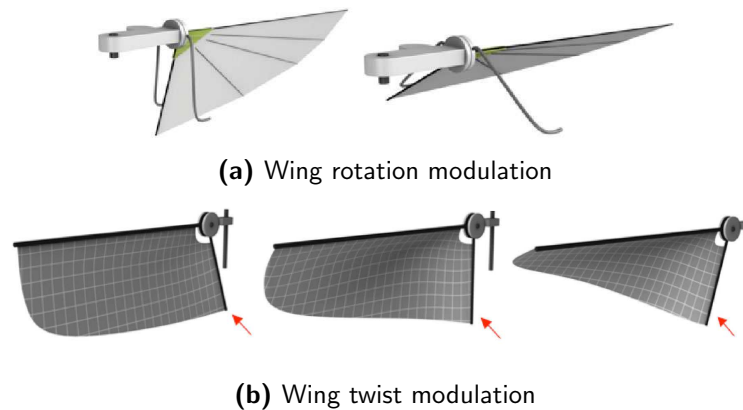
Figure 4-7: Control systems adapted from Keennon, Klingebiel, Won, & Andriukov (2012).

can conclude that on average the FWMAV flies at sub-optimal conditions, below its maximum lift. Also, the mechanism is very complex, while the goal of present research is to design a simple system to control the DelFly. However, the underlying methods, especially changing the twist distribution, are promising for present research because of the possibility of leaving the flapping mechanism the same and the high authority demonstrated by Keennon, Klingebiel, Won, & Andriukov (2012) looks promising.

Singh et al. (2005) uses wing deformation techniques as well to be able to generate different levels of thrust with a flapping wing. Although they did not have a flying prototype, they showed that with the inclusion of a torsional spring at the wing root, they could limit the passive pitch variation of the wings during flapping. By altering the torsional stiffness of the spring they could vary this pitch behaviour. This could be seen as a variation of wing rotation modulation from the Nano Hummingbird (Keennon, Klingebiel, Won, & Andriukov, 2012), but instead of modulating only the ends using 'stops', they modulate the entire passive pitching motion by using a spring.

Also in the research performed by Tokutake et al. (2009) wing deformation is used to generate control moments. Tokutake et al. (2009) however, starts with a different prototype, a four-winged FWMAV, a similar lay-out as the DelFly. In this research, the control moments are generated by actively controlling the pitch and camber of the wings. This was done by tensioning the wing skin with a thread connected to a servo motor, see Figure 4-9. With this method, an angular acceleration in pitch was achieved of $2.2 rad/s^{-2}$. This system was only tested statically for pitch. For roll, it is recommended in this paper to asymmetrically constrain the wings.

The mechanism by Tokutake et al. (2009) is simple and lightweight. It only consists of a string attached to the wings, and a servo to control the tension in this string. The method has however only been proved for pitch control, for yaw and roll control additional research is needed.

4-2-3   Synthesis: Which control system to use for the DelFly

As became clear from this section, many research groups of FWMAV design draw their inspiration from the natural flyers. The DelFly however does not as of yet use inspired-by-nature

Figure 4-8: Assembled control system as found in the Nano Hummingbird. Adapted from Keennon, Klingebiel, Won, & Andriukov (2012).
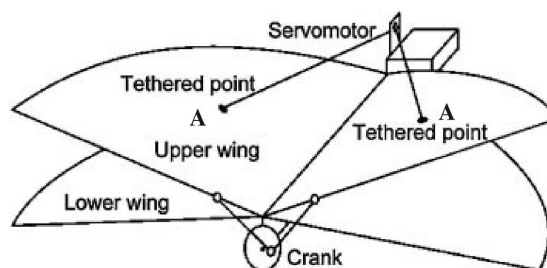
Figure 4-9: Attitude control system (pitch) by using threads connected to a servomotor. Adapted from Tokutake et al. (2009).

control methods, but uses conventional tail-surfaces. Due to the biplane configuration and linked flapping mechanism of the DelFly, the options to control the DelFly using changes in flapping kinematics or wing deformation are limited. Certainly a change in flapping kinematics will be difficult, since the entire flapping mechanism will have to be redesigned, which is not in the scope of this research.

Thus, when considering a control mechanism based on wing deformation, several options have been identified. One can change the twist angle of the wings by displacing the wing root, as is done on the Nano Hummingbird (Keennon, Klingebiel, Won, & Andriukov, 2012), however, this mechanism has a complex design, while the goal of this research is to design a simple system. In contrast, the mechanism used by Tokutake et al. (2009), which changes the angle of attack of the wings during flapping by constraining the wings with a string attached to a servo, is very simple and lightweight. Furthermore, it has been demonstrated on a biplane configuration similar to DelFly. However, Tokutake et al. (2009) have only demonstrated pitch control using this system, and recommended that lateral control can be achieved by asymmetrically tensioning the wings.

Tokutake et al. (2009)'s system only works in part of the stroke, because of the direction of the string. In this part, the angle of attack of the wings is altered due to the constrain from the string. Next to the importance of the angle of attack, it has been proven that the lift generation of the DelFly is also dependent on the stiffness of the wings (de Croon et al., 2012), since the passive rotation of the wings is dependent on stiffness of the structure. Also, in the research of Keennon, Klingebiel, Won, & Andriukov (2012), they found a dependency of the stiffness of the foil and the amount of lift generated.

It is therefore recommended to use a mechanism similar to Tokutake et al. (2009) to vary the tension, or stiffness, in the structure independently on each wing of the DelFly with a string. In this way, the passive rotation motion can be controlled with a simple system. The extent of the rotation will also change, because if the structure is more flexible, the extent of the wing rotation will also increase. The effect of this was already seen on the Nano Hummingbird (Keennon, Klingebiel, Won, & Andriukov, 2012), resulting in a modulation of the lift force of the wings. An experiment is needed where each of the four wings can be controlled independently. The results of this experiment should provide insight whether it is indeed possible to generate all of the three control moments independently with this method.

In the next part of this thesis, two concepts using wing tension modulation are described, which are experimentally tested on their moment generation.

Chapter 5

Requirements of DelFly control mechanism

In order to assess the various prototypes which are developed for this research, it is important to set quantitative and qualitative requirements, which meet the research goal of controlling the DelFly with its wings. However, a model for a four-winged tail-less FWMAV is not readily available in research. Therefore, the performance of other active control FWMAVs is studied, with a focus on moment generation magnitude and control mechanism lag time. In the rest of this chapter, first a summary of the requirements is presented, and after the ones that require more elaboration are explained in detail.

The requirements for active control, which also hold for active stabilization, are identified in order of importance:

1. **Low weight** Since the mechanism needs to be eventually able to fly, the weight of the mechanism should be low. The weight of the complete structure should be less than 23 grams (the weight a DelFly is able to lift, empty weight and payload).

2. **High control moment generation** The moments for controlling the DelFly need to be able to control the DelFly, and preferably also be able to mitigate disturbing forces and moments when flying tail-less. For stable, tail-less flight, the pitch and roll angles should be stabilised. The yaw moment controls the heading. Since a model for the DelFly tail-less dynamics is not available, it is hard to come up with an accurate requirement. From reference data from other tailless FWMAVs (see section 5-1), it is thought to be in the order of 1 to 3 Nmm.

3. **Repeatable and spectrum wide** For the vehicle to be controllable, the moments that are generated should be repeatable, i.e. a certain control input should always generate the same control moment. Also, the vehicle should be able to generate both positive and negative moments, and the moments should preferably be able to be generated with a linear relationship between input and resulting moment.

4. **Low cross-coupling** All three of the axes need to be controlled **independently**. If cross-coupling exists between the various servo commands, a combined command should be able to nullify this coupling, else undesirable movements will result, and drift will be likely.

5. **Fast actuation** The lag time of the control mechanism should be low (i.e. the time between a command and the moment production). This requirement is mostly necessary for the tail-less case, in order to timely mitigate disturbances. An initial requirement is set in the order of 0.1s for full actuation, reference data is used from comparable vehicles, see Section 5-2.

5-1   Required control moments for control and stabilization of the DelFly

As mentioned in the previous section, the requirement for the minimum control moments is set by taking reference vehicles as an example. Keennon, Klingebiel, & Andriukov (2012) mention that *"one of the more dramatic flight demonstrations was an autonomous 360° flip in the roll axis"*, and that the servos were fully deflected during this manoeuvre. This manoeuvre is shown in Figure 5-1.

In order to produce this figure, the graph from Keennon, Klingebiel, & Andriukov (2012) for the roll velocity was digitalized. The integral and derivative was taken for this data to get the roll angle and roll acceleration, respectively. From Newton's second law of rotation:

$$M_x = I_{xx}\ddot{\phi} \tag{5-1}$$

where M_x is the roll moment, I_{xx} is the roll moment of inertia and ϕ is the roll angle.

However, this considers M_x as the external moment, which consists of both the moment due to control input, but also effects acting in the opposite direction, such as skin friction, and flapping counter-torque (Cheng & Deng, 2011).

When capturing these effects in a roll damping term, L_p, which is equated with the roll velocity and moment of inertia to get the counter torque, this equation can be written as

$$\ddot{\phi} = \frac{L_p}{I_{xx}}\dot{\phi} + \frac{1}{I_{xx}}M_x \tag{5-2}$$

This equation can also be considered as a one degree of freedom excerpt of the model of Armanini et al. (2015), with a moment input instead of a control deflection.

Cheng & Deng (2011) provides semi-analytical equations to calculate the roll damping term. However, this requires details about the flapping kinematics of the Nano Hummingbird which are not available. Therefore, the non-dimensional value for the Hawkmoth (*Manduca sexta*) is taken, $L_p^+ = -0.81$ (Cheng & Deng, 2011), which is the closest insect described in the paper compared to the Nano Hummingbird in size.

This value for L_p^+ is nondimensionalized by (Cheng & Deng, 2011):

(a) Roll angle

(b) Roll rate

(c) Roll acceleration

(d) Required roll moment
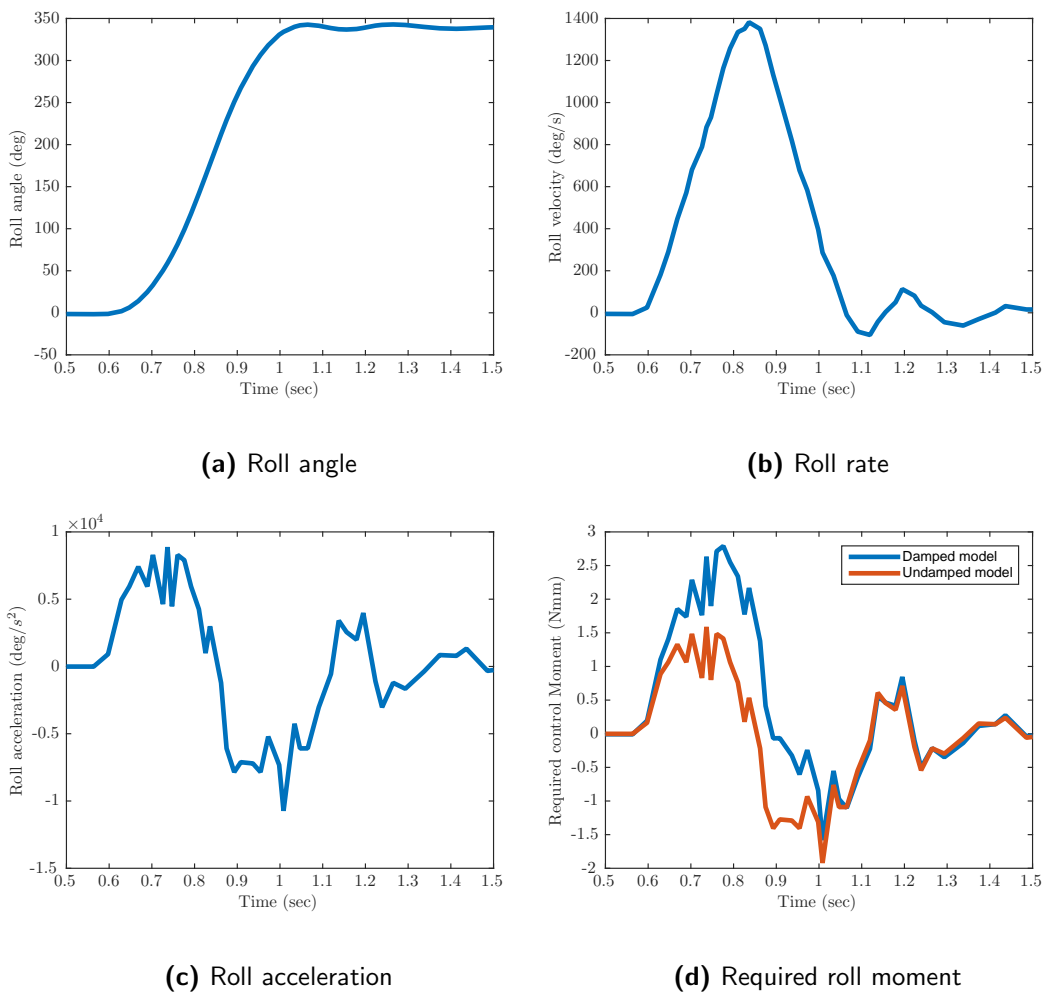
Figure 5-1: 360° lateral flip by the Nano Hummingbird. Data for angular velocity from Keennon, Klingebiel, & Andriukov (2012)

Table 5-1: Dimensions and other constants of Nano Hummingbird. Data from Keennon, Klingebiel, & Andriukov (2012) and estimations.

Variable	Value	Unit
R	7.4×10^{-2}	m
$\bar{c}$	2.5×10^{-2}	m
ρ	1.225	kg/m^3
Φ	170	deg
n	30	Hz
$\hat{r}_2$	0.505	[-]
L_p^+	-0.81	[-]
I_{xx}	1.026×10^{-5}	$kg \cdot m^2$

$$L_p = \rho U^2 R \bar{c}^2 L_p^+ \tag{5-3}$$

where $U = 2\Phi n R \hat{r}_2$.

This result in a damping coefficient of $L_p = -6.77 \cdot 10^{-5}$. The dimensions of the Nano Hummingbird used to calculate L_p, which are either from Keennon, Klingebiel, & Andriukov (2012) or by estimation, are summarized in Table 5-1.

With these parameters, an estimate can be made for the required roll control moment needed to perform this manoeuvre with the Nano Hummingbird. The result of the undamped and damped one degree of freedom model is shown in Figure 5-1d, indicating a maximum M_x of 2.8 Nmm.

With this value for M_x, it is possible to make a fast 360° roll flip. Clearly, the 360° roll flip described above is an extreme manoeuvre and is not the value that is required for regular manoeuvres and stabilization, also, the dimensions and flapping frequency for the Hummingbird are different. However, it does provide a benchmark to which we can later test the generated moments in this thesis. For now, we can estimate that the order of magnitude for the moment generation of a tail-less FWMAV is 1-3 Nmm.

Also the attitude hold mode of the robotic fly by Ma et al. (2013) is analysed. In Figure 5-2 the commanded and measurement torque is depicted, as well as the resulting angular rate. For stabilisation, a roll torque in the order of $1\mu Nm$, a pitch torque of $0.4\mu Nm$ and a yaw torque of $0.5\mu Nm$ was commanded, for a device of 80 mg (Ma et al., 2013). Note that for the yaw axis, no proportional term was used, since by design Ma et al. (2013) only control the yaw rate, since the specific yaw angle for stabilisation does not matter. These features of the robotic fly are however hard to relate back to the DelFly because of the scale differences.

5-2 Required actuation speed for control and stabilization of the DelFly

In order to control the DelFly with the proposed mechanism, it would also be desirable to reduce the lag time, and a low lag time is even required in order to stabilize the DelFly to timely mitigate destabilizing external forces and moments. For this requirement, the lateral
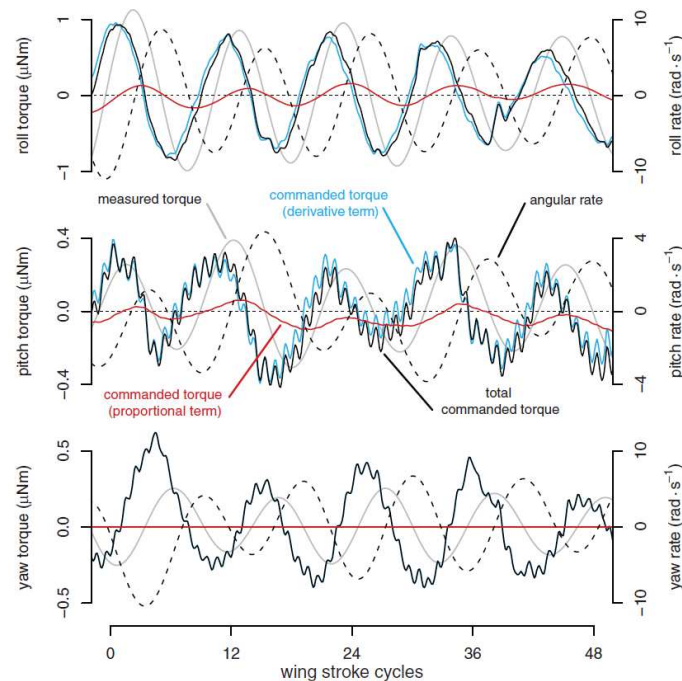
Figure 5-2: Commanded torque magnitudes during hover of the Harvard Robotic Fly, Adapted from Ma et al. (2013)

flip of the Nano Hummingbird (Keennon, Klingebiel, & Andriukov, 2012) can again be used as a reference. In Figure 5-3 the roll position command and feedback for the lateral flip described in the previous section is plotted. It takes $0.09s$ between the step command and when the command is actually reached, which gives an indication of the time it for the Nano Hummingbird to switch from extreme servo positions. This in turn is indicative for the servo speed that we need to fly tailless.

For the Harvard Robotic Fly (Figure 5-2), the delay is approximately two wing-stroke cycles. With a flapping frequency of 120 Hz, this means a lag time in the order of $0.02s$.

Concluding, for the DelFly, the required actuation speed is expected to be in the order of 0.1s for full stroke actuation.
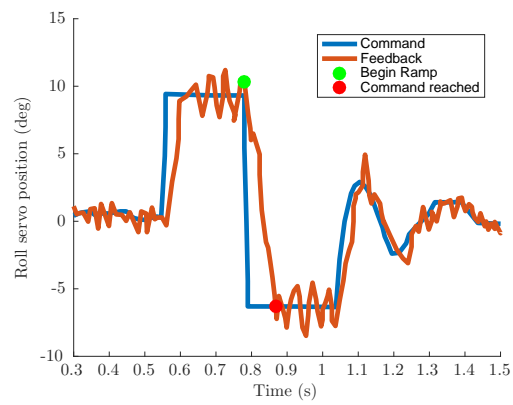
Figure 5-3: Roll servo position command and feedback for the 360° lateral flip of the Nano Hummingbird. Data retrieved from Keennon, Klingebiel, & Andriukov (2012)

Chapter 6

Methods and materials

In order to assess the concepts which will be described in chapters 7 and 9, a test setup is built which can measure the various forces and moments that are being generated, and also consists of other components that are used to explain the physical phenomena behind the control moment generation. In this chapter, first the requirements for the setup will be given, and in Section 6-2 the various components of the resulting test setup will be elaborated. This setup is used for concept A, and slightly adapted for testing concept B. The changes for the setup to measure concept B are described in Section 10-1.

6-1   Test setup requirements

To be able to assess the criteria as posed in section 5, the prototypes have to be experimentally tested. Experimentally, since to date it is still hard to accurately simulate flapping wings by solving the Navier-Stokes equations directly, because of the complex wing kinematics and deformation (De Clercq et al., 2009a).

The test setup has to be able to deform all of the four half-wings of the DelFly incrementally. These four inputs are the independent variables of this experiment. Additionally, to have the same conditions throughout, the flapping frequency should stay constant. The flapping frequency is chosen as 10 Hz, which is about the flapping frequency of the DelFly during flight (de Croon et al., 2012).

In the experiment it is important that all of the six forces and moments are measured with accuracy, to be able to assess the performance of both the control moment generation and to measure any changes in the other axis, notably the thrust force. These are the six dependent variables in the experiment. Also, to get an insight what happens with the wing motion during the wing warping control, high-speed photography needs to be incorporated in the test setup design such that the wing deformation at every flapping angle can be studied.

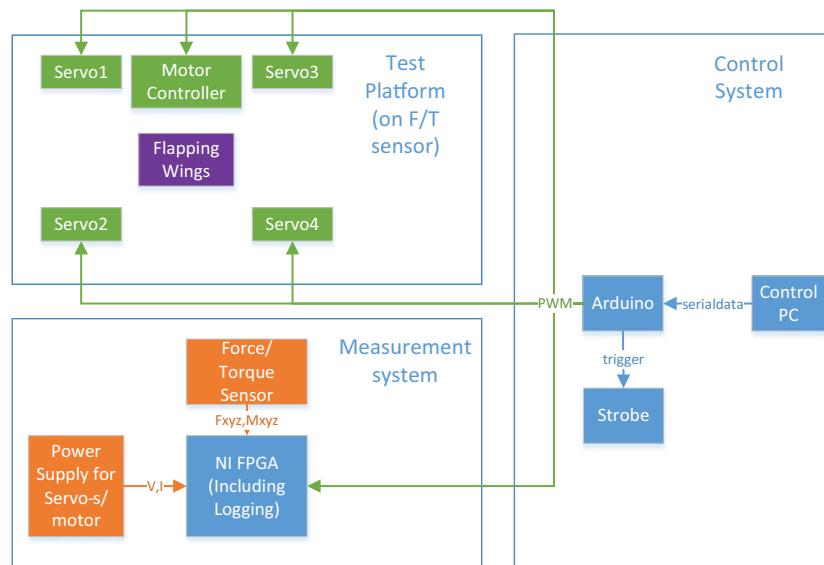In the next section the setup will be presented that is used measure these aspects of the DelFly prototypes.

Figure 6-1: Test setup overview

6-2   Measurement setup

A test setup is designed to allow the control of the independent variables and to measure the dependent variables, as described in the previous section. A schematic of this setup is shown in Figure 6-1. This setup consists of a 3D printed platform, on which the Delfly and four servo's are mounted. The motorcontroller of the DelFly and servo's are commanded by an Arduino Uno. The servos and motorcontroller are powered by a power supply with remote sensing, to compensate for the voltage drop across the output cables. This platform including DelFly and servos is mounted on a 6-axis force/torque sensor, which is connected to a National Instruments FPGA. Lastly, a stroboscope is connected to the Arduino, such that it will be synchronized with the flapping motion. In the following sections these modules are explained in more detail.

6-2-1   Mounting platform

For the test a mounting platform is designed and 3D printed. A picture of the setup is included in Figure 6-2. The platform has mounting points for a DelFly adapter, for four servos and for the force/torque sensor. The adapter features cable guides for the control threads that transfer the forces from the servos to the wings. The platform is designed such that the DelFly can easily be replaced and multiple designs can be tested.

6-2-2   DelFly

For the test a dedicated DelFly is built, consisting of four wings measuring 28 cm in span from tip to tip. The wings are made from 10 micron polyester membrane. They are hand built by using a template and a vacuum table, such that a high accuracy and repeatability is achieved and they are stiffened by carbon rods. The wing design is based on the wing optimisation by
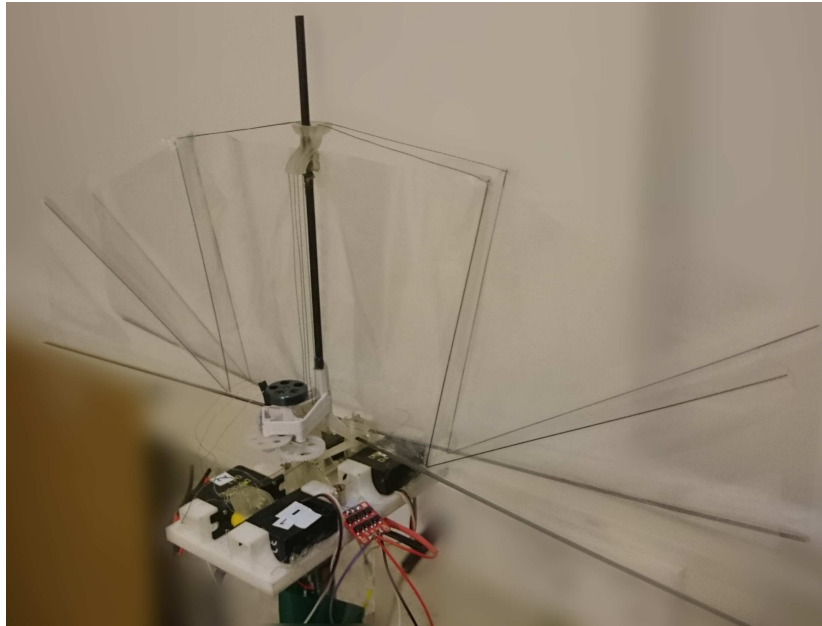
Figure 6-2: Picture of test platform with servos and DelFly

Groen et al. (2010). To eliminate any asymmetric effects in the flapping motion, a symmetric hinge flapping mechanism was 3D-printed, without a dihedral.

6-2-3 Control mechanism

In order to test the first prototype, in which the stiffeners of the wings are pulled inwards, four Dymond D47 servos are mounted on the Mounting platform. Attached to each wing is a $\varnothing 0.14$ mm Dyneema fishing line, which is led through the DelFly adapter to the servos, such that each wing can be deformed separately. On the servos a pulley system is designed such that the input to the servo relates linearly to the stroke output in the fishing line, see Figure 6-3 which relates the command in [%] to stroke in [mm] as will be used in the results for concept A. In section 7 is explained how the wings are deformed. The speed of the motor is controlled by a motor controller. This motor controller is programmed to give feedback by means of a pulse at each commutation of the motor. In turn, this feedback is used in a PID controller to control the frequency of the motor.

The servos and motor controller are commanded by an Arduino Uno. The Arduino Uno also houses the PID controller for the motor, keeping it constant at 10 Hz. The control signals to the servos and motor controller are PWM signals with a frequency of 50 Hz. A serial connection to the Arduino from a PC is used to enable the pulse width and flapping frequency to be adapted by using a simple GUI written in C# running on the PC.

6-2-4 Force/torque sensor

The platform rests on a Nano17 Titanium, a 6-axis transducer by ATI industrial automation. In Table 6-1 the calibration is shown for this sensor, which is the most sensitive calibration
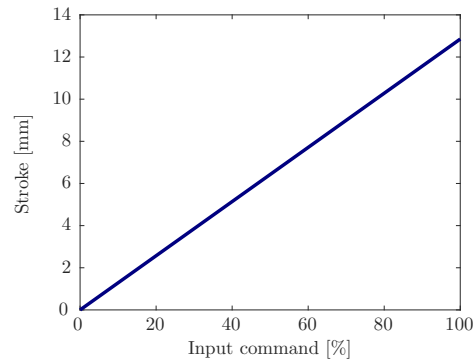
Figure 6-3: Command in [%] versus stroke in rope.

Table 6-1: Calibration of Nano17 Titanium sensor (SI-8-0.05)

Sensing ranges				Resolution			
Fx,Fy	Fz	Tx,Ty	Tz	Fx,Fy	Fz	Tx,Ty	Tz
8 N	14.1 N	50 Nmm	50 Nmm	1/682 N	1/682 N	3/364 Nmm	5/728 Nmm

for this sensor available.

6-2-5   Stroboscope and camera

To determine the deformation of the wing foil, a stroboscope synchronized with the flapping frequency is used. This was done by using the commutation feedback of the motor controller. By using the C# application, it is possible to freeze the motion at any location throughout the flapping cycle, by sending a pulse to the stroboscope each time the wing is at the requested position. A Canon DSLR is used to capture the images for closer inspection.
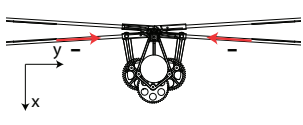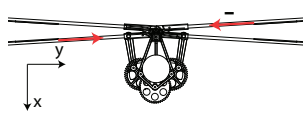
Chapter 7

Prototype design concept A
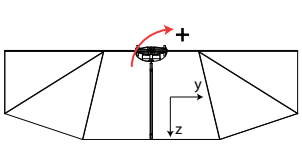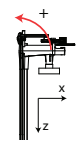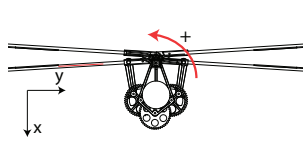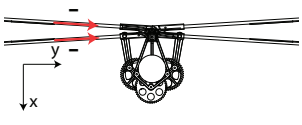
From the literature review it became clear that this research should focus on control by wing deformation. In the following chapters, a first concept is tested, consisting of threads connected to the first stiffener of the wings, connected to a servo motor. This philosophy of the control mechanism is similar to the one used in Tokutake et al. (2009). However, Tokutake et al. constrained the wings in a different direction to change the camber of the wings, in present research the stiffeners are pulled towards the root to increase the tension of the Mylar foil, see the schematic Figure 7-1 and picture of the test setup in Figure 6-2. This is done since research by Keennon, Klingebiel, Won, & Andriukov (2012) showed that for their prototype, a tight foil results in more thrust, and a slack foil results in a decrease of thrust.

Using this concept, each wing has a separate rope, allowing the tension of each wing foil to be controlled independently. This is represented in Figure 7-1 with C_1-C_4. Based on an early qualitative in-flight test, different control modes have been identified. By tensioning either the top two wings or the bottom two wings, the DelFly was found to pitch. By tensioning the left pair of wings or the right pair of wings (hereafter referred to as pair-input), the DelFly
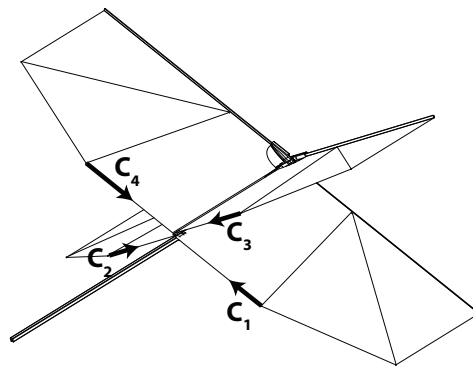
Figure 7-1: Prototype wing tensioning concept A. C_1-C_4 are the various degrees of freedom for control.

Table 7-1: Inputs and hypothesised resulting motion

Axis	Roll	Pitch	Yaw
Desired motion			
Hypothesized			

was found to make a turn. Also by tensioning the left top wing and right bottom wing or vice versa (hereafter referred to as cross-tensioning) the DelFly made a turn, although with a faster rotational speed than by pair-input. The turn was more effective and direct if cross-tensioning was applied. Unfortunately this test was performed before this research and was not documented, resulting in the directions of control being unknown.

The hypothesis for the mechanism of this test is defined as follows:

By pulling a wing stiffener towards the root, the wing foil is tensioned and as such this wing generates more thrust.

This hypothesis can be extended to explain why the DelFly was found to turn and why it could pitch in the early flight test using the wing tensioning control, see Table 7-1. If the left wing pair is tensioned, the thrust is increased on that side, and the vehicle will roll to the right. When the top wing pair is tensioned, the thrust on the top wing pair will increase and the DelFly will pitch down. Note that this hypothesis is not able to explain why the vehicle turns when a cross-tension input is applied, but it could be that next to a change in magnitude of he thrust force, also the direction changes. This hypothesis therefore also does not explain in which direction the DelFly will yaw if a yaw control input is given.

In order to test this hypothesis, to fully understand which moments are generated and how the wings are deformed during control, an experiment is designed, which is described in the next section.

Chapter 8

Experimental results of concept A

In order to be able to generate the control- and stabilisation moments about the axes, the thrust force of each wing needs to be either vectored or changed in magnitude, or the drag of a wing throughout the flapping cycle should be changed. To get more insights on the moment generation, first this thrust force (the force parallel with the hull) generated during the flapping cycle is studied, see section 8-1. Next, an attempt is made to control this force, in both direction (vectoring) and magnitude, conforming to the hypothesis. However, during testing it appeared that the hypothesis that states the moments are generated due to a change in wing foil tension and therefore thrust is not true, it appeared that another mechanism is responsible for the moment generation. In section 8-2 a theory is posed that captures the mechanism of this moment generation. This theory is based on force and moment measurements and photography with a stroboscope. After having explained this theory, the results of the experiment are shown and discussed in section 8-3. For the various control modes (cross-tensioning-, wing pair- and pitch input), the moments and forces generated due to the variations in wing input is shown. In this results section, the theory of section 8-2 is explained to explain the phenomena that occur.

8-1 Flapping cycle and thrust force

The force variations during a flapping cycle are shown in Figure 8-1. The filtered thrust is calculated by averaging ten flapping cycles, and then filtering it with a butterworth filter with a cut-off frequency of 30Hz. This will show the first three harmonics of the flapping motion. Percin (2016) shows that these first three harmonics can be reliably used for analysing the free-flight estimated forces, and this cut-off frequency will be used throughout this report when considering forces and moments within one flapping cycle. The time is non-dimensional, with $\tau = 0$ being the moment the hall effect sensor is triggered and $\tau = 1$ being the start of the next cycle. The wing motion during the cycle was already studied by De Clercq et al. (2009b), see Figure 8-2.

Starting from the instant $\tau = 0$, which is near the maximum leading edge stroke amplitude, the leading edge starts to decelerate and reverse direction. Due to inertia, the trailing edges
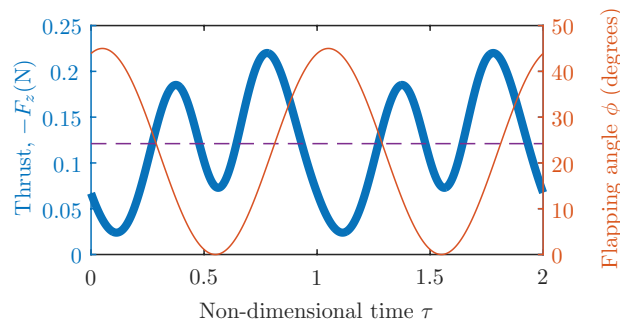
Figure 8-1: Thrust force variations and flapping angle ϕ during a flapping cycle. The dashed line indicates the average over the whole flapping cycle.
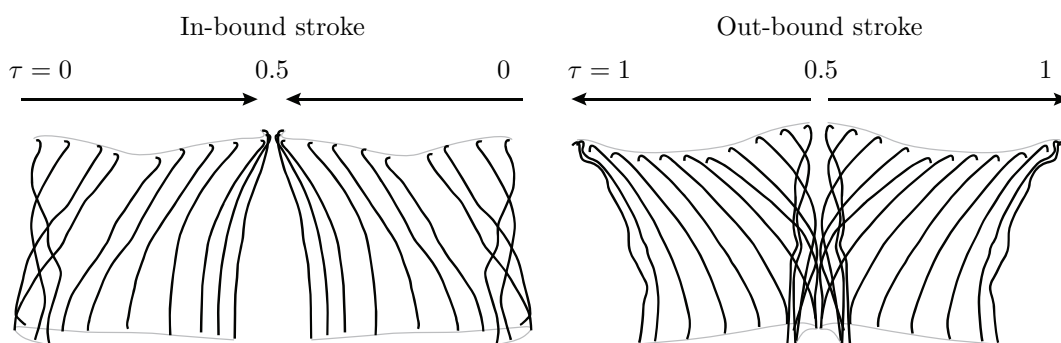
Figure 8-2: Wing deformation throughout the flapping cycle. Adapted (and editted) from de Croon et al. (2012), using the time-scale τ as presented in this paper.

remain temporarily stationary, and since he leading edge is already moving inbound again, this causes the wing to flex. At this moment, the force has a minimum value as seen in Figure 8-1. The DelFly has 'delayed rotation' (Section 3-4-2), since the wing starts to rotate after the stroke reversal has already occurred. According to the research of Dickinson et al. (1999), this has an adverse contribution to the thrust generation, however, he found this result by studying inflexible wings. Therefore this might not be an accurate theory for the flexible DelFly wings.

Continuing at $\tau = 0.25$ the two leading edges accelerate inbound and reach their maximum velocity. The force reaches a maximum due to foil being unflexed and the angle of attack being at its highest (De Clercq et al., 2009b). At $\tau = 0.5$ the leading edge spars start to approach each other and decelerate again, causing the camber of the wing to decrease. A second minimal peak is measured at the point the leading edges meet and reverse their direction. After the leading edges have met, the wing foil starts to clap together, with the contact point starting from the leading edge and moving towards the trailing edge. Next, the leading edges move outbound, increase their speed and the wings are cambered again. The foil starts to peel apart and is highly deformed. At this point, a maximum is measured, over a longer time span than the first peak; this 'peel' phase is most effective in thrust generation, and this marks the end of the clap-and-peel mechanism as was already explained in section 4-1-3.

Concluding, throughout the flapping cycle, it varies greatly how much thrust the wings generate. This feature can be exploited: a way to generate moments can be to spoil the thrust generation of (a pair of) wings, which has more effect when being done at the phases of maximum thrust generation. This is being used when designing the control mechanism of concept B, Section 10-2.

8-2 Theory of wing scoop control

To come up with a theory about the mechanism that generates the moments as will be shown in section 8-3, the individual flapping cycles were studied on both deformation and force/moment generation. This analysis is already presented before the force and moment results, since with the knowledge from this section the results can be explained more easily. To thoroughly test in what way the air is displaced, PIV measurements are necessary during flapping, which is outside the scope of present research. However, hypotheses can already be posed based on studying the stroboscopic pictures, and relating this to the time-history of forces and moments during a single flap.

The effect of controlling the wings using the ropes is studied using a stroboscope. The stroboscope was synchronised with the flapping motion by utilising the commutation feedback from the motor controller as explained in chapter 6. Using this stroboscope, it is possible to study each phase of the flap by freezing the motion. A Canon DSLR camera was used to capture this frozen motion.

As explained earlier, the reason behind pulling the wings inwards during flapping was to tension the foil of the wing. However, since the foil hardly has any stretch, it was found that during deformation also the leading edge bended inwards due to the stiffener moving towards the root. This results in a fold in the foil, which leads to another, unexpected method of moment generation.

In Figure 8-3 the stroboscopic pictures are shown for a neutral command, 40% single-winged command and 40% double winged command. The single-winged command picture is both a part of the pitch input and the cross-tension input. Figure 8-3c indicates a 40% wing-pair command. Apparent is that the string pulls the stiffener towards the root, which results in a fold in the foil of the controlled wing between the first stiffener and the hull. During the inbound flapping motion, as depicted in the figures, this results in a bubble in the foil.

Pictures throughout the flapping cycle for various τ are depicted in Figure 8-4. In these pictures, the top wing is tensioned with a command of 40%. An air bubble is both visible during in-bound and out-bound flapping.

The theory postulated here, is that this bubble generates extra drag and/or generates an extra momentum jet inwards, see the arrow representing the direction of the resultant force in Figure 8-3b. For the wing-pair command, the theory is that the useful components of the two drag forces cancel each other and therefore do not have a significant effect on any of the moments, as will be further explained in section 8-3.

8-3 Force and moment variations

The scoop(s) generated during the various inputs have implications on the moments generated during flapping. The various axes used throughout this chapter are defined in Figure 8-5. The moments shown in this section are calculated around the quarter chord point, on the axis of wing-rotation, as also indicated in the figure.

As already indicated earlier, the control modes are pitch input, cross-tension input and wing-pair input. These will be individually discussed in this section.

Pitch input

For the pitch input, which is generated by either tensioning the top two wings or the bottom pair, the relevant moment and force variations within a single flap are shown in Figure 8-6h and 8-6d. A positive pitch input is defined as tensioning both bottom wings with the corresponding servo input; a negative pitch input is achieved by tensioning the top pair of wings. In Figures 8-6a-c the cycle averaged moments are shown for a range of pitch inputs.

From Figure 8-6d it can be concluded that the input has an effect on the force F_x: during inbound motion of the leading edges the scoop generates a positive contribution for a positive command, with a maximum at the point of maximum velocity of the leading edge, at $\tau = 0.25$, and during outbound a negative one. This effect is proof for the scoop theory, both during inbound and outbound motion the formation of a scoop due to the control input results in a force perpendicular to the scoop. This force has, dependent on the location of the application point of the force with respect to the location of the center of gravity, an effect on the pitching moment. Figure 8-6h shows that the part where the scoop generates the highest drag force, also has the highest influence on the M_y pitching moment. During inbound flapping, a positive pitch input results in a higher moment than the neutral case, however, during outbound flapping the effect is the opposite. Concluding, a positive contribution of F_x generates a positive contribution to M_y. This would indicate that the point of application of
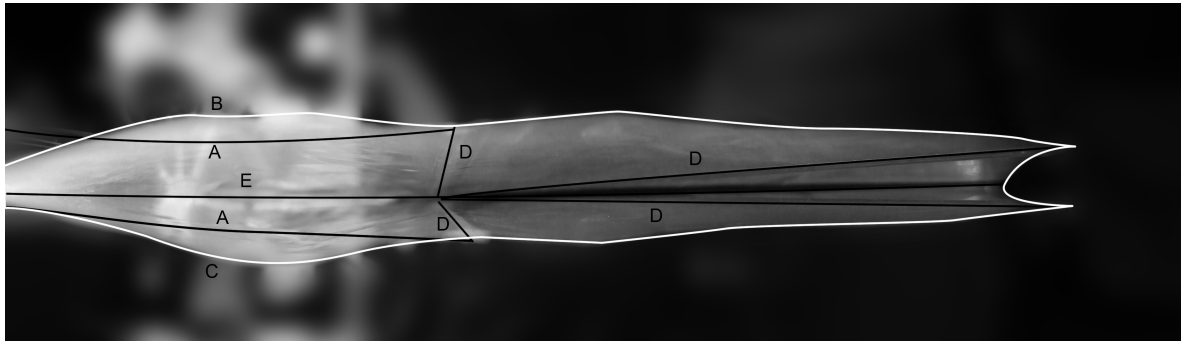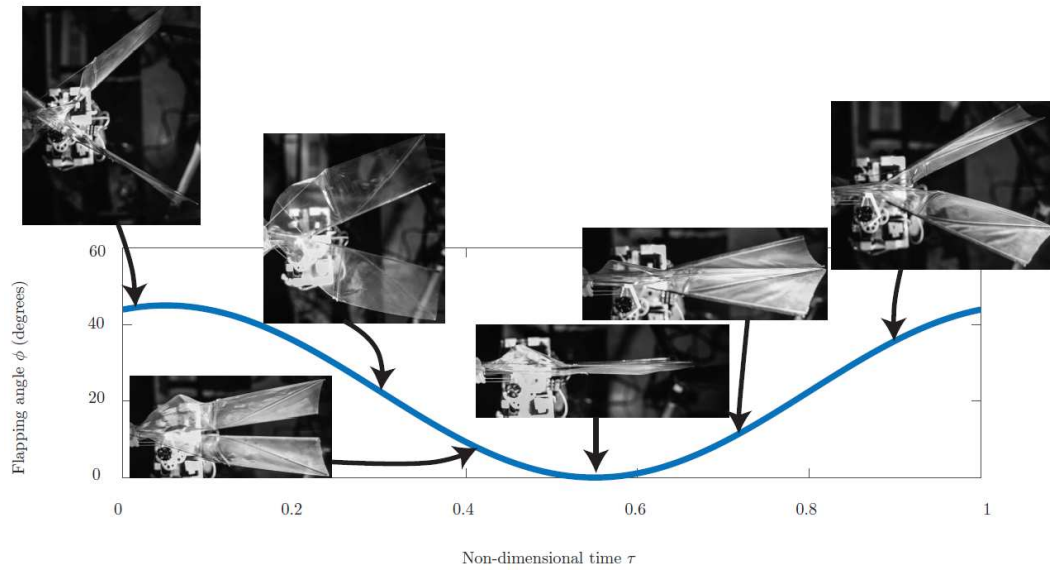
(a) Neutral command.
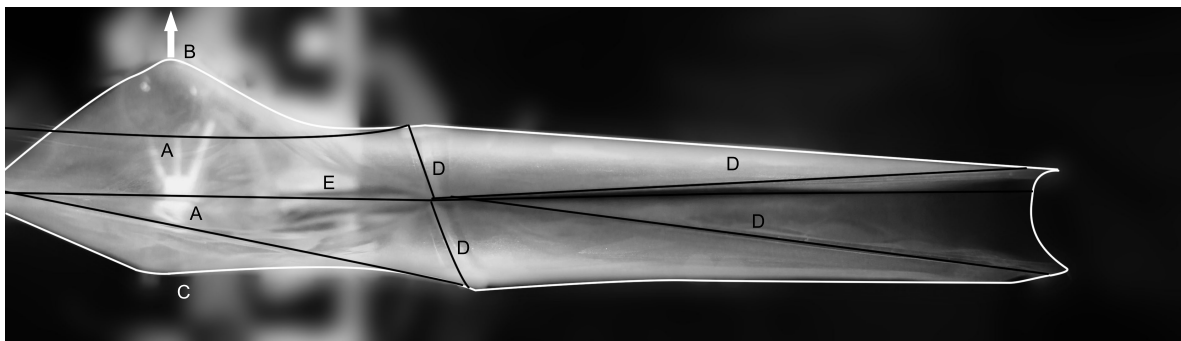
**(b)** One-sided command. The arrow represents the direction of the resultant force.
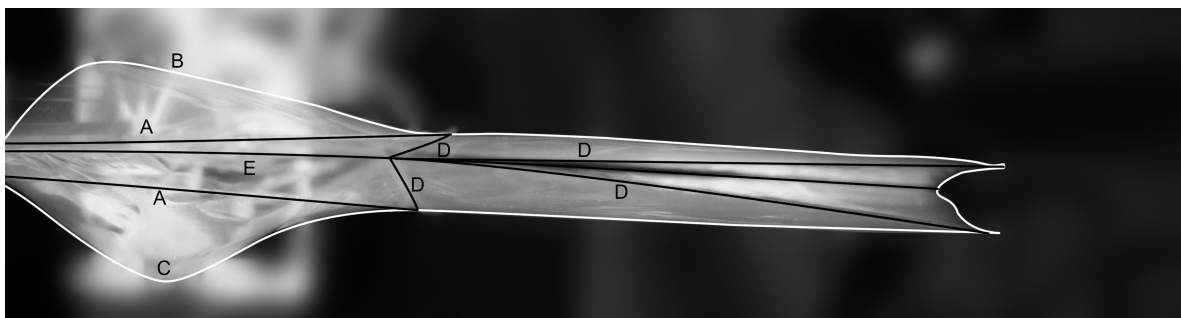
(c) Wing-pair command.

Figure 8-3: Enhanced stroboscopic pictures of wing with commands during fold-in. A: string, B: trailing edge of free-flapping wing, C: trailing edge of free-flapping wing, D: Stiffeners, E: Leading Edge
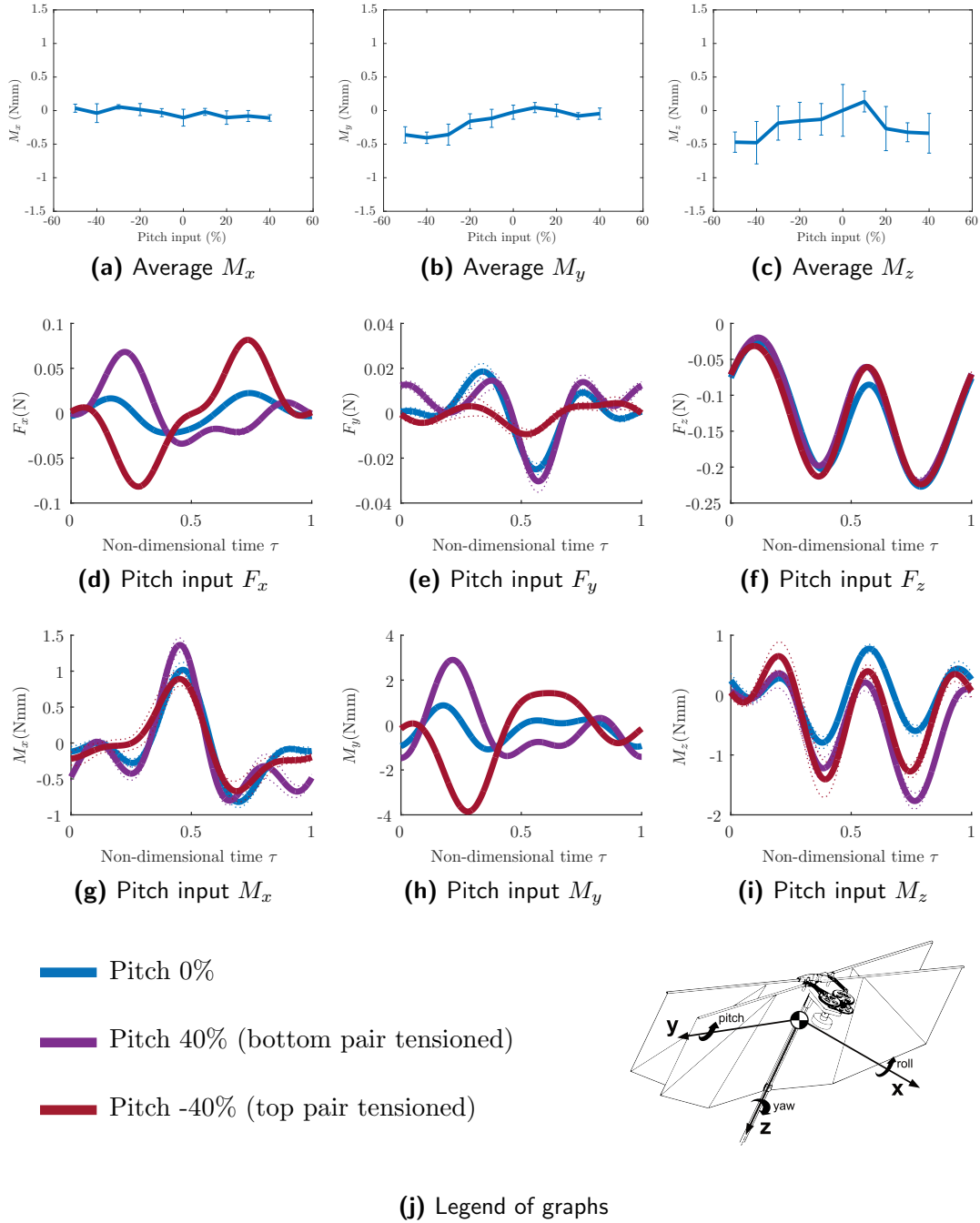
Figure 8-4: Wing deformation one-sided command through flapping cycle. In the picture, the top wing is tensioned.
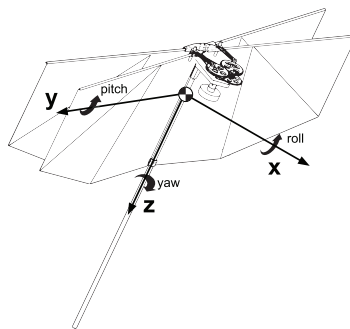
Figure 8-5: Axis definition (right-handed) and location measurement origin.

Figure 8-6: **(a)-(c)**: Cycle-averaged Moments versus Pitch inputs at 10Hz. The error bars represent the standard deviation. **(d)-(i)**: Average Forces and moments of neutral and 40% and -40% pitch input compared in a timespan of a single flap. Dotted lines indicate standard deviation. The data is filtered using a butterworth low-pass filter with a cut-off frequency of 30 Hz

the force due to the scoop is below the quarter chord point (the location of the virtual center of gravity), which is also expected by the high-speed photography picture in Figure 8-9, since the foil is loosest near the trailing edge, where the air scoop thus has the highest effect. In a later stage this would also mean that great care needs to be exercised in placing the center of gravity, since the arm of this force has an influence on both magnitude and direction of the pitching moment.

In Figures 8-6a-c, the trend line indicates the average moment for four experiments, where for each experiment the unfiltered data is averaged over an integer number of flapping cycles (ten flapping cycles are recorded). The error bars represent the corresponding standard deviation. For the averages of Figures 8-6a-c, it is clear that a positive trend is measured for the pitch moment M_y, although not very linear and the results of a positive input are not symmetric with respect to their negative input counterparts.
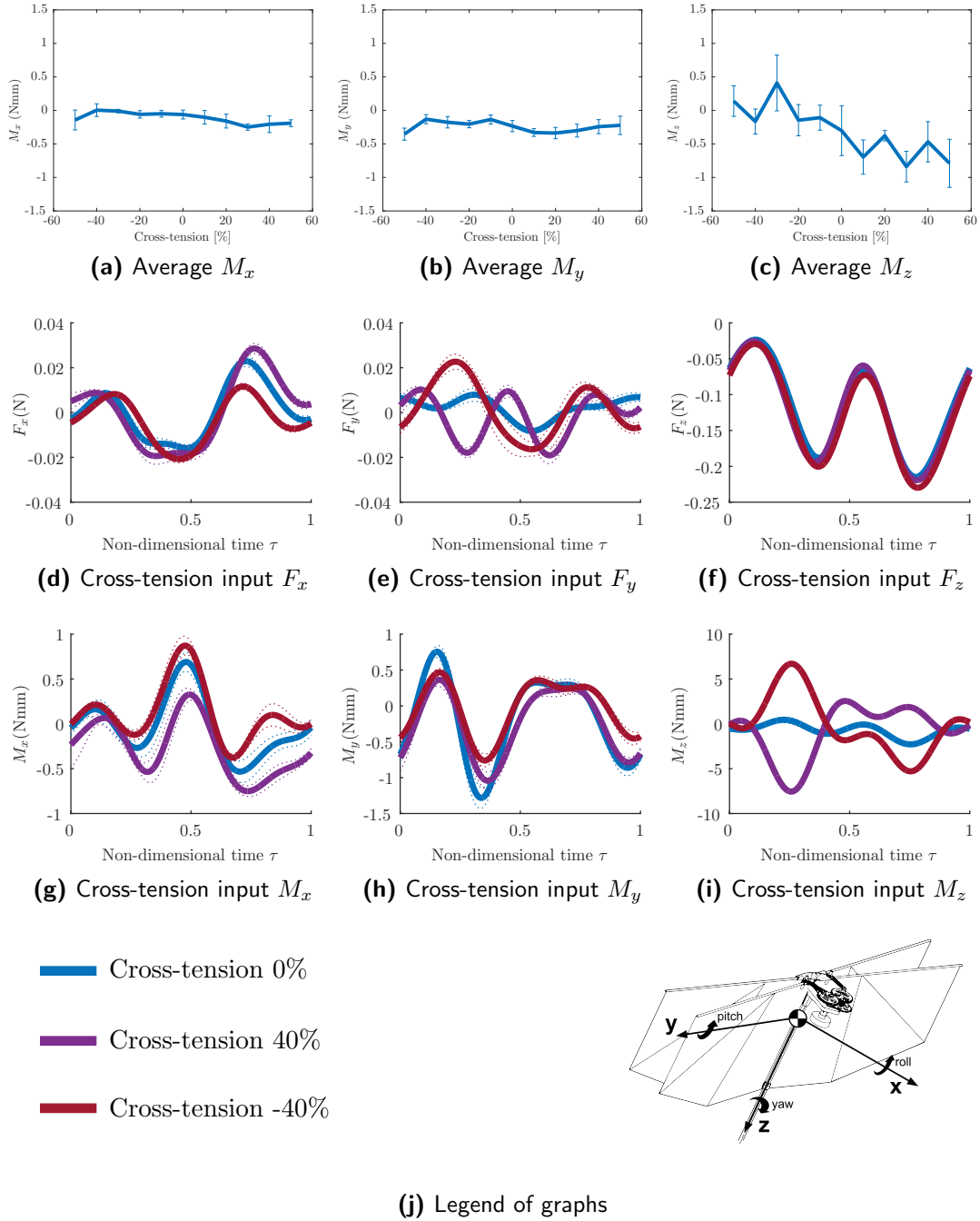
Tensioning the top pair of wings (i.e., a negative input), results in a negative M_y, or a *pitch down* moment, as expected from the explanation above. Tensioning the bottom pair of wings (positive input) however has less conclusive results, which also follows directly from the F_y graph. What is not expected is that a symmetric input (on both sides of the hull the same input is applied), also results in an unexpected coupling effect on the M_z, however with a high standard deviation. Unexpected, since a moment on this axis can only result from left-right asymmetries. Most likely this is the result from asymmetry and other inconsistencies in the prototype or measurement setup.

Concluding, the pitch input certainly has an effect on the pitch moment, although not meeting the requirements. The result is not linear and does meet the requirement for the magnitude of the moments that are generated. Also, it possibly has cross-coupling with the yaw moment, but the validity of this conclusion is questionable.
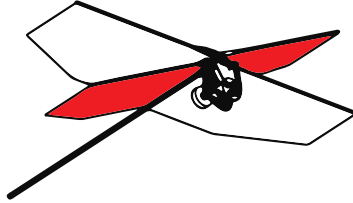
Cross-tension input

The next control mode, cross-tension input, is achieved by tensioning the left top wing and right bottom wing or vice versa. A positive input is defined as controlling both the left top wing and right bottom wing with the corresponding servo command (Figure 8-8).

The cycle average moment variations for various levels of cross-tension input are shown in Figures 8-7a-c, showing a trend in M_z, while the other moments show little variation. This dominant moment variation, M_z, is plotted in Figure 8-7i, where the moment variations within one flap cycle are shown for inputs of 0%, 40% and -40% in cross-tension. In this figure again the effect of the scoops are visible at a τ of 0.25 and 0.75, where the values are at their maximum because this is the point of maximum velocity of the leading edge. For this yaw moment, the two scoops on both sides of the leading edge generate drag forces as a couple, resulting in the aerodynamic moment. The direction can again be explained by the earlier conclusion that the drag force of an inbound flapping scoop is higher than for the outbound scoop. This causes the net-moment generation for M_z. In conclusion, cross-tension input is successful in generating a yaw moment (M_z).

(a) Average M_x

(b) Average M_y

(c) Average M_z

(d) Cross-tension input F_x

(e) Cross-tension input F_y

(f) Cross-tension input F_z

(g) Cross-tension input M_x

(h) Cross-tension input M_y

(i) Cross-tension input M_z

Cross-tension 0%

Cross-tension 40%

Cross-tension -40%

(j) Legend of graphs

Figure 8-7: (a)-(c): Cycle-averaged moments versus cross-tension inputs at 10Hz. The error bars represent the standard deviation. **(d)-(i)**: Forces and moments of neutral and 40% and -40% cross-tension input compared in a timespan of a single flap. Dotted lines indicate standard deviation. The data is filtered using a butterworth low-pass filter with a cut-off frequency of 30 Hz

Figure 8-8: A positive cross-tension input is defined as controlling both the left top wing and right bottom wing with the corresponding servo command from Figure 6-3
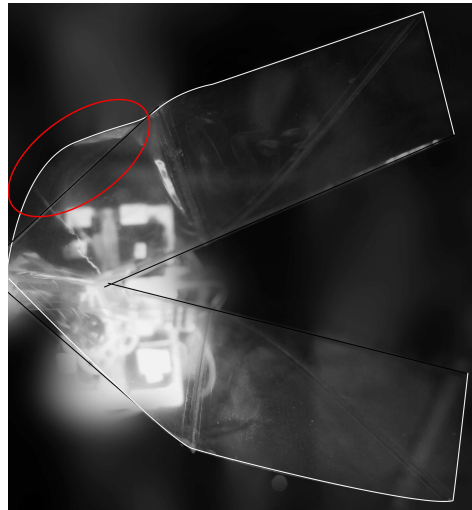
Figure 8-9: Point of maximum moment generation for Pitch and Cross-tension input. Circled is the airscoop.

Wing-pair input

Immediately apparent in Figure 8-11 is that none of the moments are controlled with the authority as seen with the cross-tension input. In the figure, a positive wing-pair input is defined as tensioning the right wing pair. This wing-pair input was expected to generate roll, by having an asymmetry between the left and right wing pair in terms of thrust creation. From Figure 8-10 can be concluded that there is indeed a significant increase of thrust F_z. Also, it appeared that, when looking at the forces during an individual flap, extra thrust is generated throughout the entire flapping cycle. However, M_x does not show significant differences, which suggests that the mean of the extra thrust is generated very close to the root. Figure 8-10 that the extra thrust force being generated at a deflection of 40%, is 0.008 N. In order to generate a moment of $1\,\mathrm{Nmm}$, an arm is needed of $125\,\mathrm{mm}$. Compared to the wing span ($280\,\mathrm{mm}$), this arm would be significant, since it is almost at the wing tip. However, as became clear, the effect in wing deformation which was visible with the stroboscope was close to the root, and therefore the actual arm of the force to the COG is expected to be small.

In Figure 8-11g the roll moment M_x is plotted during one stroke cycle. It appears that, while certainly roll moments are generated during a flap, the flap-cycle averaged effect of these moments is close to zero. It was hypothesized that an asymmetrical thrust of the wings would be the primary driver for M_x. Also visible in the graphs is that F_y is influenced by the control input. Depending on the distance of the application point with reference to the center of gravity (i.e. the arm), this F_y influences the roll moment M_x.

The F_x and F_y forces are thought to be generated in the following manner: due to the scoops which are formed during flapping for the tensioned wings (section 8-2), the wings that are tensioned create extra drag during the flapping cycle. When a wing-pair is tensioned, these forces will cancel each other in the F_x component, however, they add in the F_y component, as can be seen in Figure 8-11. This figure shows that for the F_x component, the three commands have a similar result on F_x, reflecting the cancellation of forces in this component. However, for F_y the result is oscillating. During inbound movement ($\tau = 0.25$), a positive input results in a negative F_y. This situation is drawin in the free body diagram in Figure 8-12. After this, the clap-and-fling at $\tau = 0.5$ generates a high oscillating movement, which is most likely due to the complex interactions of fluid and structure and because we filter after the first three harmonics. When the wing fling is completed, the situation is the other way around, since the scoop is now formed in the other direction, and now a positive F_y is generated. This results in a M_y which cycle averages to close to zero, since the two effects cancel each other. This leads to the conclusion that wing-pair input is not effective for attitude control.
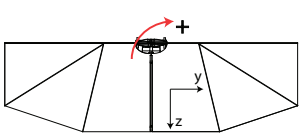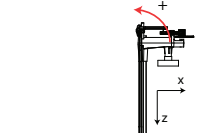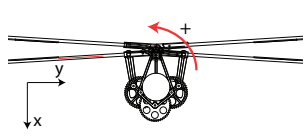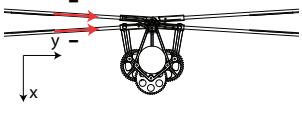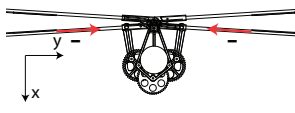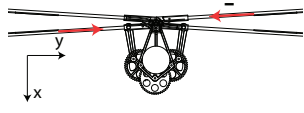
8-4   Reflection on the design of concept A and its consequences for future flyers

In this section concept A will be reflected, and also it will be discussed whether concept A would work on another DelFly flapping mechanism, the 90 degree flapper.
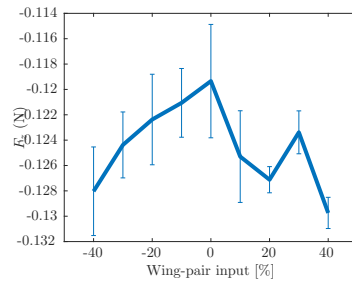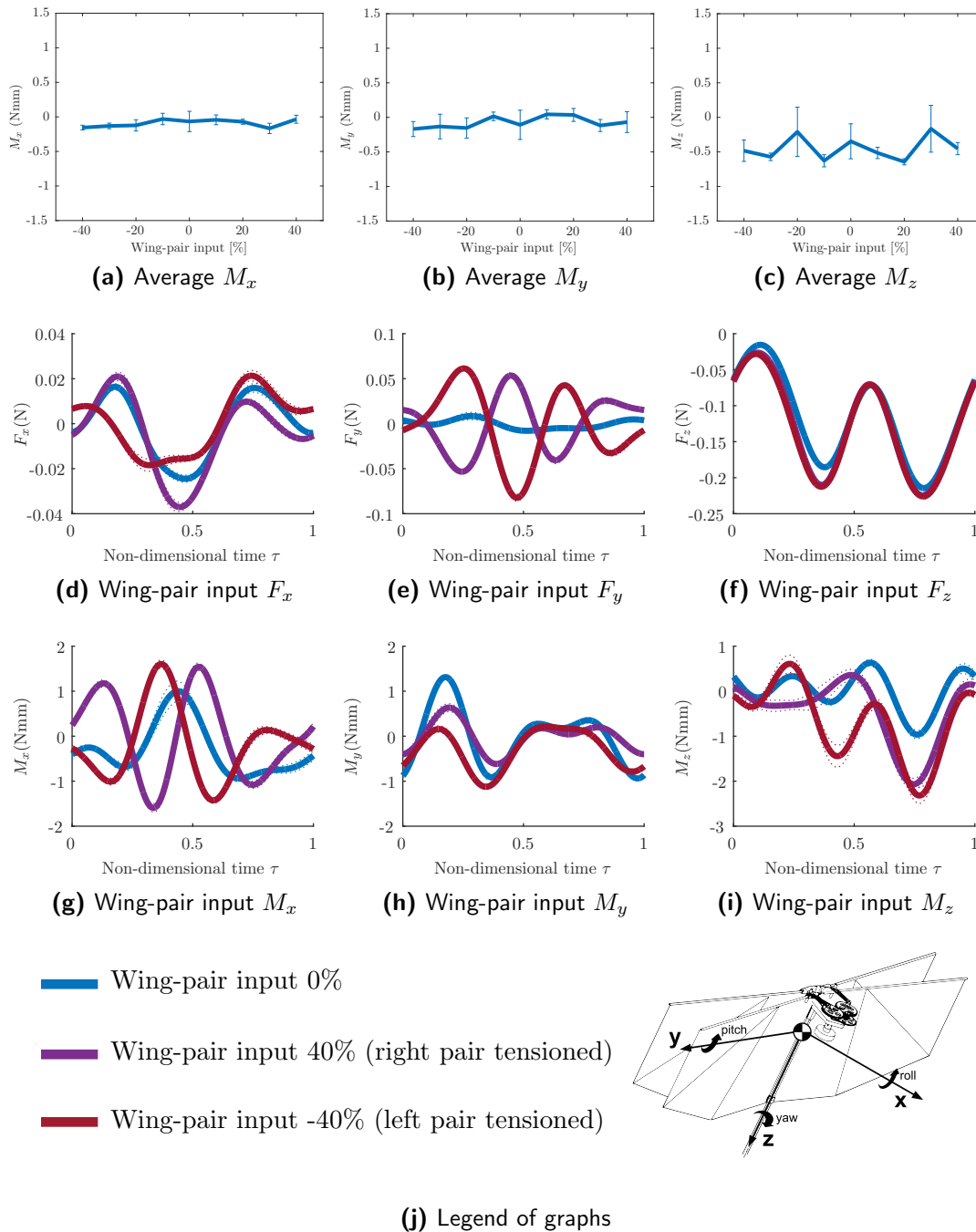
Figure 8-10: Cycle-averaged F_z versus wing-pair input. The error bars represent the standard deviation.

Table 8-1: Summary of concept A results

Axis	Roll	Pitch	Yaw
Desired motion			
Hypothesized			
Results in desired motion?	✖	✖	✔
Uncoupled with other axes?	N/A	N/A	✔

(a) Average M_x **(b)** Average M_y **(c)** Average M_z

(d) Wing-pair input F_x **(e)** Wing-pair input F_y **(f)** Wing-pair input F_z

(g) Wing-pair input M_x **(h)** Wing-pair input M_y **(i)** Wing-pair input M_z

— Wing-pair input 0%

— Wing-pair input 40% (right pair tensioned)

— Wing-pair input -40% (left pair tensioned)

(j) Legend of graphs

Figure 8-11: (a)-(c): Cycle-averaged moments versus wing-pair inputs at 10Hz. The error bars represent the standard deviation. **(d)-(i)**:Forces and moments of neutral and 40% and -40% wing-pair input compared in a timespan of a single flap. Dotted lines indicate standard deviation. The data is filtered using a butterworth low-pass filter with a cut-off frequency of 30 Hz

8-4-1 Reflection on wing foil tensioning of concept A

Comparing the results with the statement in the hypothesis, it appears that the hypothesis of the mechanism behind the moment generation in concept A was not correct. Not the changes in individual wing's thrust forces seem important, what is more important is the change in direction of the wing's force resultant due to drag creation. The theory posed here is that due to the scoop formation, a force is generated perpendicular to the wing surfaces, which can only control the yaw moment, see the summary in Table 8-1.

In the hypothesis was mentioned that the forces would be generated by changes in the tension of the foil. However, since the middle stiffener of the wing was forced inwards, Figure 8-13, only the part on the outer side of the stiffener was tensed. This part is already stiff due to the presence of the second stiffener and as thus might be less effective. Instead of the stiffening of the foil, the leading edge gets bent, which also resulted in a significantly higher power requirement due to friction of almost 25% for full actuation when all four wings are tensioned, see Figure 8-14a.

Still, the mechanism does generate control moments, most notably during the cross-tension input. It was hypothesized that this effect is created due to the formation of an air scoop, which creates a higher drag force or creates a momentum jet perpendicular to the wing foil. When a wing-pair is controlled, a significant increase in thrust is measured, however, no significant changes in the roll moment M_x were measured. It is likely that this thrust effect is on average generated too close to the root to be effective in influencing the roll moment. This effect can also be measured when all four wings are tensioned. The net moments and F_x and F_y are constant, however, an increase in thrust can be measured (see Figure 8-14b), but this is a very inefficient way of thrust creation because of the higher power required. Also, we already saw that it is likely that this extra thrust is generated close to the root, making it unable to modulate the control moments. This again forms proof for the theory that the mechanism primarily generates drag on the wings. When all four wings are tensioned, the net effect of these drag forces is zero since these forces are canceling each other with four-wing input, however, it does generate more thrust.

In conclusion, the mechanism can be primarily employed to control the yaw moment of the DelFly, with a maximum cycle-averaged moment generation of $|M_{z_{max}} - M_{z_{neut}}| =$
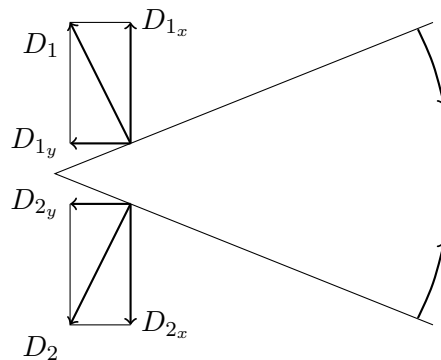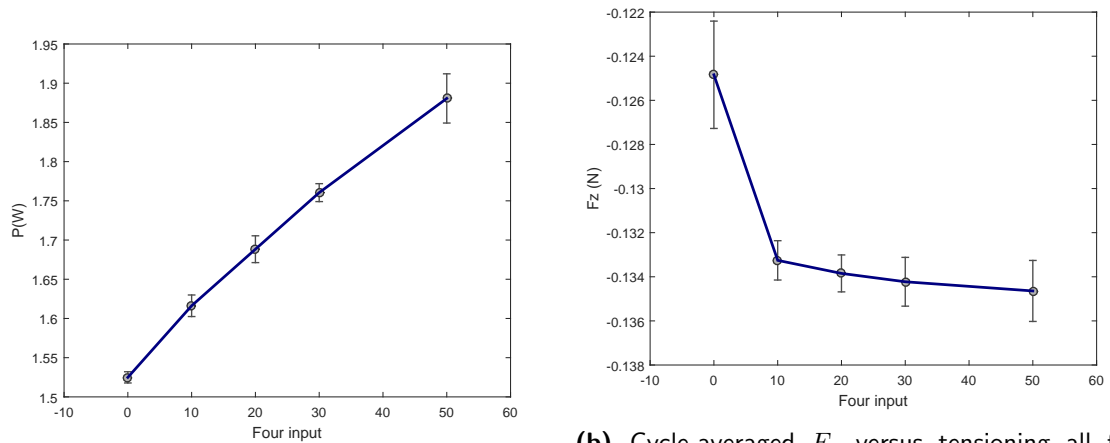

Figure 8-12: Top view free body diagram during wing-pair command with inbound motion. D_1 and D_2 represent the extra drag forces due to the control input.
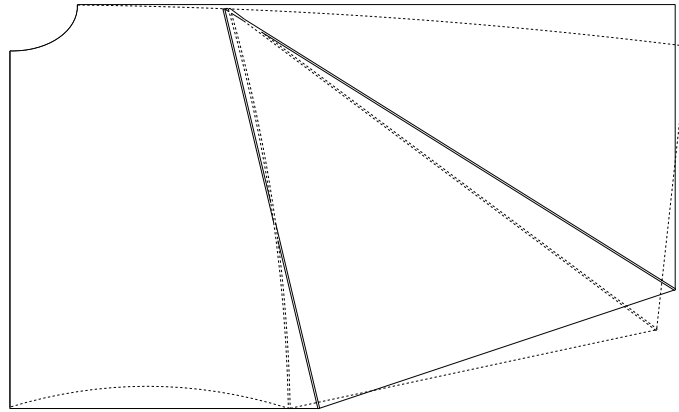
Figure 8-13: Deformed wing during actuation

(a) Power required during four-wing actuation

(b) Cycle-averaged F_z versus tensioning all four wings. The error bars represent the standard deviation.

Figure 8-14: Tensioning all four wings at once.

0.71 [Nmm] and with little cross-coupling. For the tail-less DelFly, a moment of inertia of $I_{zz} = 1.29 \cdot 10^{-5} \left[kg \cdot m^2 \right]$ is calculated, by assuming that all of the components are point masses. The servo system has not been included in this calculation, since the layout of this system still remains unknown. Newton's second law for rotation can then be applied to calculate the angular velocity generated:

$$\tau_{net\ ext} = I\alpha_{acc} \tag{8-1}$$

where I is the moment of inertia, α_{acc} the angular acceleration and $\tau_{net\ ext}$ is the net external torque. This results in an maximum angular acceleration of $\alpha_{acc} = 55\,rad/s^2$ (without damping).

Another requirement specified that the moments generated should be repeatable and spectrum wide, and preferably linear. If we look at the graph for cross-tension input, the result is certainly not linear, and also not very repeatable (the moments have a high standard deviation, which causes an uncertainty on the moments that are generated for a certain input).

In order to assess the last design criteria, the required low weight, first a servo needs to be selected that can handle the loads required to pull on the strings. Unfortunately, with this test setup it was not possible to measure the loads in the strings. However, during the test the carbon leading edges needed to be bent, requiring a considerable amount of force. It was already shown in the early flight test that sufficient control moments could be generated to control the DelFly, however, this prototype had a tail as a damper. Further research is required to determine whether the yaw axis can be actively controlled using low-weight servos.

8-4-2   Hypothesis for concept A on 90-degree flapper

Another project for possible improvement of the DelFly is the development of a 90 degree flapper. This flapper is being developed to make the DelFly more symmetric and to have the advantage of two clap-and-peel mechanisms, since each single wing has a stroke of 90 degrees.

A possibility is that the present research, on control through wing deformation, will at some point be implemented on this new 90-degree flapping mechanism. Therefore, the prototypes for control should also work on the new envisioned flapping mechanism.

The present wing tensioning concept is presently working due to the inherent difference in the inbound and outbound stroke. When a wing is tensioned, the dominant effect (as hypothesized) is the creation of the scoop which creates extra drag during the translational stroke. This drag is higher in magnitude during the inbound flap than during the outbound flap, resulting in a net moment when the whole cycle is considered.

When considering the 90 degree flapper, one of the main features will be that there is no difference between the up and down stroke anymore, they both result in a clap-and-fling. Therefore, if the device would indeed be truly symmetric, the drag created during both half-strokes would be identical. This would result in a net moment of zero.

8-5   Recommendations on concept A and test setup

The concept of wing tensioning as currently implemented only works for yaw. In the next section, it will be discussed how (also) roll and pitch can be generated by using wing tensioning. Next, in section 8-5-2 some recommendations will be given for the methodology of testing the prototypes.

8-5-1   Recommendations for further improvement of wing tension modulation

In the current concept, the first stiffener was pulled towards the fuselage, resulting in a bent leading edge. The part that was pulled to tension - the outer part of the wing next to the first stiffener - already had inherent stiffness due to the outer stiffener and the stiffness of the foil itself, see section 8-4-1. The concept hypothesis was based on a desired ability to change the tension in the Mylar foil. However, in the present concept, this Mylar foil was already tensioned to its limit. When trying to stretch this foil even more, the leading edge will be bent instead, which is not what was desired.

On a regular DelFly, the four wings are tensioned at the root of the wing, and the wings are connected in pairs. To be able to apply tension and to release tension in all of the four wings, it is recommended to disconnect the wings from each other, resulting in four single wings. A bar will be glued to each of the wings, acting as the wing root. By displacing this wing root inwards or outwards, the wing can be tensioned and slackened, respectively. This can then potentially be used to control the amount of the thrust the wing generates, and if this can be done individually for each wing, it can control the pitch and roll moments.

8-5-2   Recommendations for the methodology of the experiments

Concept A was tested using a 3D printed adapter with servos, mounted on a force-torque sensor. During the assembly of this setup, it proved to be difficult to exactly match the tension of all of the strings, such that all wings will be equal in neutral position. Also, even while a high stiffness and strength rope was used, it is possible that the strings will deform because of the forces, as well as have hysteresis. It is recommended that for the next setup it is attempted to initially not use strings in order to mitigate these effects, and instead have measurements that closer represent the effects of purely the wing deformation.

Chapter 9

Prototype design concept B

Concept A is based on tensioning the wings by pulling the first wing stiffener to the root, see Figure 9-1a. In the previous chapters it became clear that the Mylar foil is not actually tensioned by this method, since it was already in tension in the outer wing area. By pulling on the wing stiffener, instead the leading edge is bent and a wing scoop is formed, which could only effectively control yaw.

For a regular DelFly, the wings are already in tension during flapping due to the way the DelFly wings are built. In order to control the DelFly, the design of the wings should therefore be altered, in order to also have the possibility of flying with slacker wings. Therefore, for the next concept, concept B, instead of trying to tension the Mylar more than the regular DelFly, the tension of the wings of the DelFly is released by disconnecting the wing pairs, and by not fixing them to the fuselage anymore. Instead of two pairs of wings, the concept now has four separate wings, and each half-wing is connected to a carbon rod at the root (see Figure 9-1b). This rod is flexibly connected to the hinge at the top of the vehicle, and will be controlled at the bottom. By moving these rods outbound, it is possible to regulate the slackness of the wing. By moving the rod outbound, the wings become slacker, by moving the rod towards the fuselage, the foil has a higher surface tension.

A similar effect was seen in the Nano Hummingbird (Keennon, Klingebiel, & Andriukov, 2012), he regulates the tightness of the foil by moving the root to various directions (also see Section 4-2-2). However, since Keennon, Klingebiel, & Andriukov (2012) only use two wings for their FWMAV, the wing roots need to be controlled in various directions, in order to shift the application point of the resultant of total thrust. In Figure 9-2, it is depicted that for pitch the roots need to be deflected vertically. This causes the foil to be slacker during the extremal flapping angles, which causes the mechanism to generate less thrust at one extremal flapping angle (when the wings are slack), and more thrust at the other extremal flapping angle (when the wings are in tension). By moving the roots horizontally, one wing has increased slackness during the entire stroke (most dominantly during a flapping angle of zero), and the other wing foil has a higher tension. This causes the FWMAV to roll.

However, for the present DelFly this bi-directional degree of freedom of the wing-roots is potentially not needed. Since the DelFly has four wings, one can for example generate pitch
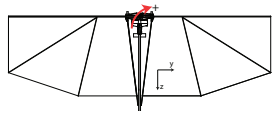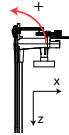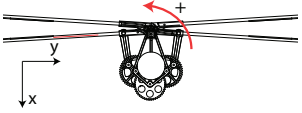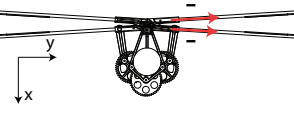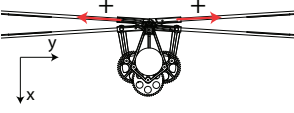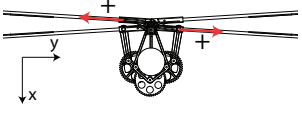
(a) Concept A   **(b)** Concept B
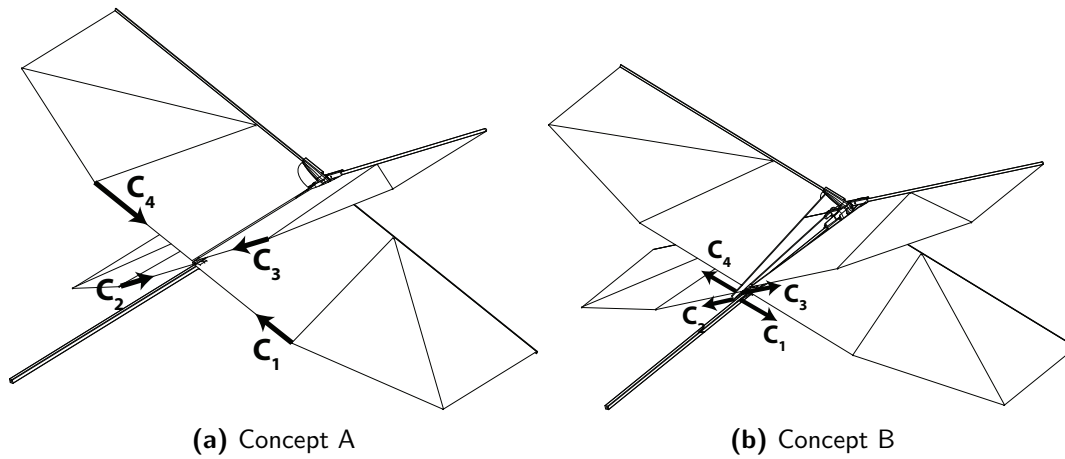
Figure 9-1: Prototypes for wing tensioning concepts A and B. C_1-C_4 are the various degrees of freedom for control.
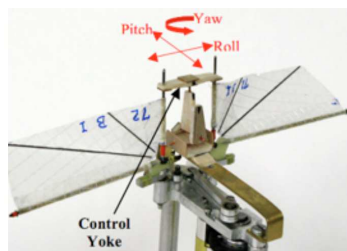
Figure 9-2: Mockup of the Nano Hummingbird with arrows indicating the direction of the root spars to generate the desired moments. Adapted from Keennon, Klingebiel, Won, & Andriukov (2012)

Table 9-1: Inputs and hypothesised resulting motion for concept B

Axis	Roll	Pitch	Yaw
Desired motion			
Hypothesized			

by increasing slackness on either the upper or the lower two wings. In this way, one pair of wings generate more thrust than the other pair, generating a control moment. The same can be done for roll, by increasing slackness of either the left or right pair of wings. The hypotheses for these motions are summarised in Table 9-1.

In the next chapter the validity of these hypotheses is tested, again by performing experiments with the force-torque sensor Nano17 Titanium.

Experimental results of concept B

Similarly as for concept A, concept B was tested for its moment generation by using a force-torque sensor. In the next section, the differences in experimental methodologies between concept A and concept B are explained. Next, in section 10-2, the optimal displacement direction for the wing roots will be explained, after which this displacement direction is used in section 10-3 to see whether the prototype is able to generate all control moments. In section 10-4 an analysis is made regarding the COG location. Lastly, in sections 10-5 and 10-6, concept B is reflected, and recommendations are made, respectively.

10-1   Methodologies for concept B testing

Instead of using the 3D printed adapter with servos for the DelFly, which caused problems with alignment, (see section 8-5-2), for the initial force-balance test of concept B the wing roots are hold in place by a CNC-milled grid, see Figure 10-2a. Also, since the servos are not needed in this test, the DelFly is fixed to the sensor using a metal clamp.

For the measurements in this chapter, unless stated otherwise, the moments are calculated in the flapping axis, at the quarter chord point.

10-2   Optimal displacement direction of the wing roots

It is likely that there is an optimal direction of displacement for the wing roots in terms of moment generation. In Figure 10-1 the resulting moments and forces are indicated for various directions of displacement of the top-left half-wing (Figure 10-2a). Ten measurements of one second duration were taken per data-point, with direction increments for both horizontal and vertical direction of $3\,\mathrm{mm}$. The average for the forces and moments was taken, resulting in the average force and moments for one flapping cycle. The results are linearly interpolated to produce Figure 10-1.

When analysing Figure 10-1, it is clear that a roll moment is produced when displacing the roots in a horizontal direction. In contrast, little to no moment at all is generated when moving the rods in vertical direction. The roll moment which is generated has a negative sign. This means that the vehicle rolls towards the side of the displaced bar, suggesting that when the foil is slacker the wing produces less thrust. This is consistent with the hypotheses stated in Section 9 and of the finding of the Nano Hummingbird (Keennon, Klingebiel, Won, & Andriukov, 2012).

When the bar at the root of the wing is displaced in a horizontal fashion, also a pitch moment is generated. This pitch moment which is generated is even higher when displacing the rods diagonally. Again, the vehicle generates a pitch moment towards the slacker wing.

For yaw however, the results are less linear. As can be seen from the M_z graph, yaw can be generated when deflecting the bar vertically, while keeping $d_{HOR} = 0$, however, the result is less conclusive.

The information that these figures show for one-wing control can be extended when considering the control of multiple wings. For example, when not only the top left wing is displaced, as was done in Figure 10-1, but instead both left half-wings are displaced, both of these wings will generate less thrust, and consequently, the measured moment M_x will be higher. However, it is expected that the upper and lower wing will both generate an opposite contribution to the pitch moment M_y, such that in total no pitch moment will be generated. The hypothesis is therefore that roll can be generated without coupling to pitch by controlling either the left or right pair. Similarly, for pitch either the top pair or bottom pair can be controlled to end up with an uncoupled pitch moment M_y. That this is indeed the case, will be shown in the next section.

Summarizing the results, for roll the optimal direction of control is horizontally, for pitch diagonally and for yaw vertically. In the next section, the bars will be displaced diagonally, with an angle of 22.5^o from the horizontal, which is half the maximum flapping angle. This would mean that the foil is the slackest at a flapping angle of 22.5^o, which is the point when the thrust generation is maximal (during an outstroke, see Figure 8-1), since the translational velocity at that point is the highest. This would suggest that in this direction, the effect due to the modulation of the magnitude of thrust will be most effective.

10-3   Concept B moment generation when moving the wing roots diagonally

In this section, the results of the experiment of the diagonal wing root deformation for concept B is shown. Each of the three moments, respectively roll, pitch and yaw, will be dealt with in the next subsections. The results of these experiments are summarised in Table 10-1. The various inputs are again applied by moving the root bars connected to the individual wings through a milled grid.

10-3-1   Roll generation of Concept B

As was already mentioned in the previous section, for roll generation (M_x), either the roots of the two left or two right wings are moved outwards, see Figure 10-4d. The other wing pair
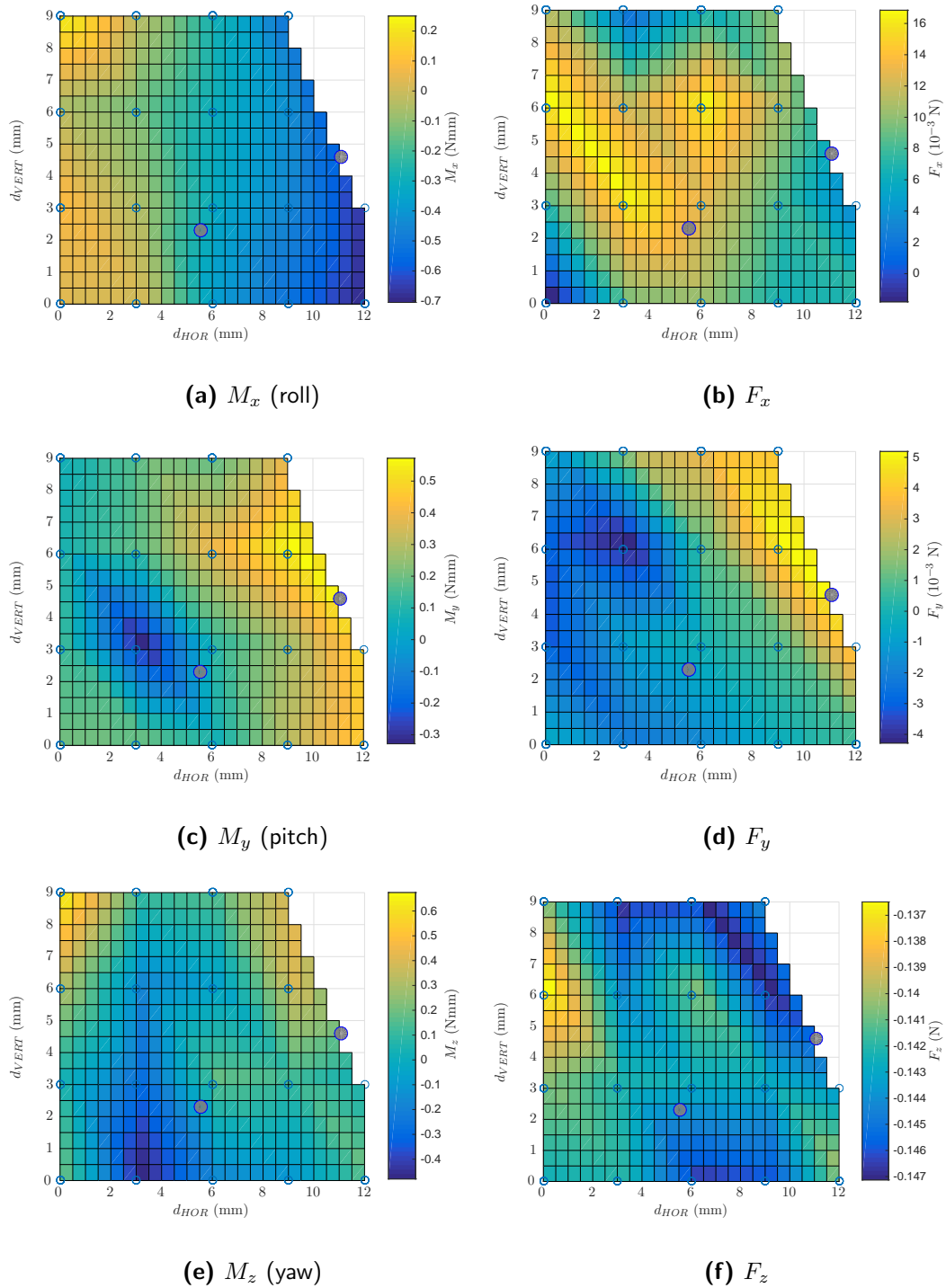
Figure 10-1: Forces of moments resulting from a displacement of the wing roots, as indicated in Figure 10-2a. The axis are defined similarly to concept A, see Figure 10-2b
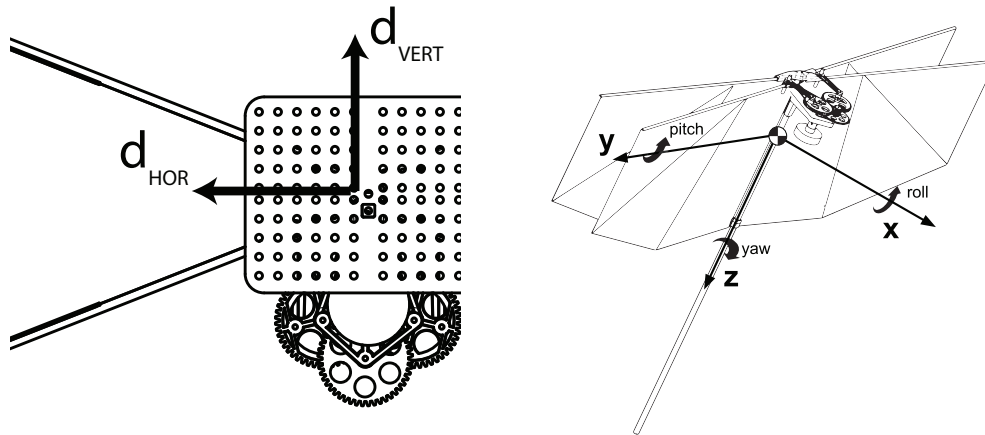
(a) Bottom view of DelFly, indicating root displacement directions. **(b)** Axis definition (right-handed) and location measurement origin.

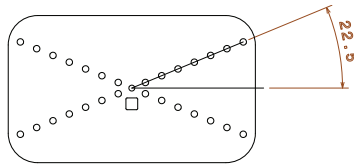**Figure 10-2:** Axis and control definitions concept B

Figure 10-3: Milled diagonal displacement grid

is fixed in the neutral position.

The results for roll are shown in Figure 10-4. Indeed, as was already expected from the results of last section, the roll moment M_x varies linearly with the root bar displacement, while the pitch moment M_y is approximately constant. As was already expected, the vehicle rolls towards the wings that are slack, which again proves that slack wings generate less thrust than stiff wings, for equal frequency. The measurements for the yaw moment M_z have a high variation, but there is no clear dependency on the root displacement for the roll case.

These observations indicate that the roll input is effective in modulating the roll moment M_x.

10-3-2   Pitch generation of Concept B

Hypothesised for the pitch generation is the slackening of either the top or the bottom pair of wings. The results and a drawing of the input method is shown in Figure 10-5.

For this input, the pitch moment M_y varies linearly with the displacement, with a slight asymmetry. The source of this asymmetry is likely due to an asymmetry of the prototype and the COG location, see Section 10-4. The roll moment M_x is approximately constant with respect to displacement at 0 Nmm, hence the pitch input is generating a pitch moment uncoupled with the roll moment. Similarly to the roll input, the yaw moment due to pitch input has a high variation, but does not show dependency on the input.

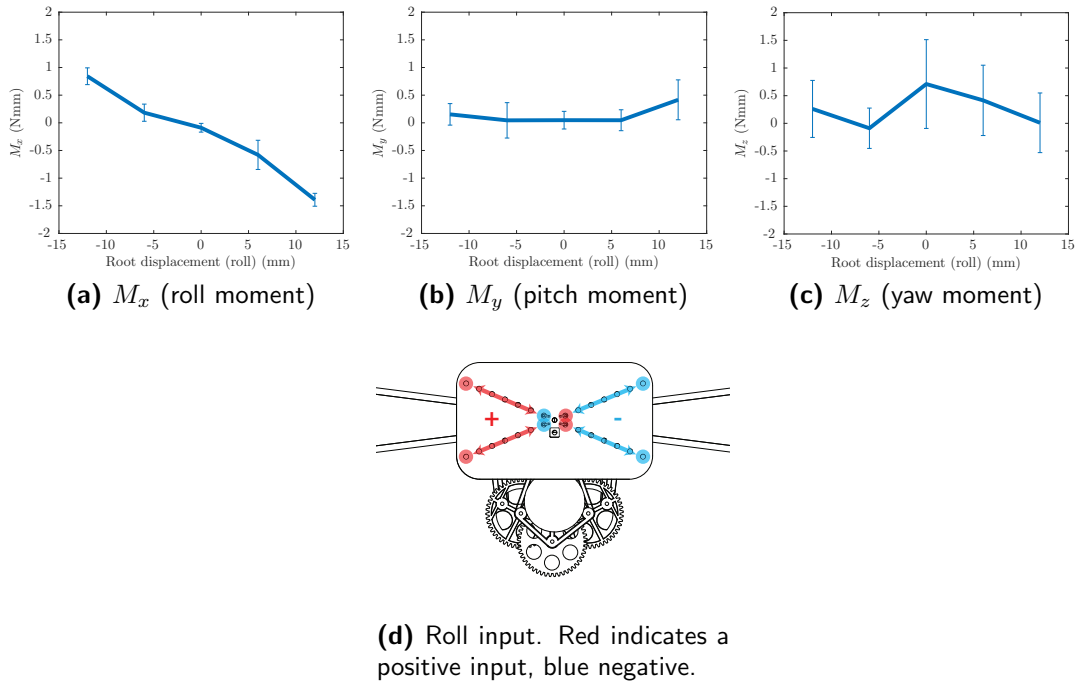Concluding, it is shown that the pitch input is effective for controlling the pitch moment M_y.

(a) M_x (roll moment)

(b) M_y (pitch moment)

(c) M_z (yaw moment)

(d) Roll input. Red indicates a positive input, blue negative.

Figure 10-4: Moment generation due to roll input for Concept B

(a) M_x (roll moment)

(b) M_y (pitch moment)

(c) M_z (yaw moment)

(d) Pitch input. Red indicates a positive input, blue negative.
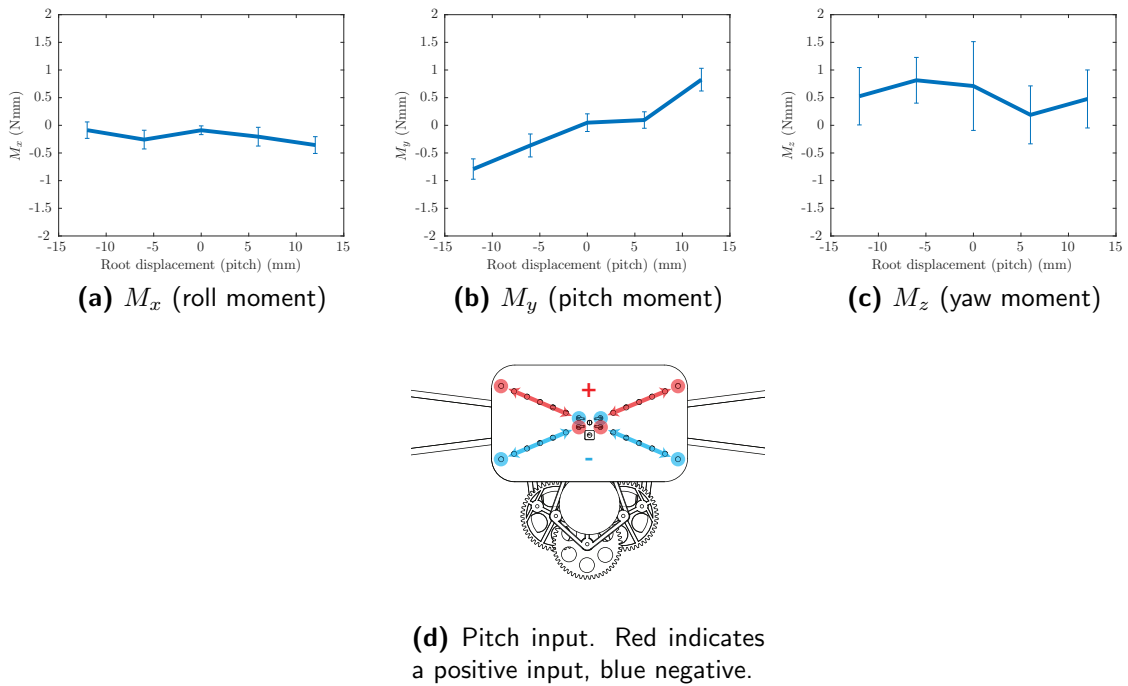
Figure 10-5: Moment generation due to pitch input for Concept B

(a) M_x (roll moment)

(b) M_y (pitch moment)

(c) M_z (yaw moment)

(d) Yaw input. Red indicates a positive input, blue negative.
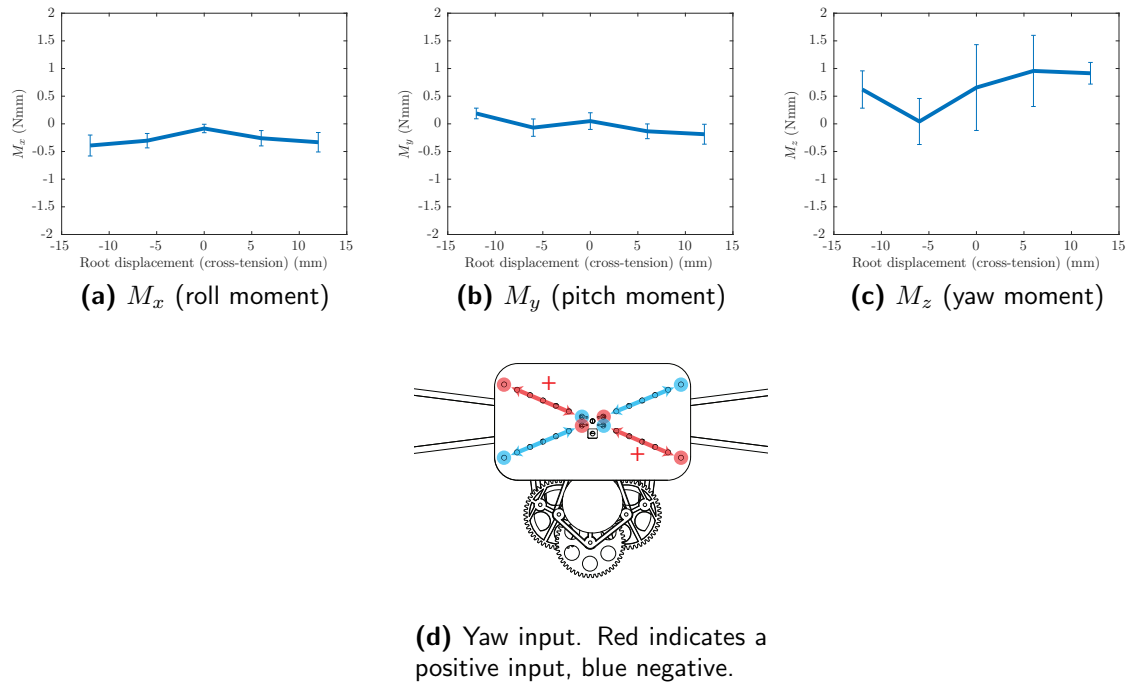
Figure 10-6: Moment generation due to yaw input for Concept B

10-3-3   Yaw generation of Concept B

As was already expected from the results of the grid, it is not possible to generate a linear yaw moment when displacing the roots diagonally, as can be seen in Figure 10-6. The roll and pitch moments do not vary with the input, and additionally also the yaw moment M_z does not show any significant dependency on the root displacement. It appears that concept B, in contrast to concept A, does not produce the wing scoops that alter the drag during the stroke.
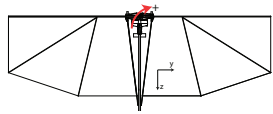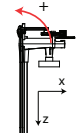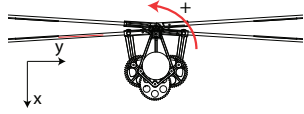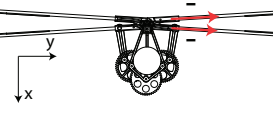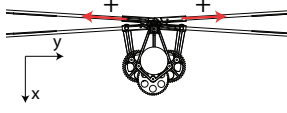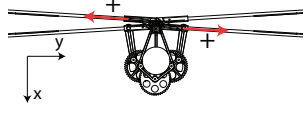
10-4   Center of gravity location for (tail-less) flight

As mentioned in Section 10-1, for the previous measurements the location about which the moments are calculated, was at the flapping axis near the quarter chord point. This location is representing the COG during free flight. As will be explained in this section, the location of this COG both has influence on the static stability, dynamic stability and the derivative of the moment generation with displacement, and therefore the COG should be placed with care in the design of free-flight models during further research.

10-4-1   Roll moment dependency on COG position

The magnitude of roll moment generation is dependent on the COG position. Naturally, the COG should be placed in the symmetry axis of the Delfly ($y_{COG} = 0$), to not cause any roll moment due to the weight vector. Moreover, Figure 10-7a shows that the side-force F_y

Table 10-1: Summary concept B results

Axis	Roll	Pitch	Yaw
Desired motion			
Hypothesized			
Results in desired motion?	✔	✔	✖
Uncoupled with other axes?	✔	✔	N/A

is dependent on the displacement of the root bars. This will also influence the total roll moment, depending on the position of the COG position relative to the application point of this side-force. In Figure 10-7 the Free Body Diagrams (FBDs) and resulting roll moment are given for a high and low COG. These figures show that the COG is preferably in the top of the DelFly, since in that position both the side force and thrust couple contribute to the roll moment.

10-4-2   Pitch moment dependency on COG position

Similarly as for roll, also the pitch moment is dependent on the COG position, see Figure 10-8. For positive inputs, next to a moment couple, also an F_x force is generated (indicated in the FBDs as P), which has an adverse contribution to the total pitch moment M_y if the COG is located at the trailing edge. Therefore, similarly as for roll, it is beneficial to have the COG in the top of the DelFly for optimal moment generation.

10-4-3   Dynamic pitch behaviour due to COG position

A regular tailed DelFly has its COG near the trailing edge. For the tail-less version of the DelFly, this situation is drawn for the hover condition in Figure 10-9a. Immediately apparent is that the thrust force vector is in line with the weight vector. If this was not the case, then in the neutral position (tension of all the wings the same), the vehicle will pitch. This means that the COG will need to be in line with the thrust vector in neutral position, which is on the flapping axis.

When a pitch input is given in this configuration, the thrust vector will shift either in positive or negative x-direction, depending on the sign of the input, see Figure 10-9b. This will cause the DelFly to pitch (Figure 10-9c), and the DelFly will fly forward. However, now also a normal force N will be generated due to the forward velocity V_∞. This normal force generates an opposite moment, when the COG is behind the normal force application point. This is not necessarily an unwanted phenomenon, since this will make the vehicle dynamically stable in
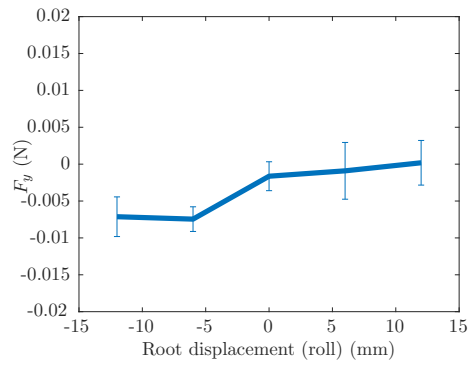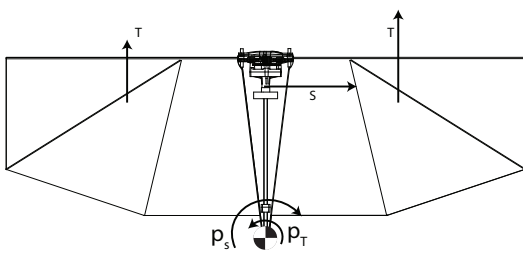
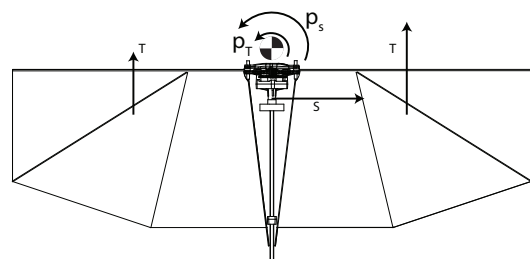**(a)** Side force F_y due to displacement of root bars
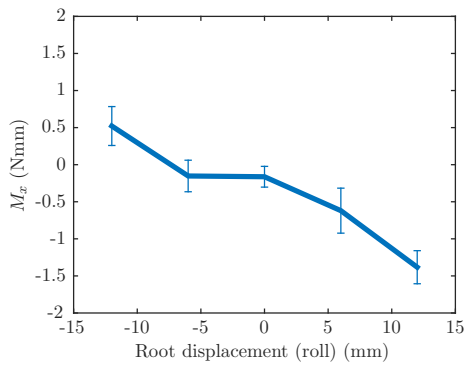
(b) Roll moment with COG at trailing edge
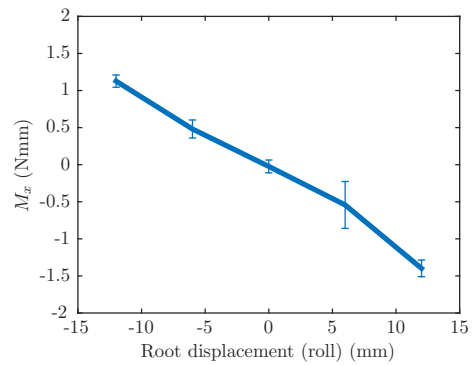
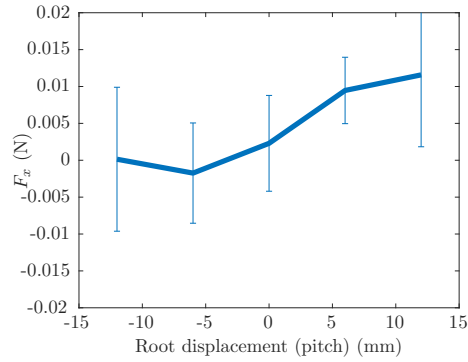**(c)** Roll moment with COG at leading edge

(d) FBD with COG at trailing edge

(e) FBD with COG at leading edge

Figure 10-7: Roll input with COG at various positions. The application point and magnitudes of the forces is indicative and not to scale.

(a) F_x due to displacement of root
bars

(b) Pitch moment with COG at trailing edge

(c) Pitch moment with COG at leading edge
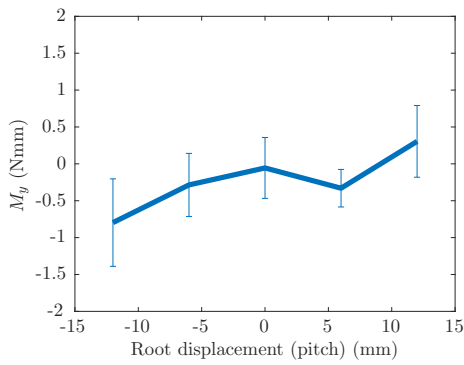

(d) FBD with COG at trailing edge

(e) FBD with COG at leading edge

Figure 10-8: Pitch input with COG at various positions. The application point and magnitudes of the forces is indicative and not to scale.
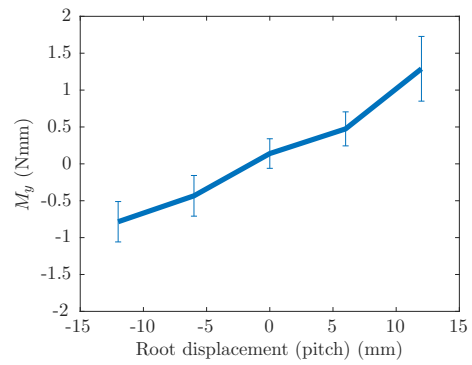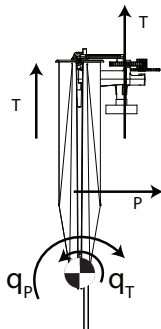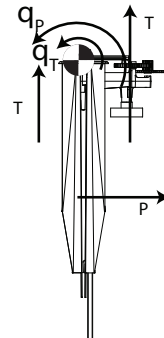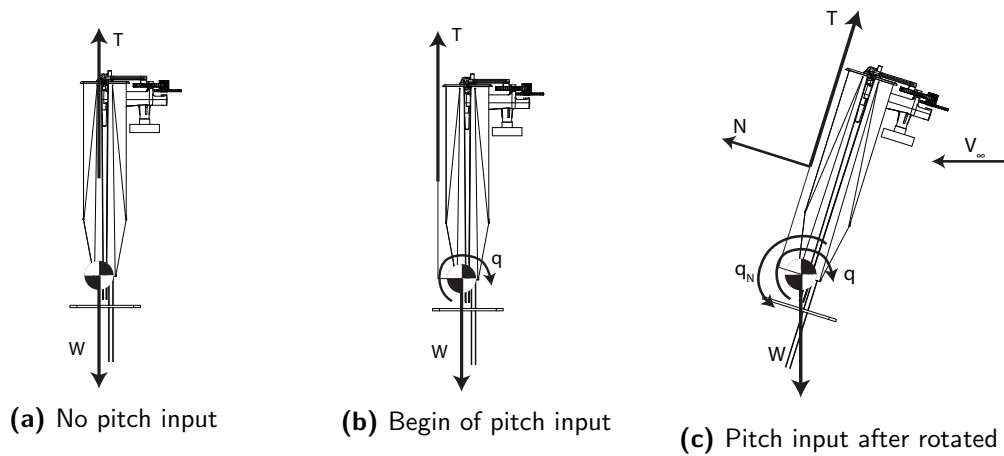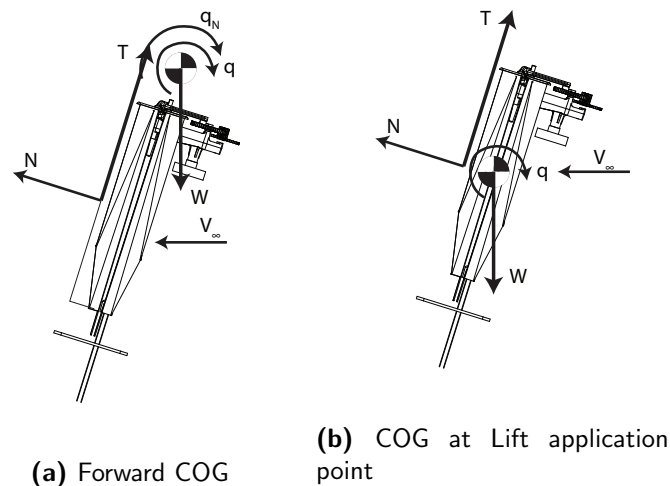
(a) No pitch input   **(b)** Begin of pitch input

(c) Pitch input after rotated

Figure 10-9: Pitch input with COG near trailing edge

(b) COG at Lift application point

(a) Forward COG

Figure 10-10: Pitch input with COG at various positions for forward flight

the pitch motion. However, in order to be able to achieve forward flight, this counter-torque may not be too high, otherwise it will always pitch back and the displacement of the average thrust vector can not counter this moment anymore. This may cause undesired oscillations in pitch.

The other extreme is drawn in Figure 10-10a. Now this normal force generates an extra contribution to the pitch moment, making the vehicle pitch faster as the DelFly speeds up, making it unstable.

In Figure 10-10b the third case is drawn, when the normal force does not influence the pitching moment. This is when the COG is located at the application point of the normal force. This discussion would suggest that the ideal location for the COG is close to this point, which is assumed to be at the quarter-chord point (from classic lift theory).

Summarising, the center of gravity has three main boundary conditions. The center of gravity should be on the flapping axis, in order to have neutral pitch moment with neutral input and not cause any roll moment due to the weight vector. The second condition is that the center

of gravity should be near the quarter-chord point for the dynamic pitch behaviour, and the third one is that it should be in the top of the vehicle in order to increase the slope of the roll and pitch commands with respect to control input. Therefore, it is recommended to place the center of gravity for a tail-less flapper using concept B in the first quarter of the chord.

10-5 Reflection on the design of concept B and its consequences for future flyers

10-5-1 Reflection on wing foil tensioning of concept B

While concept A did not meet the hypothesis that due to tensioning of the wings the thrust of each wing can be modulated, concept B proved to be more successful. By displacing the root bar of the separate wings outwards, it was possible to alter the thrust in that wing, and thus create moments by asymmetrically changing the thrust distribution. In this way, it was possible to generate pitch and roll moments. However, since these alterations in the thrust vectors are parallel to the yaw-axis, it did not result in any yaw control.

Relating the results back to the requirements, we can conclude that for pitch and roll, we satisfy all requirements related to the static moment generation. The magnitude of the control moments which are generated was in the order of 1.5 Nmm, and at maximum deflection, the results linear for all control inputs, also the boundaries, so it is likely that we can even generate higher moments. The moments are furthermore generated without cross-coupling. The mechanism used to control the wing roots, as will be explained in the recommendations (section 10-6), can be a lightweight string based servo system. Whether the last requirement regarding the actuation speed is met remains uncertain, since we first need to select the servos and test them.

10-5-2 Hypothesis concept B on 90-degree flapper

Similarly as was done for concept A in section 8-4-2, in this section an hypothesis is given for the result when including the wing tension modulation of concept B on the 90-degree flapper. As described in the previous sections, concept B, in contrast to concept A, is generating moments by modulating the amount of thrust generated on each wing. This effect is thought to still exist when each wing has a 90-degree stroke. However, the mean wing position, which is equal to half of the flapping angle, is now 45°, see Figure 10-11. This will shift the application point of the mean thrust vector, therefore the hypothesis is that relatively more pitch is generated, and relatively less roll. For the 90-degree flapper in now becomes a matter of definition what is roll and what is yaw, since they are in principle the same.

10-6 Recommendations on concept B: moving towards free-flight

The control inputs for the measurements on concept B were achieved by displacing the root bars over a CNC-milled grid. For flight however, a mechanical system is needed to displace the bars. For the force balance measurements, the root bars were fixed in position, however,
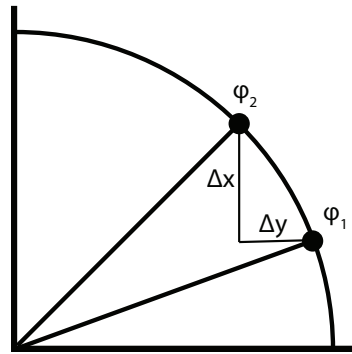
Figure 10-11: Top view of the mean flapping angle ϕ_1 of the regular DelFly compared to that of the 90-degree flapper ϕ_2, for one wing. The mean thrust application point is therefore displaced with Δy, Δx

in order to have a lightweight system, the philosophy of using ropes connected to servos is still promising for this concept.

When either a spring in the root bar near the leading edge is used, or an elastic bar is used as a root bar, the individual wings can all be deliberately slackened, and consequently by applying an input with a servo the bar can be pulled towards the root, making the foil stiffer. In this way, the control by displacing of the root bars can be recreated with a lightweight system.

Unfortunately, in this way only pitch and roll can be controlled; as was shown in the previous sections the yaw moment was not correlated with the slackening of the wings by moving the wing roots.

Chapter 11

Conclusions of preliminary research

In this preliminary work, two concepts for the control of the DelFly using its wings were presented, both using the principle of modulating the tension of the wings in order to change the thrust generated by the wing. A force-torque sensor was used to measure the resulting moments and forces. For the first concept, the stiffeners of the wing, at half-span, are pulled towards the root. This did not result in any significant altering of the thrust of the wing, however, it did cause the controlled wing to generate more drag. The result of this drag is that we were able to generate a yaw moment. The yaw moment is uncoupled and in the order of 0.5 Nmm, but with a high standard deviation. Also, the result is not linear. For the pitch and roll moment we did not measure significant results.

For concept B the mechanism on the tensioning and slackening of the wing foil has been revised. Instead of pulling the stiffener towards the root, the roots of the wings itself are disconnected from the fuselage, and they are moved outbound for slackening of the wing. Measurements showed that the best direction to move the roots towards, is equal to half of the flapping amplitude. This is also the point when the wing speed reaches its maximum during the flapping motion, and is also the point when the highest thrust force is created. For concept B, we were able to generate both the pitch and roll moments, and meet all requirements for free-flight. However, it did not result in yaw control, but for attitude stabilisation this is not required, since the yaw control is only needed to control the heading of the DelFly.

When moving towards a free-flight prototype, a mechanism needs to be developed to actuate each wing seperately. In this way, the roll and pitch moments can be generated that are required to stabilise and control the aircraft. For the flying prototype design, the center of gravity should be placed near the leading edge, close to the quarter chord point, in the flapping axis, to make sure that moment generation is optimal and to improve the dynamic stability of the (tail-less) DelFly.

Bibliography

Alexander, D. E. (1986). Wind tunnel studies of turns by flying dragonflies. *Journal of Experimental Biology*, *122*(1), 81–98.

Anderson Jr, J. D. (1985). *Fundamentals of aerodynamics*. Tata McGraw-Hill Education.

Ansari, S. A., Knowles, K., & Zbikowski, R. (2008, November). Insectlike Flapping Wings in the Hover Part I: Effect of Wing Kinematics. *Journal of Aircraft*, *45*(6), 1945–1954.

Armanini, S. F., Visser, C. C. de, Croon, G. C. H. E. de, & Mulder, M. (2015, December). Time-Varying Model Identification of Flapping-Wing Vehicle Dynamics Using Flight Data. *Journal of Guidance, Control, and Dynamics*.

Arora, N., Gupta, A., Sanghi, S., Aono, H., & Shyy, W. (2014). Lift-drag and flow structures associated with the clap and fling motion. *Physics of Fluids (1994-present)*, *26*(7), 071906.

Birch, J. M. (2003, July). The influence of wing-wake interactions on the production of aerodynamic forces in flapping flight. *Journal of Experimental Biology*, *206*(13), 2257–2272.

Cheng, B., & Deng, X. (2011, October). Translational and Rotational Damping of Flapping Flight and Its Dynamics and Stability at Hovering. *IEEE Transactions on Robotics*, *27*(5), 849–864.

Coleman, D., Benedict, M., Hrishikeshavan, V., & Chopra, I. (2015). Design, Development and Flight-Testing of a Robotic Hummingbird. In *AHS 71 st Annual Forum, Virginia Beach, Virginia, May 57, 2015*.

De Croon, G., De Clercq, K. M. E., Ruijsink, Remes, & De Wagter, C. (2009). Design, aerodynamics, and vision-based control of the DelFly. *International Journal of Micro Air Vehicles*, *1*(2), 71–97.

de Croon, G. C., Groen, M. A., De Wagter, C., Remes, B., Ruijsink, R., & Oudheusden, B. W. van. (2012). Design, aerodynamics and autonomy of the DelFly. *Bioinspiration & biomimetics*, *7*(2), 025003.

De Wagter, C., Tijmons, S., Remes, B. D., & de Croon, G. C. (2014). Autonomous flight of a 20-gram flapping wing mav with a 4-gram onboard stereo vision system. In *Robotics and Automation (ICRA), 2014 IEEE International Conference on* (pp. 4982–4987). IEEE.

De Clercq, K., Kat, R. de, Remes, B., Oudheusden, B. van, & Bijl, H. (2009a). Aerodynamic experiments on DelFly II: unsteady lift enhancement. *International Journal of Micro Air Vehicles*, *1*(4), 255–262.

De Clercq, K., Kat, R. de, Remes, B., Oudheusden, B. van, & Bijl, H. (2009b, June). Flow Visualization and Force Measurements on a Hovering Flapping-Wing MAV 'DelFly II'. In *Proc. 39th aiaa fluid dynamics conference.* American Institute of Aeronautics and Astronautics.

Dickinson, M. H., Lehmann, F. O., & Gotz, K. G. (1993, September). The active control of wing rotation by Drosophila. *Journal of Experimental Biology*, *182*(1), 173–189.

Dickinson, M. H., Lehmann, F.-O., & Sane, S. P. (1999). Wing rotation and the aerodynamic basis of insect flight. *Science*, *284*(5422), 1954–1960.

Ellington, C. P. (1999). The novel aerodynamics of insect flight: applications to micro-air vehicles. *Journal of Experimental Biology*, *202*(23), 3439–3448.

Fry, S. N., Sayaman, R., & Dickinson, M. H. (2003). The aerodynamics of free-flight maneuvers in drosophila. , *300*(5618), 495–498.

Götz, K. G. (1968). Flight control in Drosophila by visual perception of motion. *Kybernetik*, *4*(6), 199–208.

Groen, M., Bruggeman, B., Remes, B., Ruijsink, R., Van Oudheusden, B. W., & Bijl, H. (2010). Improving flight performance of the flapping wing MAV DelFly II. In *Int. Micro Air Vehicle Conf. and Competition (IMAV 2010)(Braunschweig, Germany).*

Hatch, G. (1966, July). Structure and Mechanics of the Dragonfly Pterothorax. *Annals of the Entomological Society of America*, *59*(4), 702–714.

Karásek, M., Hua, A., Nan, Y., Lalami, M., & Preumont, A. (2014). Pitch and Roll Control Mechanism for a Hovering Flapping Wing MAV. *International Journal of Micro Air Vehicles*, *6*(4).

Keennon, M., Klingebiel, K., & Andriukov, A. (2012). Tailless flapping wing propulsion and control development for the nano hummingbird micro air vehicle. In *American helicopter society future vertical lift aircraft design conference.*

Keennon, M., Klingebiel, K., Won, H., & Andriukov, A. (2012). Development of the nano hummingbird: A tailless flapping wing micro air vehicle. In *50th AIAA Aerospace Sciences Meeting Including the New Horizons Forum and Aerospace Exposition, Nashville, TN. January* (pp. 9–12).

Ma, K. Y., Chirarattananon, P., Fuller, S. B., & Wood, R. J. (2013, May). Controlled Flight of a Biologically Inspired, Insect-Scale Robot. *Science*, *340*(6132), 603–607.

Percin, M. (2016). *Aerodynamic Performance of the DelFly II.* (unpublished thesis)

Sane, S. P. (2003, December). The aerodynamics of insect flight. *Journal of Experimental Biology*, *206*(23), 4191–4208.

Sane, S. P., & Dickinson, M. H. (2001). The control of flight force by a flapping wing: lift and drag production. *Journal of experimental biology*, *204*(15), 2607–2626.

Singh, B., Chopra, I., Ramasamy, M., & Leishman, J. (2005, April). Experimental Studies on Insect-Based Flapping Wings for Micro Hovering Air Vehicles. In *46th aiaa/asme/asce/ah-s/asc structures, structural dynamics and materials conference.* American Institute of Aeronautics and Astronautics.

Sun, M. (2005, February). Dynamic flight stability of a hovering bumblebee. *Journal of Experimental Biology*, *208*(3), 447–459.

Sun, M. (2014, May). Insect flight dynamics: Stability and control. *Reviews of Modern Physics*, *86*(2), 615–646.

Sun, M., Wang, J., & Xiong, Y. (2007). Dynamic flight stability of hovering insects. *Acta Mechanica Sinica*, *23*(3), 231–246.

Taylor, G. K. (2001). Mechanics and aerodynamics of insect flight control. *Biological Reviews*, *76*(4), 449–471.

Tokutake, H., Sunada, S., & Ohtsuka, Y. (2009). Active Control of Flapping Wings Using Wing Deformation. *Transactions of the Japan Society for Aeronautical and Space Sciences*, *52*(176), 98–103.

Weis-Fogh, T. (1973). Quick estimates of flight fitness in hovering animals, including novel mechanisms for lift production. *Journal of Experimental Biology*, *59*(1), 169–230.

Wootton, R. J. (1981). Palaeozoic insects. *Annual review of entomology*, *26*(1), 319–344.

Xu, N., & Sun, M. (2013, February). Lateral dynamic flight stability of a model bumblebee in hovering and forward flight. *Journal of Theoretical Biology*, *319*, 102–115.

Zanker, J. M. (1988a). How does lateral abdomen deflection contribute to flight control ofDrosophila melanogaster? *Journal of Comparative Physiology A*, *162*(5), 581–588.

Zanker, J. M. (1988b). On the mechanism of speed and altitude control in Drosophila melanogaster. *Physiological entomology*, *13*(3), 351–361.

Zhang, Y., & Sun, M. (2010, May). Dynamic flight stability of a hovering model insect: lateral motion. *Acta Mechanica Sinica*, *26*(2), 175–190.